

Technische Universität München
Professur für Entwicklungsbiologie der Pflanzen

**The role of the Arabidopsis AGCVIII kinase UNICORN (UCN)
in plant development and flowering time determination**

Janys Peter Pleßmann

Vollständiger Abdruck der von der Fakultät Wissenschaftszentrum Weihenstephan für Ernährung, Landnutzung und Umwelt der Technischen Universität München zur Erlangung des akademischen Grades eines

Doktors der Naturwissenschaften

genehmigten Dissertation.

Vorsitzender:

Prof. Dr. Erwin Grill

Prüfer der Dissertation:

1. Prof. Dr. Kay H. Schneitz
2. Prof. Dr. Ralph Hüchelhoven

Die Dissertation wurde am 12.09.2017 bei der Technischen Universität München eingereicht und durch die Fakultät Wissenschaftszentrum Weihenstephan für Ernährung, Landnutzung und Umwelt am 04.12.2017 angenommen.

Summary

Plant development is strongly regulated in *Arabidopsis thaliana* and often depends on the perception, transduction and integration of extrinsic and intrinsic signals. These signals are frequently transferred by kinases, proteins that phosphorylate their targets thereby modulating their activity. One of these kinases is UNICORN (UCN) from the AGCVIII family. It was shown that *UCN* is a tumor suppressor, regulating planar cell division in integuments. This ovule organ shows protrusions in the *ucn-1* mutant that carries a missense mutation which putatively destroyed the kinase function of the protein.

In this work, I performed a detailed analysis of the *ucn-1* mutant, carrying a mutation in the genome of the Landsberg *erecta* (*Ler*) accession. I compared it to the *ucn-2* mutant that carries a putative *UCN* null allele in Columbia (Col-0) background. In this study, I used comparative analysis of the mutant phenotypes which revealed that *UCN* affects many more developmental processes of the plant than only ovule development. The results I present here show that *UCN* is expressed in all plant organs, above and below ground presumably representing a role for *UCN* in cell division. Furthermore, I showed that some phenotypical differences of *ucn-1* and *ucn-2* are due to genetic background effects rather than due to the differences in the respective mutations.

I further showed that *UCN* affects the epigenome. The *ucn-1* mutant has the capability to inherit an early flowering phenotype to its offspring independent of the mutated allele. In addition, I showed that other plant organs affected by the gain-of-function of *UCN* were still affected even after the T-DNA segregated out and the lines had a wild-type genome.

My analysis also revealed that *UCN* affects the transition to flowering. Depending on the genetic background flowering time was accelerated or delayed in *UCN* gain-of-function lines. In addition, I demonstrated that *UCN* physically interacts with ARABIDOPSIS TRITHORAX-RELATED7 (*ATXR7*), a protein of the trithorax-family that enhances the expression of *FLOWERING LOCUS C (FLC)*. Moreover, I showed that *UCN* regulates flowering through *ATXR7*. Finally, I demonstrated that *UCN* is required for the control of *FLC* expression and the repression of *FT* and therefore represses flowering in Col-0.

Zusammenfassung

Die Entwicklung der Pflanze ist in *Arabidopsis thaliana* streng reguliert und hängt oft von der Wahrnehmung, der Weitergabe und der Vernetzung extrinsischer und intrinsischer Signale ab. Diese Signale werden häufig durch Kinasen, Proteine, die ihre Zielobjekte phosphorylieren und dadurch ihre Aktivität modulieren, weitergeleitet. Eine dieser Kinasen aus der AGCVIII Familie ist UNICORN (UCN). In einer *ucn-1*-Mutante, welche eine Missense-Mutation trägt, die wahrscheinlich die Kinasefunktion des Proteins zerstört, zeigen Integumente irreguläre Zellteilung. Es wurde daher vorgeschlagen, dass UCN ein Tumorsuppressor ist, welcher planare Zellteilung in den Integumenten reguliert.

In dieser Arbeit wurde die *ucn-1*-Mutante, eine Mutation im Genom von Landsberg *erecta* (*Ler*), einer phänotypischen Analyse unterzogen. Sie wurde mit der *ucn-2*-Mutante verglichen, welche vermutlich eine Null-Mutation im Genom von Columbia (*Col-0*) trägt. In dieser Studie wurde durch vergleichende Analysen der Phänotypen der Mutanten gezeigt, dass *UCN* wahrscheinlich an viel mehr Entwicklungsprozessen der Pflanze als nur der Ovulenenwicklung beteiligt ist. Die Ergebnisse, die hier präsentiert werden, zeigen, dass *UCN* in allen Pflanzenorganen exprimiert wird, sowohl überirdischen als auch unterirdischen, was auf eine Rolle *UCNs* in der Zellteilung hindeutet. Darüber hinaus wurde gezeigt, dass die phänotypischen Unterschiede von *ucn-1* und *ucn-2* mehr vom genetischen Hintergrund der Mutation abhängen als von den unterschiedlichen Mutationen selbst.

Ferner zeigte ich, dass *UCN* das Epigenom beeinflusst. Die *ucn-1*-Mutante besitzt die Fähigkeit, ihren Frühblühphänotyp unabhängig vom mutierten Allel an ihren Nachwuchs zu vererben. Darüber hinaus zeigte ich, dass andere Pflanzenorgane, die von der gain-of-function von *UCN* betroffen waren, dies auch noch waren, wenn die T-DNA ausgesegregiert war und die Linien ein Wildtyp-Genom hatten.

Die Analyse ergab auch, dass *UCN* den Übergang zur Blüte beeinflusst. Abhängig vom genetischen Hintergrund wurde durch die gain-of-function eine beschleunigte oder verspätete Blüte eingeleitet. Zusätzlich konnte belegt werden, dass *UCN* physisch mit ARABIDOPSIS TRITHORAX-RELATED7 (*ATXR7*) interagiert, einem Protein der Trithorax-Familie, welches die Expression von *FLOWERING LOCUS C* (*FLC*) verstärkt. Mit dieser Studie wird gezeigt, dass *UCN* über *ATXR7* den Blühzeitpunkt reguliert. Letztlich wird belegt, dass *UCN* an der ordentlichen Expression von *FLC* und der Repression von *FT* beteiligt ist und dadurch die Blüte in *Col-0* reprimiert.

Table of contents

1	Introduction	1
1.1	The plant's life cycle in a nutshell	1
1.2	The transition to flowering	4
1.3	Flower and ovule development	6
1.4	DNA and chromatin – location matters	8
1.5	The AGCVIII kinase UNICORN (UCN)	10
1.6	Aim of this work	11
2	Material and Methods	12
2.1	Plant work	12
2.2	Cloning	12
2.3	Generation of various constructs	15
2.3.1	Construction of overexpression constructs	15
2.3.2	Construction of pGGZ001::pUCN:3xVenus-NLS	15
2.3.3	Constructing BiFC vectors	16
2.3.4	Constructing Y2H vectors	16
2.4	Phenotyping and microscopy	17
2.5	Generation of transgenic lines	18
2.6	Yeast two-hybrid (Y2H)	19
2.7	Bimolecular fluorescence complementation (BiFC)	19
2.8	Semiquantitative real-time PCR (sqRT-PCR) to verify <i>UCN</i> overexpression	20
2.9	Quantitative real-time PCRs (qRT-PCRs)	20
3	Results	22
3.1	Investigating the spatial expression pattern of <i>UCN</i>	22
3.2	Phenotypical comparison between two mutant alleles of <i>UCN</i> – <i>ucn-1</i> and <i>ucn-2</i>	27
3.3	Analysis of heterozygous <i>ucn-1</i> and <i>ucn-2</i> mutants	33
3.4	The flowering phenotype of a segregating F ₂ population of <i>ucn-1</i>	37
3.5	Influence of the length of day on <i>ucn-1</i> and <i>ucn-2</i>	38
3.6	Overexpression of <i>UCN</i>	40
3.7	Overexpression of <i>ucn-1</i>	45
3.8	Some features of the plants are inherited epigenetically	49

3.9	<i>UCN</i> is putatively involved in processes that affect flowering	55
3.9.1	<i>UCN</i> interacts with <i>ATXR7</i> in yeast	55
3.9.2	<i>UCN</i> interacts with <i>ATXR7</i> in protoplasts	56
3.10	Testing the influence of <i>ATXR7</i> on <i>UCN</i> and vice versa	57
3.10.1	Phenotypical characterization of <i>atxr7-1</i>	58
3.10.2	Phenotypical characterization of <i>atxr7-1 ucn-2</i>	60
3.11	Overexpressing <i>ATXR7</i>	63
3.11.1	Overexpression of <i>ATXR7</i> in wild-type plants	64
3.11.2	Overexpressing <i>ATXR7</i> and <i>UCN</i> in wild-type plants	67
3.11.3	Overexpressing <i>ATXR7</i> in <i>ucn-1</i> and <i>ucn-2</i>	72
3.11.4	Overexpression of <i>UCN</i> in <i>atxr7-1</i>	77
3.12	qRT-PCR results	79
3.12.1	The influence of <i>UCN</i> on <i>ATXR7</i>	79
3.12.2	The influence of <i>ATXR7</i> on <i>UCN</i>	80
3.12.3	The influence of <i>UCN</i> on the expression of <i>FLC</i>	81
3.12.4	The influence of <i>UCN</i> on the expression of <i>FT</i>	83
3.12.5	The influence of <i>ATXR7</i> gain-of-function on the expression of <i>FLC</i> and <i>FT</i>	84
3.12.6	Epigenetic influence on the expression of <i>FLC</i> and <i>FT</i> in EFC	85
4	Discussion	87
4.1	<i>UCN</i> is involved in processes of multiple plant organs	87
4.2	The <i>ucn-1</i> allele displays a dominant negative behavior	90
4.3	<i>UCN</i> is involved in epigenetic modifications	92
4.4	<i>UCN</i> and <i>ATXR7</i> share pathways	93
4.5	<i>UCN</i> is involved in flowering time regulation	96
5	Conclusion	100
6	Supplements	102
7	References	106
8	Acknowledgements	112
9	Curriculum Vitae	113

1 Introduction

1.1 The plant's life cycle in a nutshell

The life cycle of *Arabidopsis thaliana* can be divided into several developmental stages. After germination, the new plant starts with the vegetative phase. In this phase *Arabidopsis* builds up biomass by growing a rosette and performing photosynthesis. It builds up nutrients and stores them not only for the plant itself but also for the subsequent reproductive phase [1]. In the subsequent reproductive phase, *Arabidopsis* starts to reproduce by growing flowers, the reproductive organs of a plant. In parallel to the reproductive phase, the senescence already begins. The plant is gathering the nutrients and otherwise stored energy from its vegetative organs to support its offspring [2]. In case of *Arabidopsis*, an annual plant, the life cycle of the plant terminates with the end of senescence. At the same time, the seeds, and therefore the offspring, are mature and the end of one life cycle is also the beginning of several hundred new ones.

Germination of a seed is regulated by the plant hormones abscisic acid (ABA) and gibberellins (GA) where ABA supports dormancy and GA counteracts the effects of ABA and supports germination [3]. External signals can also support germination. The uptake of water by the seed and finally the rupture of the seed coat represents the beginning of the vegetative phase [4]. The embryo that developed in the seed with the help of nutrients delivered by the endosperm already contains cotyledons and the root [5].

The root is characterized by four zones, which are already established in the seed itself [6]. The root cap, the meristematic zone, the elongation zone, and the maturation zone: the root cap at the most distal end serves to save the meristematic tissue from damage when the root is growing deeper into the soil [7]. The meristematic zone bears cells acting as initials that characteristically divide. Thereby they produce cells that further divide and differentiate into the cells that make up the root. The elongation zone is where extensive cell elongation takes place. Although some cells still divide in this zone, cell division decreases to zero with increasing distance from the meristem. Finally, the maturation zone contains the mature cells. Here, cell division and elongation ceased, the cells acquire their differentiated characteristics. In this zone, lateral roots and root hairs develop [8].

For the patterning of the different root tissues and the formation and maintenance of the root meristem the plant hormone auxin plays a major role. In the root tip, there is an auxin maximum needed for the maintenance of the quiescent center (QC), a group of rarely dividing cells in the meristematic zone [9]. The auxin is further transported in the root by the polarized distribution of PIN-FORMED (PIN) proteins, thereby establishing a flow comparable to an inverted fountain, with a rush towards the QC in the stele and a rush away from the QC in the epidermis [10]. This auxin gradient and transcription factors (TF) that selectively react to certain auxin concentrations therefore build up the different root tissues. In addition to the root formation, auxin is also involved in the initiation of lateral roots [11]. Lateral roots emerge from pericycle founder cells and auxin primes the pericycle cells from which the lateral root emerges [6, 12]. The architecture of a lateral root is not very different from the architecture of the main root. It contains the same zoning as the main root. In *Arabidopsis*, lateral roots emerge in a left-right alternation on the main root developing at the edge of elongation and maturation zone [11].

Above ground, the shoot apical meristem (SAM) is responsible for indeterminate growth. It localizes in the middle of the future rosette at the base between the cotyledons. The SAM is divided into certain zones: the central zone (CZ, see figure 1.1.1) contains slowly dividing, undifferentiated cells. Around that zone, the peripheral zone (PZ, see figure 1.1.1) contains more frequently dividing cells that later form lateral organs. Beneath the central zone lies the rib zone (RZ, see figure 1.1.1) with dividing cells that later form the internal tissue of the stem. On top of the SAM lie three cell layers, L1, L2, and L3 (see figure 1.1.1) which also contribute to the tissue of the shoot [13].

The size of the meristem is controlled mainly by *WUSCHEL* (*WUS*) and *CLAVATA1* and 3 (*CLV1*, *CLV3*) [14]. *WUS* gives the SAM its identity and is expressed in the organizing center (OC). From there, the protein moves into the central zone (CZ) where it promotes the expression of *CLV3* which in turn represses *WUS* (see figure 1.1.1) thereby controlling SAM size [15].

Rosette leaves are initiated at the peripheral zone of the SAM (see figure 1.1.1). The first two leaves grow between the cotyledons. From here, the rest of the leaves grow anticlockwise in a spiral arrangement [16]. The leaves of *Arabidopsis* have a lanceolate shape and grow from their proximal to their distal end. Therefore, cell division takes place at the proximal end of the leaf while at the distal end, the cells elongate [17]. The planar shape

of the leaves is achieved through the generation of an adaxial-abaxial axis. Amongst other factors, axis identity is regulated by KANADI and YABBY transcription factors that promote abaxial fate. The adaxial identity is promoted by class III HD-ZIP transcription factors [18].

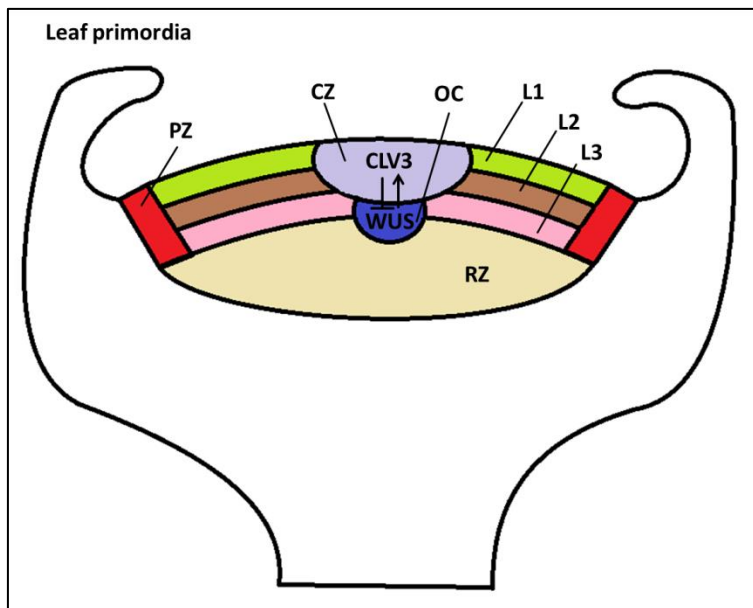


Figure 1.1.1: Schematic picture of the shoot apical meristem of *Arabidopsis* [19].

Picture shows the central zone (CZ, purple), the organizing center (OC, blue), the peripheral zone (PZ, red), the three layers L1 to L3 (green, brown, pink), and the rib zone (RZ, light brown). *CLV3* and *WUS* act together in a negative feedback loop to determine meristem size. Leaf primordia develop in the periphery.

The vegetative phase is followed by the reproductive phase where the plant starts producing flowers and with it, offspring. The transition to flowering is highly regulated and will be described in more detail later. It is accompanied with the transformation of the SAM into an inflorescence meristem (IM) which produces flowers instead of leaves [20, 21]. Genes such as *TERMINAL FLOWERING1 (TFL1)*, *AGAMOUS (AG)*, and *LEAFY (LFY)* but also *WUS* are involved in floral meristem identity [14, 22].

In plants, a double fertilization takes place. Therefore, the pollen sticks to the stigma, a small, sticky tissue on the most distal end of the carpel that starts developing when the ovules are ready for fertilization. The pollen then grows into the carpel. Amongst other factors, it is chemically attracted by the synergids of the ovules [23]. When reaching the ovule the tip of the pollen tube grows into the micropyle, a small “whole” that is generated by the integuments. There, it releases two nuclei, one fertilizing the egg-cell and the other one fertilizing the central cell [24]. The zygote now develops into the plant embryo while the central cell develops into the endosperm.

After fertilization, embryogenesis starts with an unequal cell division, dividing the zygote, the fertilized egg cell, into an apical and a basal cell [25]. The above ground tissue will develop from the apical cell while the root develops from the basal cell. When embryogenesis continues, certain stages of the embryo are visible [26]. In the so called early heart stage, the anlagen of the cotyledons are already visible while in the following late heart stage and the torpedo stage, the root and the shoot apex can already be clearly distinguished. In the mature embryo, cotyledons and the two apices are completely available. The endosperm was consumed by the embryo, supporting it with energy and the embryo is now completely taking the place in the seed, persisting in dormancy and waiting for the right signals for germination [4]. Then the cycle can begin from the start.

1.2 The transition to flowering

The transition to flowering that separates the vegetative phase from the reproductive is tightly regulated since the right time to flower is a question of survival and, more important, a question of the offspring's survival. Therefore, the plant permanently processes external signals, for example temperature, and internal signals, for example plant age to find the perfect time for flowering.

In *Arabidopsis* two different "strategies" can be observed in the different accessions reflecting their geographical localization. There are strains that need a prolonged time of cold treatment called vernalization as a signal for flowering, the winter-annual strains. Other strains are independent of vernalization and flower without cold treatment, the summer-annual strains [27] such as *Ler* and *Col-0*. Winter-annual plants usually grow a rosette in autumn which rests over winter. At that time, genes that prevent the flowering transition are repressed by the low temperature. Subsequently, milder temperatures and longer days in spring then promote flowering. In summer-annual strains, the vegetative phase is not separated from the reproductive phase by winter and therefore, all developmental phases are passed in one year. Therefore, the lines are independent of vernalization [1].

Temperature and the length of the days (photoperiod) are only two of multiple external signals that the plants use to find the right time for flowering. Also nutrients, light quality, and stress influences flowering time [1, 28]. The external signals are interconnected with internal signals such as plant age. They are summarized in the autonomous flowering pathway that promotes flowering by repressing *FLOWERING LOCUS C (FLC)* [29], a very

potent flowering repressor. Also the plant hormone GA plays a role as an intrinsic signal in flowering time regulation [30, 31] especially in short days (SD) [32].

Vernalization, at least in winter-annual plants, is the most potent signal for flowering and depends mainly on the repression and subsequent silencing of *FLC* [33]. *FLC*, a MADS box (for **M**CM1, **A**GAMOUS, **D**EFICIENS, **S**RF) protein that binds to CA_nG boxes (CC(A/T)_nGG), the consensus sequence recognized by this protein family, in turn directly represses the flowering activator *FLOWERING LOCUS T (FT)* by binding to its first intron [34]. FT is a small protein comparable to a flowering promoting hormone and therefore described as florigen.

FLC expression strongly depends on *FRIGIDA (FRI)*, a transcriptional mediator that assembles the transcription complex for *FLC* [35]. In fact, most of the summer-annual plants that are independent of vernalization lack a functional *FRI*, *FLC* or both [36]. The *Arabidopsis* Col-0 strain for example has a non-functional *FRI* allele and the dependency of vernalization can in part be re-established by transforming a functional *FRI* allele into the plant [37]. The *Ler* strain of *Arabidopsis* on the other hand contains a non-functional *FLC* allele that carries a mutator-like transposon in the 3' end of its first intron [36], an intron which also plays a role in the regulation of *FLC* expression [38]. Due to these differences, the two accessions likely also use different pathways to initiate the transition to flowering.

For the activation of flowering, repressors like *FLC* have to be repressed and flowering activators need to be expressed. Therefore, it is distinguished between flowering promotion, which is the repression of the flowering repressors, and flowering activation by floral integrators such as *FT*, which is the actual transition of the SAM to an inflorescence meristem (IM) that produces flowers [39]. The transition of the meristem is, amongst other floral integrators, regulated by *FT*. *FT* activates flowering over long distances from the leaf [40], where it is activated in the phloem [41], to the SAM. There, it acts together with other proteins to reprogram the meristem into an IM. The activation of *FT* in one leaf is thereby sufficient to activate flowering [42]. *FT* is induced under LD conditions in the ploem. In cooperation with other proteins, *FT* then activates floral meristem identity genes, such as *APETALA1 (AP1)* [43] to induce flowering. *AP1* and *LEAFY (LFY)*, two proteins acting downstream of *FT*, regulate floral meristem identity. In fact, the expression of these two genes in the floral anlagen of the IM is one of the earliest events in floral transition [44, 45].

1.3 Flower and ovule development

After flowering transition, flower primordia are constantly formed in the periphery of the IM. Flowers are by far the most complex organs of the plant. *Arabidopsis* flowers consist of four sepals in the outer whorl, four petals, six stamens and finally two fused carpels in the innermost whorl. It has been greatly accepted that the identity of the four different whorls is regulated by an ABC system (see figure 1.3.1). This ABC system is built by the homeotic flower genes, *APETALA1* (*AP1*) and *AP2*, *AP3* and *PISTILLATA* (*PI*), and *AGAMOUS* (*AG*). The expression of these genes is giving the four whorls of the flower their identity [46]. In the inner whorl *AG*, the C class gene of the ABC system, is giving the carpels their identity [47] (see figure 1.3.1, red). In the next whorl the B class genes *AP3* and *PI* are co-expressed with *AG*. Together they are giving the stamen their identity [48] (see figure 1.3.1, yellow). The expression of the C class gene excludes the expression of the A class genes and vice versa. Therefore, in the next whorl, the A class genes *AP1* and *AP2* are expressed. Together with the B class genes *AP3* and *PI* which are giving the petals their identity (see figure 1.3.1, green). In the outermost whorl only *AP1* and *AP2* are still expressed giving the sepals their identity [44, 49, 50] (see figure 1.3.1, blue). Each loss-of-function mutant of these genes shifts the ABC system to the benefit of the other genes and therefore alters the structure of the flower. The flower of *ag1* mutants for example lack stamen and carpels which are replaced by petals [47].

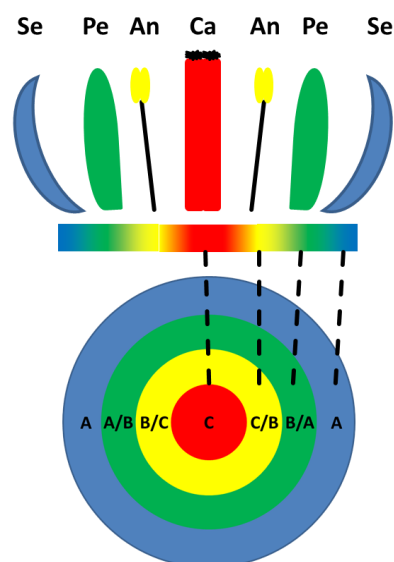


Figure 1.3.1: Scheme of the ABC model of floral organ identity.

Floral organs develop by the different expression of class A, B, and C genes which give the organs their identity. Thereby, A class genes (in blue) give the sepals (Se) their identity and together with B class genes (in green) they give identity to the petals (Pe). B and C class genes (in yellow) give identity to the stamens (An) while C class genes (in red) give rise to the carpels (Ca). Figure shows a scheme of the floral organs (upper figure) and a top view of the whorls (lower figure)

In *Arabidopsis*, the anthers on top of the stamen bear the pollen that contains the haploid paternal genome while the maternal haploid genome is found in the ovules which grow in the carpels in the inner whorl. Every carpel contains about 50 to 75 ovules which after fertilization develop into seeds. Ovules appear in rows along the placenta in the carpel. As cell division continues forming a small dome, three distinct tissues can be distinguished: on proximal end, the funiculus connects the ovule with the motherplant. The tissue in the middle is called chalaza and later develops the integuments, an outer one and an inner one. These integuments, each contains an adaxial and an abaxial cell layer, grow strictly by anticlinal cell division and later surround the megaspore mother cell (MMC), developing from the nucellus at the most distal tissue primordium of the ovule. The integuments, which later form the seed coat are, in contrast to the MMC and later the embryo, built-up from diploid maternal tissue and therefore differs from the seedling in its genomic composition [51].

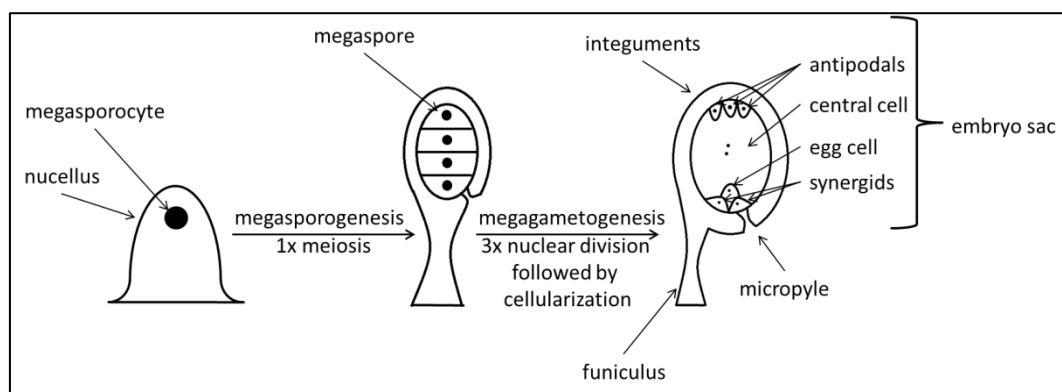


Figure 1.3.2: Schematic diagram of the development of the ovule.

During megasporogenesis the megasporophyte meiotically divides into a tetrad. The megaspore proximal to the chalazal side then undergoes megagametogenesis while the other three megaspores degenerate. The megagametogenesis then results in the embryo sac containing seven cells.

The MMC develops from the megasporocyte that undergoes a meiotic divisions building a tetrad of megaspores. One of these megaspores proximal to the chalaza survives, giving rise to the embryo sac by undergoing three round of mitosis followed by cellularization. The embryo sac then contains seven cells, three antipodal cells, a central cell with two haploid nuclei, the egg cell, and two synergids (see figure 1.3.2) [52, 53]. When double fertilization occurs, the egg cell and the central cell are fertilized. Subsequently, the egg cell develops into the embryo (see above) while the central cell develops into the endosperm. The endosperm which took up half of the seed volume is almost completely resorbed by the embryo between seven and ten days after fertilization took place. The parallel development of the seed can be roughly subdivided into three stages: accumulation

of starch in the early embryogenesis, storage of oils and proteins in the maturation phase, and water loss in the late maturation phase [54].

The seed size depends on endosperm and integuments and the cross-talk between those two tissues. Therefore, it is determined by a completely maternal tissue, the integuments, and a maternal-paternal tissue, the endosperm [51]. Furthermore, the integuments are diploid while the endosperm is a triploid tissue after fertilization (two maternal nuclei and one paternal nucleus). The two genomes derived maternally and paternally are not functionally equivalent in *Arabidopsis* endosperm [55]. Thus, seed size is also determined by a parent-of-origin effect. It therefore also depends on imprinted genes and DNA methylation [56].

1.4 DNA and chromatin – location matters

Gene expression is not only dependent on transcription factors but also on the chromatin structures found at the gene loci themselves. The chromatin is divided into euchromatin in which active genes are located in and heterochromatin in which inactive genes are located in. The chromatin structure is involved in the regulation of genes by controlling the access of the transcription machinery to the DNA locus. Amongst other modifications, it is established by direct modification of the DNA through methylation of the cytosine C5 to 5-methylcytosine. While this methylation in animals only takes place in a CG context, methylation in plants can take place in CG, CHG, and CHH (H = A, T, C) contexts [57]. The methylation of DNA is usually associated with gene silencing therefore it is often found around transposons and the centromeres [58]. On the other hand, more and more methylation patterns are found which are not associated with these functions but gene regulation [59]. It was also demonstrated that DNA methylation in promoters can function as a recognition site for proteins [60]. In plants, three pathways for the maintenance of DNA methylation are known: METHYLTRANSFERASE1 (MET1) [61], CHROMOMETHYLASE3 (CMT3) [62, 63], and DOMAINS REARRANGED METHYLASE1 and 2 (DRM1/2) [64, 65]. These DNA methyltransferases also have overlapping functions and therefore single mutants can be inconspicuous but a quadruple knock-out is causing embryo lethality demonstrating the importance of a correct DNA methylation [66].

However, DNA methylation is also meiotically inherited to the offspring and can therefore be used as a kind of “DNA memory” [61]. How this inheritance takes place is still elusive since not much is known about the “equalization” of the DNA methylation patterns

after fertilization where a maternal and a paternal epigenome come together and need to be adapted to each other. It could be shown that a global demethylation takes place although there is growing evidence that e.g. imprinted genes do not seem to be subject to this process [67]. However, the DNA methylation pattern is one possibility to modify gene expression and in addition inherit certain expression patterns trans-generationally [68].

Other modifications that influence gene expression are found on histones which are octamers the DNA is wrapped around resulting in a kind of pearl necklace structure. Histones consist of two copies of the monomers H2A, H2B, H3, and H4, although variations are possible [69]. They can be modified post-translationally for example by phosphorylation which is mostly associated with chromosome condensation [70], acetylation which neutralizes polarity and weakens the interaction of histones and DNA, methylation to regulate gene transcription, and further modifications like ubiquitination, histone tail clipping, etc. [71]. Most modifications take place at the N-terminus of histone H3 which is protruding from the molecule and therefore a great target for modifications. The different histone modifications are summarized in the term “histone code”.

Two protein groups methylate H3 to regulate gene expression: proteins from the **trithorax** (Trx) group methylate H3K4 and K36 and activate gene expression while proteins from the **polycomb group** (PcG) methylate H3K9 and K27 and repress gene expression. Both protein groups belong to the SET (for **Su**(var), **E**(z), trithorax) domain group (SDG) [72]. The histone writing can be very specific and therefore add only one histone as for example *ARABIDOPSIS TRITHORAX1* (*ATX1*) which selectively trimethylates dimethylated lysine 4 (H3K4me₂ → H3K4me₃) [73] or less specific like *ARABIDOPSIS TRITHORAX-RELATED7* (*ATXR7*) which, amongst others, can mono-, di- and trimethylate H3K4 [74, 75].

The histone code is highly variable and the modifications need to be seen in context with other modifications and the location of the histone itself. The active marks H3K4me_{2/3} and H3K36me₃ antagonize the deposition of the repressive mark H3K27me₃ [76]. Another example is the grade of methylation. While H3K36me₂ and me₃ is associated with activation, the monomethylation results in deactivation [77]. In addition, the histone code cannot be separated from transcription and *vice versa*. These reactions are interconnected: not only can the histone code influence transcription, but also can the transcription influence the histone code [78]. The same is true for DNA methylation [60, 79] which in addition can also influence the histone code and *vice versa* [80]. Therefore, the transcription of a gene can influence the regulation while it transcribes the gene.

1.5 The AGCVIII kinase UNICORN (UCN)

A common way of posttranslational modulation of proteins is phosphorylation. Phosphorylation of a protein can modulate its activity. It is carried out by kinases. The genome of *Arabidopsis* is predicted to encode more than 1000 kinases and therefore much more than the genome of any other representative metazoan organism [81]. Kinases are divided into serine/threonine kinases and tyrosine kinases, according to the target amino acid which is phosphorylated [82]. Protein serine/threonine kinases (PSTK) represent around 4% of the *Arabidopsis* proteome [83]. These kinases use the γ -phosphate of ATP or GTP to generate phosphate monoesters using the alcohol groups on serine or threonine as phosphate acceptors [84]. The PSTKs can be further divided into several families of which one of them is the AGC (for protein kinase **A** (PKA), protein kinase **G** (PKG), protein kinase **C** (PKC)) family [85] which contains 39 members [81]. The AGC kinases are further divided into five subfamilies, of which one of them is the AGCVIII subfamily. This subfamily is plant-specific and contains 23 members [81]. They are identified by a common DFD (aspartic acid, phenylalanine, aspartic acid) motif at the N-terminal end and the insertion of a variable sequence between catalytic subdomain VII and VIII [84]. The DFD motif is involved in the coordinated binding of Mg^{2+} -ATP [81].

Most AGC kinases are primary targets for 3-phosphoinositide-dependent protein kinase (PDK1), a master-kinase that activates their targets through phosphorylating their activation loop [86, 87]. This activation then allows autophosphorylation and activation of substrate kinases [86]. Although it can be shown that PDK1 interacts with multiple AGCVIII kinases *in vitro* [81], the relevance of these interactions in plants is still discussed [88]. However, AGCVIII kinases play critical roles in cellular signaling and are involved in converting developmental and environmental signals into cell responses. Known targets of AGCVIII kinases are rare [88]. In this work, the AGCVIII kinase *UNICORN* (*UCN*) is investigated.

UCN was first described in 1997, growing protrusions on the integuments and eventually fails to generate an embryo sac. It further shows semi-lethality [89]. The gene was isolated and characterized in 2012. Alignments showed that *UCN* codes for an active AGCVIII kinase, encoding two kinase domains separated by an insertion loop, a nuclear localization signal lying in the insertion loop as well as a nuclear export signal flanking the kinase domains, and a 3'-PHOSPHOINOSITIDE-DEPENDENT PROTEIN KINASE1 (PDK1) - interacting domain at its C-terminal end. Like many other AGCVIII kinases *UCN* can interact

with PDK1 *in vitro* and in yeast (unpublished data). UCN is localized in the cytoplasm as well as in the nucleus of the cells. It was further shown that the protrusions are not restricted on the outer integuments but also the inner integuments, filaments and petals. It could be demonstrated that *UCN* is involved in planar cell growth by repressing the KANADI transcription factor *ABERRANT TESTA SHAPE (ATS)*. It was concluded that the relative levels of *ATS* and *UCN* are critical for planar cell growth in the integuments. Further, former results show that *UCN* acts in an organ-specific manner in floral organogenesis and that the outgrowths develop autonomously of the plant hormones auxin and cytokinin. In addition, *UCN* acts independently of the *AUXIN RESPONSE FACTOR (ARF)* genes *ETTIN (ETT)* and *ARF4*. *ETT* is thought to form dimers with *ATS* to regulate integument development and polarity [90]. This indicates that *UCN* acts in a different pathway than the *ETT/ARF4* complex [91, 92].

1.6 Aim of this work

In this study, the spatial expression pattern of *UCN* was visualized for the first time using a *3xVenus* reporter gene coupled to the full promoter region of *UCN*. Further, the *ucn-1* mutant, a mutant in the *Ler* accession, was characterized focusing on different plant organs than the flower and the ovules. It was compared to the *ucn-2* mutant, a mutant in the *Col-0* accession carrying a putative *ucn* null-allele. I was able to show that, despite the distinct differences in phenotype, the mutants have some features in common, although *ucn-2* displays these features in a much weaker fashion. I further present data that neither *ucn-1* nor *ucn-2* carries a “real” null allele and that *ucn-1* is a negative-dominant allele. With a gain-of-function approach, I further demonstrate that differences between *ucn-1* and *ucn-2* are largely dependent on the accessions. The data presented here also suggests a role for *UCN* in processes of other plant organs than the flower.

In the later part of this study I focus on a putative role of *UCN* in flowering time determination. I will present data that shows that *UCN* likely interacts with the trithorax-like SET domain protein *ATXR7*. Evidence is presented that, in some processes, *UCN* and *ATXR7* act in the same pathways. I will further show that *UCN* putatively influences the expression of the floral repressor *FLC* and the floral integrator *FT*. The results also suggest that this influence is inherited trans-generationally through a modified epigenome in *Col-0* as well as in *Ler*.

2 Material and Methods

2.1 Plant work

Arabidopsis thaliana (L.) Heynh. var. Landsberg (*erecta* mutant) (*Ler*) and var. Columbia (Col-0) were used as wild-type strains. The *ucn-1* (*Ler* background) and *ucn-2* (Col-0 background) mutants were described earlier [89, 91] as was the *atxr7-1* mutant [74].

Plants were grown either on Murashige & Skoog (MS) medium (4,4g/L) containing 0,8% Agarose or soil (Patzter Einheitserde, extra-gesiebt, Typ T, Patzer GmbH & Co. KG, Sinntal-Jossa, Germany) mixed with perlite in either a long day cycle (LD; 16hrs light) or a short day cycle (SD; 8hrs light) using a cold-white light. The light intensity was 100 to 150 μ E in either LD or SD cycle. The growth temperature was 21°C (\pm 1°C) in the light periods and 18°C (\pm 1°C) in the dark periods. The relative humidity was 50 to 60%.

Before sowing seeds on MS, they were surface sterilized in 70% Ethanol for 3min on a rotator. Regardless the medium used, seeds were stratified for 3d at 4°C prior to incubation. Plants sown on soil were cultured under a lid for three to five days to support equal germination.

2.2 Cloning

DNA and RNA used for cloning were extracted from *Arabidopsis thaliana* using the NucleoSpin Plant II kit (Macherey-Nagel GmbH und Co. KG) and the NucleoSpin RNA plant kit (Macherey-Nagel GmbH und Co. KG), respectively, both according to the manufacturer's protocol. Before RNA was used as a template, mRNA was reverse transcribed into cDNA using the RevertAid 1st strand cDNA synthesis kit (Fermentas) and a poly-T primer according to the manufacturer's protocol. Cloning was performed using standard methods described in [93].

Vectors used in this work are listed in table 2.2.2. Q5 High-Fidelity DNA Polymerase (NEB GmbH) was used according to the manufacturer's protocol to receive the PCR-fragments needed for cloning. Restriction enzymes and T4 DNA Ligase used for cloning were also received from NEB GmbH and used according to the manufacturer's protocols. PCR products were purified using the NucleoSpin Gel and PCR clean-up kit (Macherey-Nagel GmbH und Co. KG) according to the manufacturer's protocol. Plasmids were isolated with

the NucleoSpin Plasmid kit (Macherey-Nagel GmbH und Co. KG) according to the manufacturer's protocol. *Escherichia coli* strain DH10 β was used for amplification of the plasmids. Bacteria were grown on corresponding selection media (Lacto-broth; for concentration of antibiotics, see table 2.2.1).

Table 2.2.1: Concentration of Antibiotics used in this work for selection of *E. coli*.

Antibiotic	Concentration [$\mu\text{g/ml}$]
Ampicillin	100
Kanamycin	50
Spectinomycin	100
Gentamycin	25
Rifampicin	10
Tetracyclin	12,5

Cloned plasmids were verified through sequencing by MWG-Biotech AG following the company's standards. Sequencing results were aligned with CloneManager Ver. 8.04 to reference sequences received from The Arabidopsis Information Resource (TAIR, www.arabidopsis.org).

Binary vectors used for plant transformation were based on GreenGate [94]. All primer used in this work are listed in table 2.2.3.

Table 2.2.2: Backbone vectors used in this work.

Name	Used for	Description
pGADT7-GW	Yeast 2 Hybrid	Contains activation domain for Yeast two-hybrid interaction tests
pGBKT7-GW	Yeast 2 Hybrid	Contains binding domain for Yeast two-hybrid interaction tests
pUC-SPYCE	BiFC	Contains C-terminal part of yellow fluorescence protein (YFP)
pUC-SPYNE	BiFC	Contains N-terminal part of YFP
pGGA000	GG entry vector	Entry vector for promoter region of interest
pGGC000	GG entry vector	Entry vector for CDS of interest
pGGE000	GG entry vector	Entry vector for terminator region of interest
pGGN000	GG intermediate vector	Intermediate vector used to construct double T-DNA constructs
pGGM000	GG intermediate vector	Intermediate vector used to construct double T-DNA constructs
pGGZ001	GG destination vector	Destination vector, binary vector for plant transformation
pGGA006	GG entry with pUBQ	Entry vector carrying promoter sequence of <i>UBQ10</i>
pGGB003	GG entry with N-decoy	Entry vector carrying N-decoy in case no N-tag is needed
pGGD002	GG entry with C-decoy	Entry vector carrying C-decoy in case no C-tag is needed
pGGD007	GG entry with linker:NLS	Entry vector carrying nuclear localization signal with linker as C-tag
pGGE009	GG entry with tUBQ	Entry vector carrying terminator of <i>UBQ10</i>
pGGF009	GG entry with Basta-R	Entry vector carrying Basta resistance for plant selection

Table 2.2.3: Primer used in this work.

Primer number	Sequence (5' -> 3')	Purpose
2033	GACAAATCCTCCGCATCTTCTCT	Genotyping <i>ucn-1</i>
2034	TTCCGGGTTCCGGATCCG	Genotyping <i>ucn-1</i>
3758	AACAGGTCTCAGGCTCAACAATGGTTGCGGTTGATTCC	Amplifying <i>ATXR7</i> for pGGC000
3952	AACAGGTCTCTCTGAGTTTAGCGATCCACGGCAC	Amplifying <i>ATXR7</i> for pGC000
3561	AACAGGTCTCTCTGAGAAATCAACAAACGGATTGTTTTCAGAACA	Amplifying <i>UCN/ucn-1</i> for pGGC000
3562	AACAGGTCTCAGGCTCAACAATGGAGACAAGACCATCATCATCATCTTCT	Amplifying <i>UCN/ucn-1</i> for pGGC000
3978	AACAGGTCTCAACCTGACAAACAGCGCGACGTCACC	Amplifying <i>pUCN</i> (compl.) for pGGA000
3552	AACAGGTCTCTTGTGTTGTGAGAGAAAGAGAGAGAT	Amplifying <i>pUCN</i> (compl.) for pGGA000
3688	AACAGGTCTCACTGCTCCACGCGTGGGAGAATCTATC	Amplifying <i>tUCN</i> (compl.) for pGGE000
3549	AACAGGTCTCAGTGCTTATTGTTATAGATAACTGA	Amplifying <i>tUCN</i> (compl.) for pGGE000
3690	AACAGGTCTCAGGCTCAACAGCTGTCGCTGCGGCAGCG	Amplifying <i>Venus</i> to assemble <i>3xVenus</i>
3744	AAAAAGCGGCCGAGCAGCAGCCTTGTACAGCTCGTCCATGCC	Amplifying <i>Venus</i> to assemble <i>3xVenus</i>
3745	AAAAAGCGGCCGCTGCTGCTGCTGCTATGGTGAGCAAGGGCGAG	Amplifying <i>Venus</i> to assemble <i>3xVenus</i>
3746	TCAGGGAGTGGTTCCTTGTACAGCTCGTCCATGCC	Amplifying <i>Venus</i> to assemble <i>3xVenus</i>
3747	GGAAGCGGCTCTGGAATGGTGAGCAAGGGCGAG	Amplifying <i>Venus</i> to assemble <i>3xVenus</i>
3748	AAAAATCCGGAACCACTCCCTGACTTGTACAGCTCGTCCATGCC	Amplifying <i>Venus</i> to assemble <i>3xVenus</i>
3756	AAAAAGCGCGCCATGGTTGCGGTTGATTCC	Amplifying <i>ATXR7</i> for pUC-SPYCE/NE
3946	AAAAACCCGGGGTTTAGCGATCCACGGCAC	Amplifying <i>ATXR7</i> for pUC-SPYCE/NE
3175	GGGGGGTTCGACATGGAAAAAGTTTTCTCCGAC	Amplifying <i>bZIP63</i> for pUC-SPYCE/NE
3176	AAAAACCCGGGCTGATCCCAACGCTTCAATAC	Amplifying <i>bZIP63</i> for pUC-SPYCE/NE
3975	AAAAACCCGGGCATGGTTGCGGTTGATTCC	Amplifying <i>ATXR7</i> for AD/BD
3976	AAAAACTCGAGTTAGTTTAGCGATCCACGGCAC	Amplifying <i>ATXR7</i> for AD
3977	AAAAAGCGGCCGCTTAGTTTAGCGATCCACGGCAC	Amplifying <i>ATXR7</i> for BD

2.3 Generation of various constructs

2.3.1 Construction of overexpression constructs

For the overexpression constructs, the CDS of *ATXR7* was amplified using cDNA received from Col-0 total RNA using primer 3758 and 3952. The CDS of *UCN* and *ucn-1* was amplified using genomic DNA (gDNA) of *Ler* and *ucn-1*, respectively, as template with primer 3561 and 3562. All PCR products were digested with *BsaI* and ligated into pGGC000 resulting in the entry vectors *pGGC000::ATXR7*, *pGGC000::UCN* and *pGGC000::ucn-1*, respectively.

Vectors were further assembled with pGGA006, pGGB003, pGGD002, pGGE009, and pGGF009 (all kindly provided by Jan Lohmann) to *pGGZ001::pUBQ:ATXR7:tUBQ*, *pGGZ001::pUBQ:UCN:tUBQ* and *pGGZ001::pUBQ:ucn-1:tUBQ*, respectively, following the instructions of [94].

The entry vectors mentioned above were also used to construct the double overexpression vector *pGGZ001::pUBQ:ATXR7 pUBQ:UCN* via *pGGN000::pUBQ:ATXR7:tUBQ* and *pGGM000::pUBQ:UCN:tUBQ*.

2.3.2 Construction of *pGGZ001::pUCN:3xVenus-NLS*

The destination vector *pGGZ001::pUCN:3xVenus-NLS* was assembled with the GreenGate system. To clone *pGGA000::pUCN*, the whole promoter region of *UCN* including the 5'UTR (-1bp to -8365bp) was amplified with primer 3978 and 3552 using gDNA of Col-0 as template. The amplicon was purified and ligated into pGGA000 as described before.

For *pGGE000::tUCN*, the whole terminator region of *UCN* including the 3'UTR (+1216bp to +3057bp) was amplified with primer 3688 and 3549 using from Col-0 gDNA as template. The amplicon was purified, digested and ligated into pGGE000 as described above.

For the *3xVenus* vector, the *Venus* CDS was amplified three times with different overhangs using primer 3690 + 3744, 3745 + 3746, and 3747 + 3748 using a lab-created *Venus*-plasmid as template. The amplicons were purified and subcloned into pJET1.2 using the CloneJet PCR cloning kit (Fermentas) according to the manufacturer's protocol. This resulted in the three plasmids *pJET1.2::Venus-1*, *pJET1.2::Venus-2* and *pJET1.2::Venus-3*. All three plasmids were then used to ligate *Venus-1* to -3 into pGGC000 in a single tube reaction

using the GG digest/ligate reaction of [94] as a model. This resulted in the entry vector pGGC000::3xVenus.

The final vector pGGZ001::pUCN:3xVenus-NLS was then assembled from pGGA000::pUCN, pGGB003, pGGC000::3xVenus, pGGD007, pGGE000::tUCN, and pGGF009.

2.3.3 Constructing BiFC vectors

Protein interaction studies in protoplasts were performed with bimolecular fluorescence complementation (BiFC) using the two vectors pUC-SPYCE and pUC-SPYNE. For pUC-SPYCE::ATXR7 and pUC-SPYNE::ATXR7, the CDS of ATXR7 was amplified using primer 3756 and 3946 with Col-0 cDNA as template. The amplicon was purified then digested with AscI and XmaI, as also were the vectors pUC-SPYCE and pUC-SPYNE. Ligation partners were then again purified and subsequently ligated to the final vectors pUC-SPYCE::ATXR7 and pUC-SPYNE::ATXR7.

The control vectors pUC-SPYCE::bZIP63 and pUC-SPYNE::bZIP63 were constructed by amplifying the CDS of bZIP63 with primer 3175 and 3176 using cDNA of Col-0 as template. Amplicons were purified and digested with XmaI and Sall, as was the plasmids pUC-SPYCE and pUC-SPYNE. Ligation partners were again purified then ligated to pUC-SPYCE::bZIP63 and pUC-SPYNE::bZIP63. All constructs were verified by sequencing.

All other plasmids needed for the BiFC were already constructed by former lab members [91].

2.3.4 Constructing Y2H vectors

The backbone vectors for the Yeast two-hybrid (Y2H) analysis were pGADT7 AD (further called AD) and pGBKT7 BD (further called BD). The CDS of ATXR7 was amplified with different overhangs using primer pair 3975 + 3976 to clone it into AD and 3975 + 3977, respectively, to clone it into BD. Again, cDNA of Col-0 was used as template. Amplicons were purified and digested with XhoI/XmaI for cloning into AD and XmaI/NotI for cloning into BD. The same digestion enzymes were used to digest the corresponding vectors needed. The digests were purified and the products were ligated to receive pGADT7 AD::ATXR7 and pGBKT7 BD::ATXR7.

Fragments of the ATXR7 CDS comprising 999bp were amplified using the pGADT7 AD::ATXR7 described above as template. In total, ATXR7 was divided into eight overlapping

fragments, each amplified for AD and BD (for primer used see table 2.3.1) then purified. Amplicons for AD and the plasmid itself were then digested with XhoI and XmaI, purified and ligated. Amplicons for BD and the plasmid itself were digested with XmaI and NotI, purified and also ligated. All constructs were verified by sequencing.

All other plasmids used were constructed by former lab members.

Table 2.3.1: Primer used to amplify fragments of ATXR7 for Y2H.

forward primer	reverse primer (AD/BD)	fragment amplified
3975	4333/4348	1 – 999
4334	4335/4349	502 – 1500
4336	4337/4350	1000 – 1998
4338	4339/4351	1501 – 2499
4340	4341/4352	1999 – 2997
4342	4343/4353	2500 – 3498
4344	4345/4354	2998 – 3996
4346	4347/4355	3499 – 4167

2.4 Phenotyping and microscopy

For the determination of flowering time, plants were grown as described above. When the first flower opened, rosette and cauline leaves of the plant were counted and summed up to the total leaf number (TL).

Seed size was determined by measuring the 2D seed area. Therefore, seeds were dried for one month at room temperature (RT; 20 to 25°C) after harvesting then photographed under the dissecting scope (Olympus). Pictures were transformed into binary pictures using FIJI, ver. 1.51b. Each seed was marked with the wand tool to calculate its 2D area.

To determine the germination rate, seeds from the same batch were harvested and brought out randomized on MS plates (100+ seeds per GT spread on three plates). Plates were then stratified for 3d and incubated under LD conditions for 7d. Subsequent to incubation, germinated seeds were counted and the germination rate with standard deviation was calculated with Microsoft Excel (Version 14.0.4760.1000).

To measure the root length of 5d old seedlings, seeds were plated on MS as described above. After 24h, 36h, and 48h the germination rate was checked. 5 day after germination (dag), considering the time of germination, a picture of each seedling was taken

with the dissecting scope (Olympus) and the root length was measured from the tip to hypocotyl using FIJI.

For the determination of the silique length plants were grown until short before flower termination. Then, siliques of the main stem were used for the measurement. Thereby, the first 3 to 5 siliques and the siliques of the last 3cm of the stem were skipped. The length was measured by taking a photo of the siliques with the dissecting scope and measuring their length using FIJI.

For the scatterplots and the calculations needed for comparison, RStudio, ver. 0.99.896 was used. To calculate significances, the student's t-test was used.

The analysis of the ovules was done using a Confocal Laser Scanning Microscope (CLSM; Olympus FV1000), using an inverted IX81 stand and FluoView software (FV-10 ASW version 01.04.00.09) (Olympus Europa GmbH, Hamburg, Germany). Before the analysis, ovules were stained with propidium iodide (PI) according to [95]. For CLSM, ovules were dissected in H₂O under a dissecting scope then covered with an 18 x 18 mm glass cover slip (0,17mm thickness; #1, Menzel-Gläser, Braunschweig, Germany). For visualization, samples were excited at 561nm using a multi-line argon laser and PI staining was detected at 627nm. Images were obtained with a 20x or 40x water objective, respectively (PlanApo 40x/0.90, WLSM).

The 3x*Venus* marker lines were also analyzed with the CLSM mentioned above. The preparation of the samples was also done as described before. Samples were excited at 515nm and the signal was detected at 527nm. Images were obtained using the same 20x or 40x water objectives as before.

2.5 Generation of transgenic lines

Plants were transformed with different constructs using the floral dip method [96] and *Agrobacterium tumefaciens* strain GV3101 [93] pretransformed with pSOUP needed for amplification of the GreenGate constructs and selected with corresponding antibiotics listed in table 2.2.1. Transgenic T₁ lines were selected on MS containing Phosphinoictrin (10µg/ml) or on soil using Basta (100mg/L Glufosinat-ammonium; Bayer CropScience Deutschland GmbH) treatment for selection, seven and ten days after incubation. After seven to ten days on plate or 14 days on soil, surviving seedlings were transferred to single pots for further analysis.

2.6 Yeast two-hybrid (Y2H)

For Y2H, the two *Saccharomyces cerevisiae* strains Y8800 (*MAT α*) and Y8930 (*MATa*) were used. Transformation of Yeast was done according to [97] transforming pGADT7 AD constructs into Y8800 and pGBKT7 BD constructs into Y8930. Positive transformants of Y8930 were then selected on selective dropout plates lacking tryptophan (SD-W) and positive transformants of Y8800 were selected on selective dropout plates lacking leucine (SD-L) plates.

For mating, colonies were picked from the SD-L and SD-W plates, respectively, resuspended in 100 μ l water, diluted 1:10 and 3 μ l of these suspensions were mixed on an YPD plate. Plate was then incubated at 30°C for O/N. After that, colonies were picked, again resuspended in 100 μ l H₂O and diluted 1:10. Afterwards, 3 μ l of that suspension was then plated on selective dropout plates lacking tryptophan and leucine (SD-LW) to verify the mating success. Another 3 μ l of the suspension was plated on selective dropout plates lacking tryptophan, leucine, and histidine (SD-LWH) and containing 2,5mM 3-Amino-1,2,4-triazole (3-AT) to verify protein interaction.

To reduce false positive background, the SD-LW and the SD-LWH + 3-AT plates were again plated over to fresh SD-LW and SD-LWH + 3-AT plates as described above. If colonies still grew on the 2nd plates, interaction was taken for granted.

2.7 Bimolecular fluorescence complementation (BiFC)

To study protein interaction in protoplasts, bimolecular fluorescence complementation (BiFC) according to [98] was performed. Protoplast transfection with pUC-SPYCE and pUC-SPYNE carrying the genes of interest (see table 2.7.1 for inserts and table 2.2.3 for primers used for amplification) was done according to [99]. Interaction analysis was then performed with the CLSM mentioned above.

The YFP signal was excited at 515nm with a multi-line argon laser and the emission was detected at 527nm. Images were obtained with 20x or 40x water objectives.

Table 2.7.1: Genes of interest cloned into pUC-SPYCE and pUC-SPYNE for BiFC essays.

Gene (CDS) of interest	Purpose
<i>UCN</i>	Gene of interest tested with ATXR7
<i>ucn-1</i>	Gene of interest tested with ATXR7
<i>bZIP63</i>	Homodimer used as positive control
<i>ATXR7</i>	Gene of interest tested with UCN and <i>ucn-1</i>

As a positive control, bZIP63 homodimers were used as in [98]. Empty pUC-SPYCE and pUC-SPYNE vectors were used as negative controls.

2.8 Semiquantitative real-time PCR (sqRT-PCR) to verify *UCN* overexpression

Because of an artifact in the quantitative real-time polymerase chain reaction (qRT-PCR) when using two primers annealing in the CDS of *UCN*, the verification of the overexpression of *UCN in planta* was done using a sqRT-PCR. Therefore, RNA of 10d old seedlings was extracted and 3µg of it were reverse transcribed into cDNA as described before. For the amplification of the *UCN* fragment, 1µl cDNA was used as template and the GT primer 2033 and 2034 (see table 2.2.3) were used for amplification. The PCR reaction was performed using Taq Polymerase with ThermoPol Buffer (New England BioLabs Inc.) according to the manufacturer's protocol.

After sqRT-PCR, samples were separated on an Agarose gel (1,2%) via gel-electrophoresis. The intensity of the bands was then calculated using FIJI and Excel.

2.9 Quantitative real-time PCRs (qRT-PCRs)

For quantitative real-time polymerase chain reactions (qRT-PCRs), plants were grown on MS plates as described above. 10 days after incubation (dai), three times ten seedlings per genotype were bulked representing a biological triplicate. RNA was extracted using the NucleoSpin RNA plant kit (Macherey-Nagel GmbH und Co. KG) according to the manufacturer's protocol. 3µg of total RNA was reverse transcribed into cDNA using the RevertAid 1st strand cDNA synthesis kit (Fermentas) according to the manufacturer's protocol. The reverse transcription was performed using poly-T primer to selectively reverse transcribe the mRNA.

Before used as a template in qRT-PCR, the cDNA was diluted with H₂O to a factor of 1:100. For the qRT-PCRs, the GoTaq qPCR mastermix (Promega) was used according to the manufacturer's protocol.

The CFX96 and CFX384 Touch Real-Time PCR Detection System (Bio-Rad) were used as qRT-PCR devices. Bio-Rad CFX Manager 3.1 Software was used to setup and analyze the

qRT-PCRs. The final calculations of the relative expressions were done with Microsoft Excel according to [100].

Primers used in qRT-PCRs are listed in table 2.9.1. At4g33380, At2g28390, and At5g46630 were used as reference genes.

Table 2.9.1: Primers used in qRT-PCRs.

Primer number or name	Sequence (5' -> 3')	Target gene [evtl. Ref.]
2727	TGAAGGAGAGGAAGAGCCTGAGGAA	At4g33380
2728	CCCCATCTCACTGCAGCACCAC	
2729	AGATTGCAGGGTACGCCTTGAGG	At2g28390
2730	ACACGCATTCCACCTTCCGCG	
2731	CCAAATGGAATTTTCAGGTGCCAATG	At5g46630
2732	CAATGCGTACCTTGAGAAAACGAAC	
UCN(qPCR_UTR)_F	ATTCGTCGCCGGTGAAG	UCN
UCN(qPCR_UTR2)_R	CGTTTCAGACCCACTCGTCTC	
3760	CAGCAAGCATGTTTCGTTTC	ATXR7
3761	ATGCCTCCACAGACAAGTTC	
FT(qPCR)_F	GAGAAGACCTCAGGAAGTTC	FT [101]
FT(qPCR)_R	TGGATTTTCGTAACACACAATCTC	
3969	AGTTGAACAAGAGCATCGATAC	FLC
3970	AAAGCTCTGAACTATGGTTCAC	

3 Results

3.1 Investigating the spatial expression pattern of *UCN*

In a former work it was shown that *UCN* is expressed in all plant tissues [91]. This coincides with the data from AtGenExpress (see figure S5). To verify these results, an *in-situ* hybridization approach was formerly tried but showed no result. Hence, I tested another visualization approach in this work to maybe get a better impression of the spatial expression pattern of *UCN*. For this purpose, a 3x*Venus* reporter gene coupled to a nuclear localization signal (NLS) and expressed under the control of the complete promoter region including the 3'UTR of *UCN* was transformed into Col-0. After pre-selecting the T₂ generation for the YFP-signal, I analyzed three independent T₃ lines homozygous for the T-DNA under the confocal microscope. Since in former works evidence for a role of *UCN* in ovule development was presented [89, 91], I started my analysis with this plant organ and the flower which is also impaired in *ucn-1*.

UCN expression is found throughout the ovule and also in all developmental stages (see figure 3.1.1A to D). In very young ovules (figure 3.1.1A and figure 3.1.1B), *UCN* expression is found in all cells, especially in the nucleus and the megaspore mother cell, respectively (indicated with arrows in figure 3.1.1A and B). Expression is also found in the carpel walls (see figure 3.1.1A). The expression continues throughout all developmental stages of the ovule. In later stages (see figure 3.1.1C and D) it is still found in all tissues. Before fertilization, two big nuclei show a stronger expression than the surrounding cells (see figure 3.1.1C, indicated with arrow). After fertilization, the signal is not present any more (see figure 3.1.1D).

The analysis of the *UCN* expression in other flower parts also revealed a ubiquitously observed signal. It is found in all organs of the flower (sepals, petals, stamens, carpels) (see figure 3.1.2A to D) and it remains constant throughout all the different developmental stages. While the sepals and petals show a steady expression in all their cells (see figure 3.1.2A and B), it is restricted to the filaments in the stamens. The anthers themselves do not show any expression (see figure 3.1.2C and D).

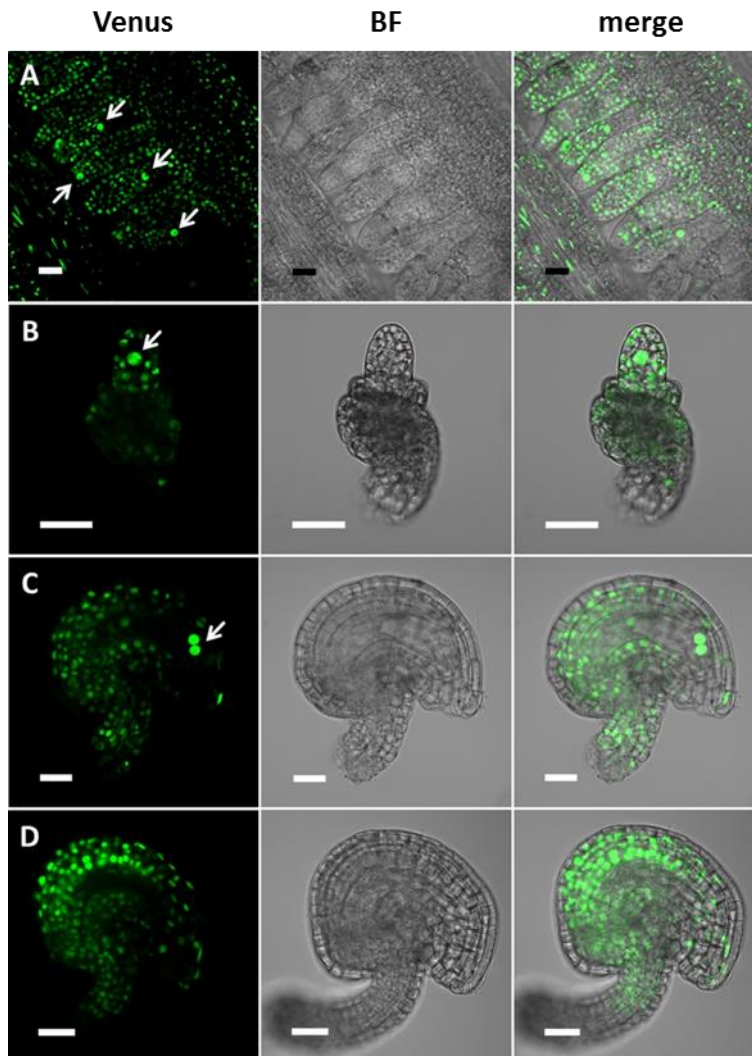


Figure 3.1.1: Investigation of the spatial *UCN* expression pattern in ovules using a *pUCN::3xVenus-NLS* reporter gene in *Col-0*.

UCN is expressed throughout all ovule stages. (A) In very young ovules (around stage 2-I) the expression is visible in all cells including a bright expression in the megaspore mother cell (MMC; indicated with arrows). The picture also shows expression in the cells of the carpel walls surrounding the ovules. (B) The bright expression in the MMC (indicated with arrow) is still visible when integuments are visible (around stage 2-V). The *UCN* expression is now also visible in developing integuments and the funiculus. (C) In the developed ovule before fertilization the *UCN* expression is still visible in all cells. The two cells showing a brighter expression (indicated with arrow) could not clearly be identified. (D) The signal is also visible in fertilized ovules. The expression is now equally distributed. Channels are mentioned above (BF = bright field). Scale bars = 20 μ m.

The expression pattern of *UCN* I found in the reproductive plant parts coincide with the phenotype described earlier [89] and further suggests that the reporter construct can be used to analyze the expression also in other plant organs. In addition to the reproductive plant parts which are affected in the *ucn-1* mutant, *UCN* expression is also found in other tissues. In five to ten days old seedlings *UCN* expression is found in the root (see figure 3.1.3A to H). Here, it is restricted to the elongation zone and the meristematic zone (see figure 3.1.3A), excluding an area in the root tip which is supposed to consist of the quiescent cells (see figure 3.1.3B). In the maturation zone, the expression is restricted to the vascular

tissue (see figure 3.1.3C and D). Because of the shape of the nuclei it can be hypothesized that these cells are companion cells. However, the expression in these cells is much weaker than the expression in the transition zone (compare figure 3.1.3A and B with C and D).

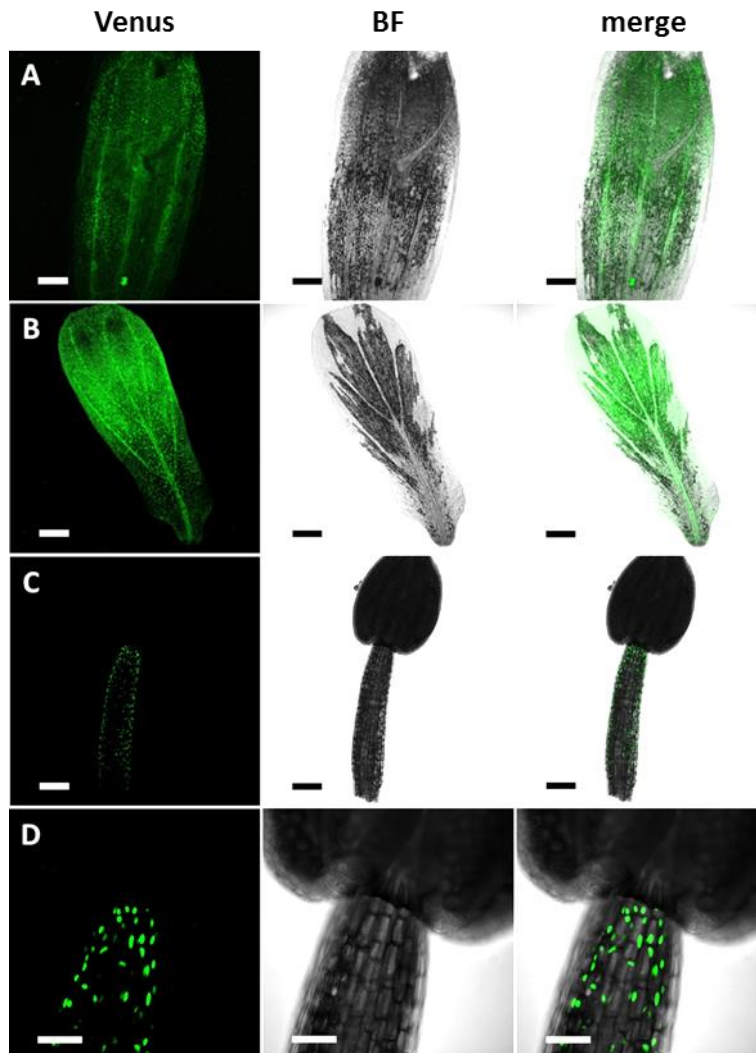


Figure 3.1.2: Investigation of the *UCN* expression pattern in flower organs using a pUCN::3xVenus-NLS reporter gene in Col-0.

UCN is expressed in all flower organs. (A) In sepals as well as in (B) petals *UCN* expression is found all over the tissue. Black spots are areas out of focus rather than areas with no *UCN* expression. In the vascular tissue the *UCN* expression seems to be enhanced. (C) and (D) In stamens *UCN* expression was only found in the filaments, not in the anther. Channels are mentioned above (BF = bright field). Scale bars = A to C: 150µm; D: 50µm.

When lateral roots emerge, the *UCN* expression in the maturation zone is re-activated in the endoderm. It is found in the very first developmental stages of the emerging lateral root (see figure 3.1.3E) and remains constant while the new root is growing (see figure 3.1.3F). In longer lateral roots it decreases again in the maturation zone, in contrast to the elongation zone and the meristematic zone where it remains constant (see figure 3.1.3G and H). Again, the expression in the meristematic zone of lateral roots leaves out the area where the quiescent cells are supposed to be (see figure 3.1.3H). Summarized, *UCN*

expression in roots takes place where cell division is found. Later it is restricted to the vascular tissue of the elongation zones, most likely the companion cells.

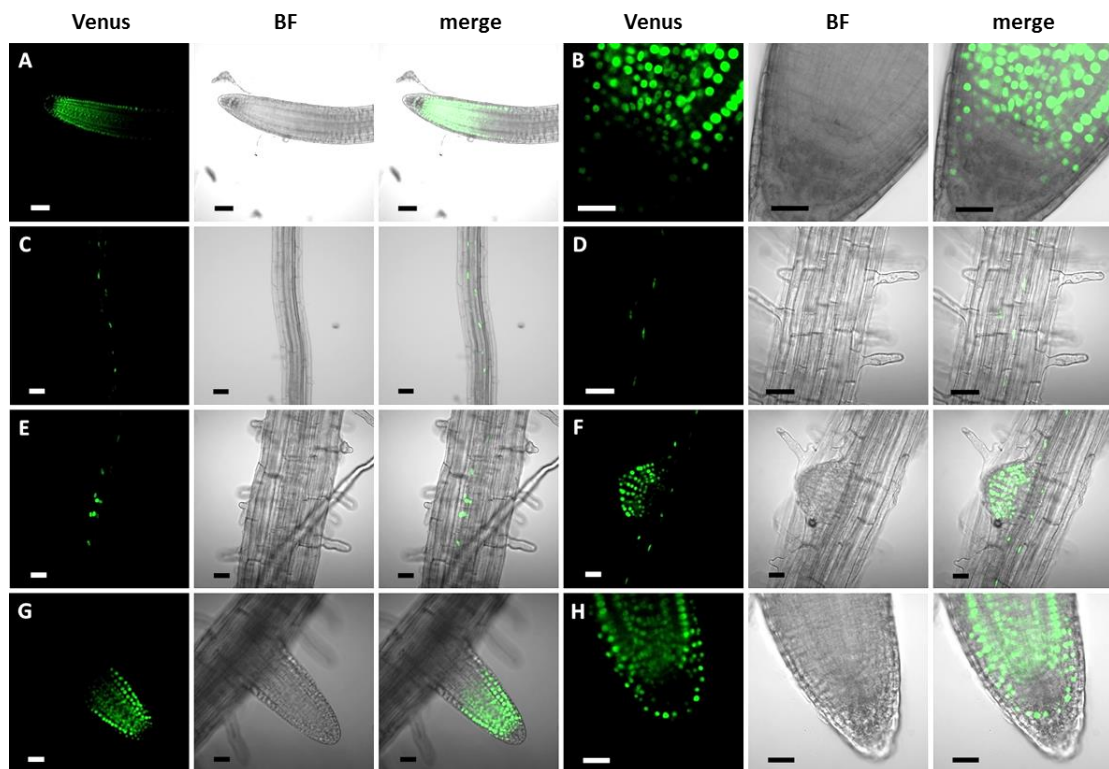


Figure 3.1.3: *UCN* expression in the root of 5 to 10d old seedlings visualized with pUCN::3xVenus-NLS in Col-0. (A) and (B) *UCN* expression is found in the root tip of seedlings, localized in the transition zone and excluding what is supposed to be the quiescent cells. (C) and (D) In the elongation zone of the root *UCN* is exclusively expressed in the vascular tissue. (E) and (F) When lateral roots are emerging *UCN* is reactivated and the expression remains stable in the transition zone as the lateral root develops. (G) *UCN* expression is again restricted to the transition zone when the lateral root grows bigger. (H) In the very tip of the lateral root (and also the main root) the expression again leaves out the quiescent cells. Channels are mentioned above (BF = bright field). Scale bars: A, C, D = 50 μ m; B, E to H = 20 μ m.

UCN is also expressed in the above ground tissue of the seedlings (see figure 3.1.4A to J). Even expression is found all over the cotyledons, the hypocotyl and also in emerging leaves (see figures 3.1.4A and B). It seems to be less in the endoderm of the hypocotyl (see figure 3.1.4A) where the signal almost disappears. On the other hand, in a growing leaf the signal is much stronger indicating a much stronger expression of *UCN*. These results are conforming to the previous observation in the root, that *UCN* expression is higher in tissues with active cell division.

The signal strength decreases in older tissues like the cotyledons of ten day old seedlings (see figure 3.1.4C), but it remains active in certain cell types. Although, the signal is very weak in the hypocotyl (see figure 3.1.4A) it remains constant in the epidermis (see figure 3.1.4D). Closer to the root, the signal is lost (see figure 3.1.4E) supporting the

observation of a local expression in the vascular tissue of the elongation zone of the root. In the shoot apical meristem (SAM) no signal is visible (see figure 3.1.4F). It is repressed around the SAM where it is restricted to the epidermal cell layer leaving out the area where the SAM is supposed to be.

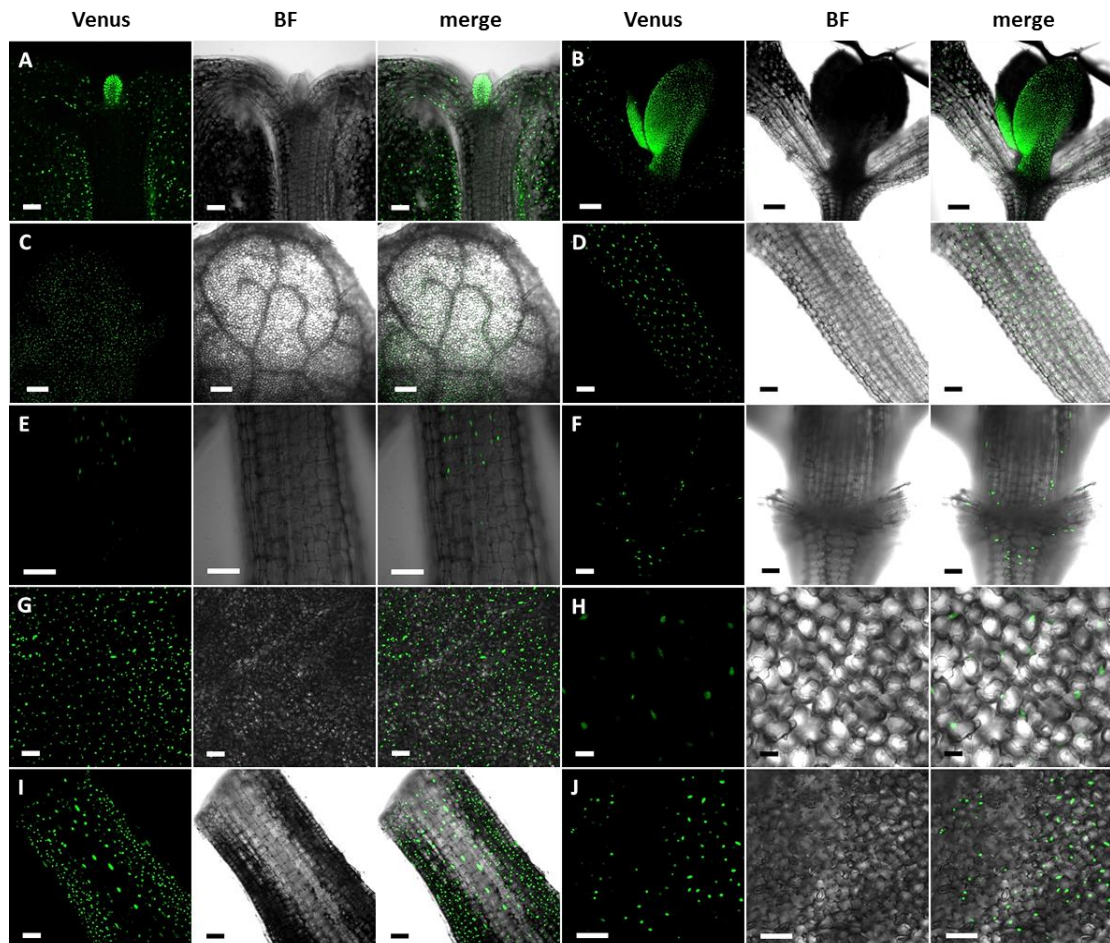


Figure 3.1.4: Analysis of the *UCN* expression in seedlings and above ground tissues of the plant visualized with pUCN::3xVenus-NLS in Col-0.

(A) *UCN* expression can be found all over the seedling, especially where cell division takes place (4d old seedling). (B) When the seedling is older, the expression localizes more and more to tissues with cell division (7d old seedling) as in the 1st leaf pair compared to the cotyledons. (C) The expression also decreases in the tip of the cotyledons (10d old seedling). (D) In the hypocotyl *UCN* expression is found in the epidermal layers (6d old seedling). (E) It is repressed where the hypocotyl joins the root (6d old seedling). (F) In the SAM, no signal was observed (10d old seedling). (G) and (H) *UCN* is also active in young leaves in the parenchyma (G: young leaf of 19d old plant; H: young leaf of 11d old plant), although the expression there is much weaker. (I) In middle aged leaves (petiole of 10d old plant) expression is active in the region with cell division while it seems to decrease from the vascular tissue on. (J) The *UCN* expression then decreases more and more near the tip of the leaf (leaf tip of 1st leaf of 11d old plant). Channels are mentioned above (BF = bright field). Scale bars = A, D, E, F, G, H, I: 50µm; B, C: 150µm; J: 100µm.

The selective expression of *UCN* in regions with active cell division is continuously found in all developmental stages of the plant. In young leaves which are still developing, the signal is very strong (see figure 3.1.4G) while it decreases with the age of the leaves (see figure 3.1.4H and J) although it never disappears completely. Also, a constant signal remains

in the vascular tissue of the leaves, even if the surrounding signals are getting weaker (see figure 3.1.4I).

In conclusion, the investigation of the reporter construct pUCN::3xVenus-NLS in Col-0 reveals that UCN is expressed in all plant organs and throughout the vegetative as well as the reproductive phase. Strong *UCN* expression is found in developing tissue with active cell division. In the root a region is left out what is supposed to be the quiescent cells. The same holds true for the shoot apical meristem. With the elongation and differentiation of the cells the expression of *UCN* decreases although it never disappears completely. In ovules *UCN* is also expressed in all cells. A stronger signal is received from the nucellus and the MMC, respectively and later in two nuclei close to the micropyle.

3.2 Phenotypical comparison between two mutant alleles of *UCN* – *ucn-1* and *ucn-2*

The *ucn-1* mutation is a missense mutation in *Ler* background and results in an amino acid exchange in the protein (G165S) [91]. Hence, the *ucn-1* allele most likely is not a null allele. Another *UCN* mutant, *ucn-2*, a loss-of-function line in Col-0 background carrying a T-DNA in the coding sequence of *UCN* (see figure 3.2.1) resulting in a STOP codon 604bp downstream of ATG, was formerly described as a *UCN* null-allele [91], although a transcription upstream of the gene and therefore a translation of a truncated protein would still be possible (see figure 3.2.1). A phenotypical comparison of both mutants in an earlier work revealed that their phenotypes, especially regarding floral organs, are clearly different [91]. Using a pUCN::3xVenus-NLS reporter line I was able to demonstrate that *UCN* is expressed not exclusively in the floral organs and the ovules but also in many other plant organs. Therefore, I re-examined both phenotypes to check if other organs are also affected in *ucn-1* or *ucn-2*. I further checked the *UCN* expression in *ucn-1* and *ucn-2* to confirm the null-allele of *ucn-2*.

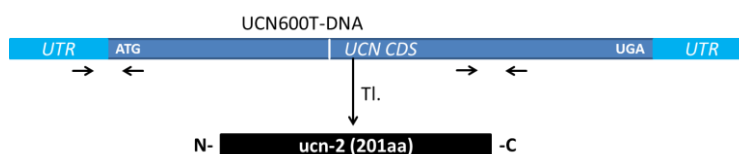


Figure 3.2.1: Schematic view of *ucn-2* mRNA and putative protein.

The T-DNA is inserted 600bp downstream of ATG (indicated with a white line) resulting in a truncated protein of 201aa. Primers used for verification of expression are indicated with arrows below DNA scheme. UTR = untranslated region, ATG = start codon, UGA = stop codon, *UCN CDS* = *UNICORN* coding sequence, TI. = Transcription.

The determination of the *UCN* expression level in ten day old seedlings of *ucn-1* reveals that it is decreased to 63% of the wild-type expression (see figure 3.2.2A). This result indicates that there is less *UCN* mRNA in *ucn-1*. To analyze the expression of *ucn-2*, qRT- and sqRT-PCRs were performed, amplifying fragments of *UCN* upstream the T-DNA insertion site and another fragment downstream the T-DNA insertion site (see figure 3.2.1, arrows). Compared to Col-0, the *ucn-2* expression upstream of the T-DNA is 27% ($p = 0,0028$) (see figure 3.2.2B). No *ucn-2* expression is found using primer annealing downstream of the T-DNA insertion site (see figure 3.2.2C). The remaining visible expression is background from the gel used to analyze the sqRT-PCR. This suggests that *ucn-2* is not a real null-allele.

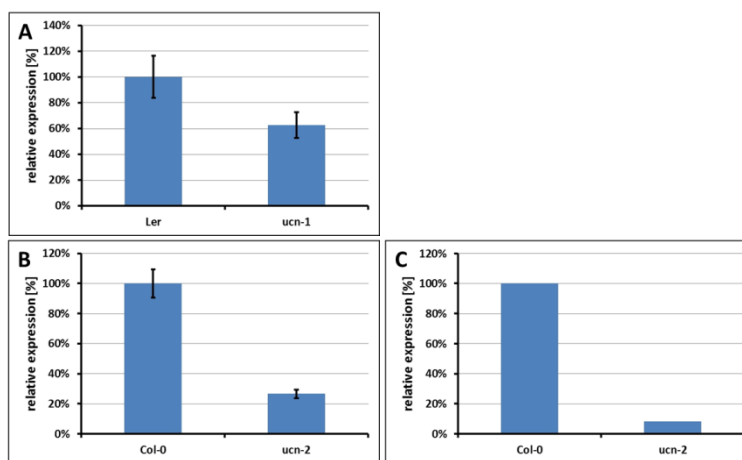


Figure 3.2.2: Expression level of *UCN* in *ucn-1* compared to *Ler* and *ucn-2* compared to *Col-0*.

(A) Ten day old seedlings of *ucn-1* still show 62,8% of the wild-type expression. (B) Upstream of the T-DNA insertion site, *ucn-2* expression constitutes 27% compared to the expression of *UCN* in *Col-0*. (C) Downstream of the T-DNA no expression of *UCN* is found in *ucn-2*, except the background of the gel. All data is from 10d old seedlings grown in LD. For primer locations, see figure 3.2.1. Bars represent mean value of biological triplicate with 1x standard deviation.

When the phenotypes of *ucn-1* and *ucn-2* were formerly described, the focus lied strongly on the flower and the ovules [89, 91]. Here, *ucn-1* displays a strong flower phenotype (see figure 3.2.3C and D). Further, it also shows protrusions on the proximal side of the integuments (see figure 3.2.3E and F). These features are not observed on *ucn-2* flower and ovules, respectively (see figure 3.2.4D to G). The observation therefore verifies former results [89, 91]. Since *UCN* expression is found in all plant organs, I re-examined the two mutant lines *ucn-1* and *ucn-2* to check if other plant organs are also affected.

The investigation of the seed size revealed that it is affected in both mutants. The survey of the 2D seed surface of *ucn-1* reveals that the seeds have an average 2D seed area of $71531\mu\text{m}^2$ ($n = 66$), whereas *Ler* seeds have an average 2D surface of $86761\mu\text{m}^2$ ($n = 103$) ($p = 8,7 * 10^{-12}$) (see figure 3.2.5A). This result suggests that seeds of *ucn-1* have smaller

seeds than the wild-type. The investigation of *ucn-2* seeds revealed that *ucn-2* seeds are bigger than Col-0 seeds. Seeds of *ucn-2* have in average an area of $96239\mu\text{m}^2$ ($n = 71$) while Col-0 seeds show an average 2D seed area of $78127\mu\text{m}^2$ ($n = 93$). Therefore, the 2D seed surface of *ucn-2* is 123% of the 2D seed surface of Col-0 ($p = 5,4 * 10^{-17}$) (see figure 3.2.5F). This result is in contrast to the result received for *ucn-1*, where the seeds are smaller than the seeds of the corresponding wild-type. However, in both cases the loss-of-function of *UCN* has an influence on the seed size.

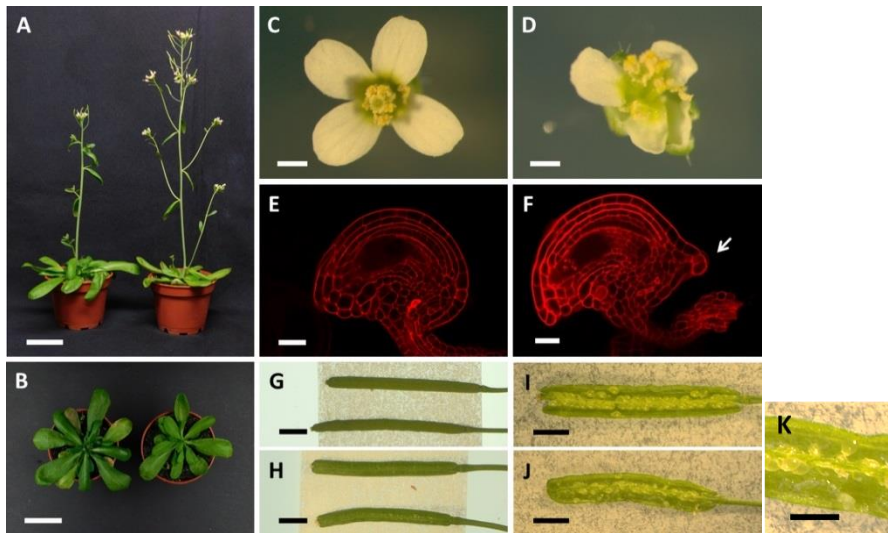


Figure 3.2.3: Phenotypical characteristics of *ucn-1*.

(A) *Ler* (left) and *ucn-1* (right), grown 23d under LD conditions. Due to early flowering, *ucn-1* is further developed than *Ler* and therefore shows fewer rosette leaves. (B) Rosettes of *Ler* (left) compared to *ucn-1* (right), 23dag, stems removed. The rosette leaves of *ucn-1* are inconspicuous regarding their shape and size. (C) and (D) Flowers of *Ler* (C) and *ucn-1* (D). Most *ucn-1* flowers show a deformed shape. (E) and (F) Ovules of *Ler* (E) and *ucn-1* (F). Ovules of *ucn-1* show protrusions at the proximal side of the integuments (indicated with arrow). (G) to (J) Fully developed siliques of *Ler* (G and I) and *ucn-1* (H and J). Siliques of *ucn-1* are shorter than wild-type siliques. Furthermore they bear degenerated ovules indicating embryo lethality. (K) Detail from (J) showing unfertilized, degenerated ovules. Scale bars: A and B: 3cm; C and D: 500 μm ; E and F: 20 μm ; G to J: 2mm.

Besides the smaller seed size, the germination rate of *ucn-1* is also affected. In total, 283 out of the 288 *Ler* seeds germinated (98,3%) while out of the 288 *ucn-1* seeds only 204 seeds germinated (70,8%) (see figure 3.2.5B). Therefore, the germination rate of *ucn-1* is 28% lower than the germination rate of the wild-type ($p = 0,0235$). This decrease is not observed for *ucn-2* seeds (see figure 3.2.5G). In summary, these results suggest that the germination of *ucn-2* seeds is not impaired like the germination of *ucn-1* seeds.

Due to the *UCN* expression found in the root transition zone where cell division takes place, the root length of the main root of five day old seedlings of *ucn-1* and *ucn-2* was also analyzed. Roots of *Ler* seedlings have an average length of 11,2mm ($n = 49$) five days after germination, whereas roots of *ucn-1* seedlings have an average length of 6,3mm

($n = 50$) ($p = 1,89 * 10^{-16}$) (see figure 3.2.5C). This result indicates that the root length of the main root is also affected in *ucn-1*. An analysis of the root length of the main root of five day old *ucn-2* seedlings revealed that *ucn-2* ($n = 37$) shows in average a root length of 13,8mm, while Col-0 seedlings grow in average a root length of 15,8mm ($n = 33$) (see figure 3.2.5H). According to the student's t-test, the difference of 2mm is significant ($p = 0,0400$). Therefore, both mutants display a shorter main root, although the difference between *ucn-1* and *Ler* is much bigger than the difference of *ucn-2* and Col-0.

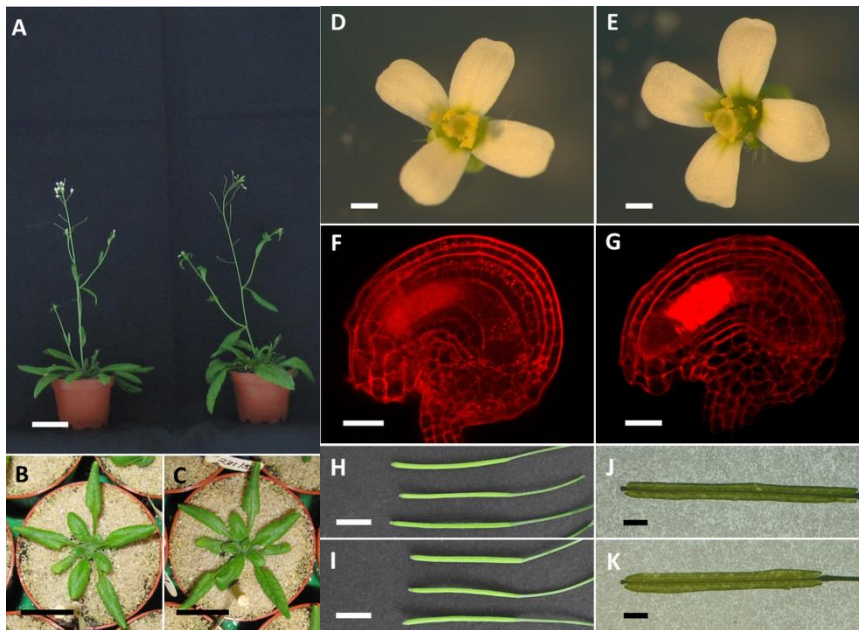


Figure 3.2.4: Phenotypical analysis of *ucn-2*.

(A) When grown in LD, *ucn-2* (right) flowers the same time as Col-0 (left). (B) and (C) Rosettes of Col-0 and *ucn-2*, 21dag, LD. No differences are found comparing the rosettes of Col-0 (B) to *ucn-2* (C). (D) to (G) Flowers and the ovules of *ucn-2* (E and G) show no striking features compared to Col-0 flowers (D and F). (H) and (I) Siliques of *ucn-2* (I) do not differ in shape and only slightly in size compared to siliques of Col-0 (H). (J) and (K) Embryo lethality as in *ucn-1* was not found in *ucn-2* siliques either (K) when compared to Col-0 (J). Scale bars: A: 3cm; B and C: 2cm; D and E: 500 μ m; F and G: 20 μ m; H and I 5mm; J and K: 2mm.

An analysis of the flowering time under long day (LD) conditions revealed that *ucn-1* starts flowering earlier than the corresponding wild-type *Ler* (see figure 3.2.3A and 3.2.5D). When the first flower opens, *Ler* has grown in average 17 total leaves while *ucn-1* grows in average only 13,6 total leaves until the opening of the first flower ($p = 1,7 * 10^{-10}$). The analysis of the flowering time of *ucn-2* under LD conditions revealed that there is no difference compared to the flowering time of Col-0 (see figure 3.2.4A and 3.2.5I). In average, *ucn-2* starts flowering with in average 17,8 total leaves ($n = 23$) while Col-0 starts flowering with in average 17,7 total leaves ($n = 23$) ($p = 0,7481$). Therefore, in contrast to *ucn-1*, *ucn-2* has no deregulated flowering time under the tested conditions.

The flowering plant of *ucn-1* shows no special features in its overall shape (see figure 3.2.3A), lateral organs et cetera show the same number as the wild-type plant. Also, the rosette and the leaves do not differ from the rosette and leaves of *Ler* (see figure 3.2.3B). The same holds true for *ucn-2*. The overall plant stature is inconspicuous compared to *Col-0* (see figure 3.2.4A). Rosette and leaves are indistinguishable from wild-type rosettes and leaves (see figure 3.2.4B and C).

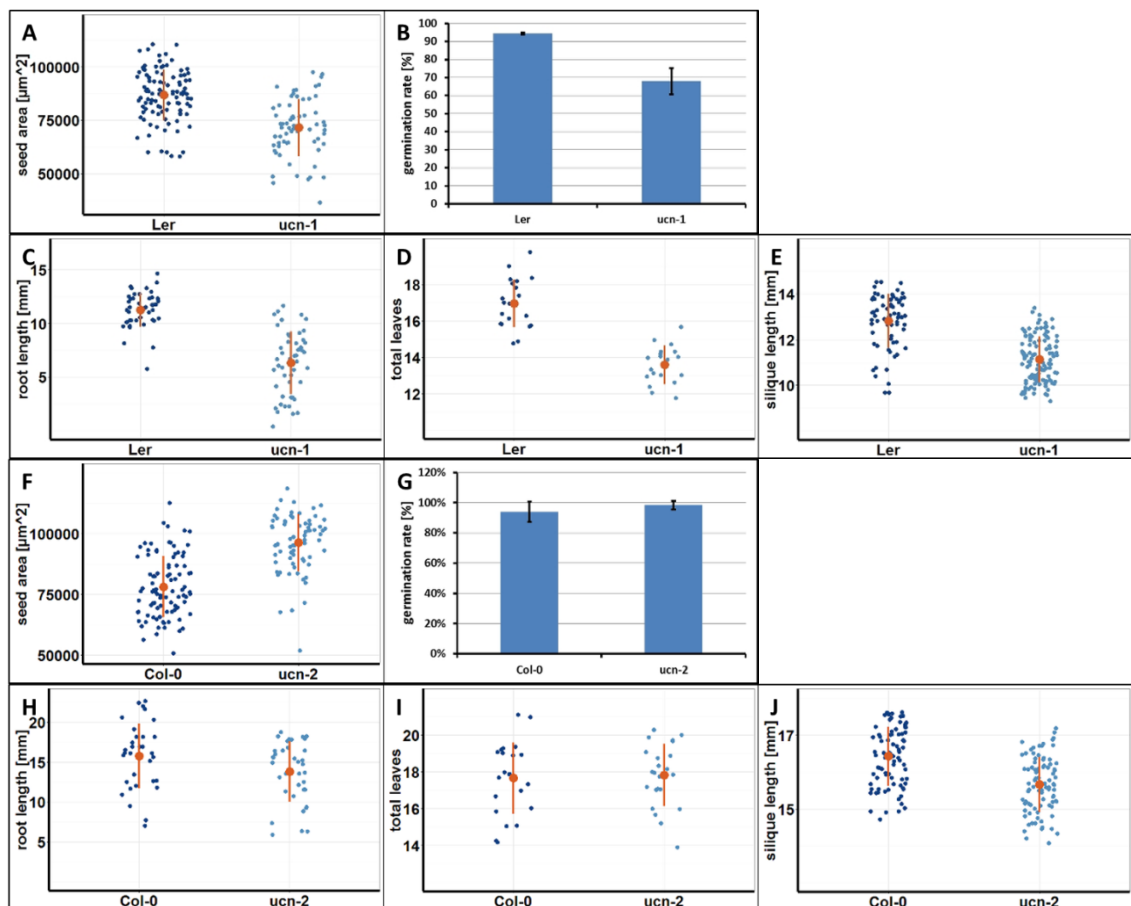


Figure 3.2.5: Analysis of the characteristics of *ucn-1* and *ucn-2*.

Plants were grown under LD conditions and compared to each other regarding specific characteristics. (A) to (E) *ucn-1*; (F) to (J) *ucn-2*. 2D seed surface of *ucn-1* (A) and *ucn-2* (F); germination rate of *ucn-1* (B) and *ucn-2* (G); root length of five day old seedlings grown on MS of *ucn-1* (C) and *ucn-2* (G); flowering time of *ucn-1* (D) and *ucn-2* (I); silique length of fully developed siliques of *ucn-1* (E) and *ucn-2* (J); Blue dots represent samples, brown dots with lines represent the mean with 1x standard deviation.

Due to the *UCN* expression in the carpel walls and the degenerated ovules observed in the siliques of *ucn-1*, the length of fully developed siliques of *ucn-1* and *ucn-2* was also investigated. This analysis revealed that the siliques of *ucn-1* are smaller than the ones of the wild-type (see figure 3.2.5E). In average, full-grown siliques of *Ler* have a length of 12,8mm ($n = 68$) while the average length of full-grown *ucn-1* siliques is 11,1mm ($n = 119$) ($p = 3,7 * 10^{-17}$). However, the overall shape of the siliques was inconspicuous (see figure 3.2.3G and H). The analysis of the silique length of *ucn-2* revealed that the siliques of *ucn-2*

are slightly smaller than Col-0 siliques (see figure 3.2.5J). Full-grown *ucn-2* siliques have an average length of 15,7mm (n = 86) while siliques of Col-0 grow in average a length of 16,4mm (n = 85). The difference is very small but according to the student's t-test it is highly significant ($p = 1,02977 * 10^{-9}$). This is again a phenotypical feature that both mutants display and again it is much weaker in Col-0 background than it is in *Ler*. The overall shape of *ucn-2* siliques is indistinguishable from the wild-type's silique shape (see figure 3.2.4H and I).

The *ucn-1* mutation also causes sterility. Siliques of *ucn-1* often contain ovules that are degenerated (see figure 3.2.3I, J, and K). The whitish color indicates that the ovules degenerate before fertilization. This sterility varies from silique to silique and from plant to plant. In contrast to *ucn-1*, no sterility is found in siliques of *ucn-2* (see figure 3.2.4J and K).

Table 3.2.1: Result of the comparison of *ucn-1* and *ucn-2* with their corresponding wild-types *Ler* and Col-0, respectively.

Analysis was done regarding seed size (2D seed area), germination rate, root length of the main root, flowering time (FT) in LD, overall plant stature, rosette leaves, and length of fully developed siliques including their ovules. Values are relative to the corresponding wild-types.

Characteristic	<i>ucn-1</i>	<i>ucn-2</i>
Expression level	62,8%	27%
Seed size	82%	123%
Germination rate	72%	wild-type
Root length	56%	87%
FT (LD)	75%	wild-type
Overall plant stature	wild-type	wild-type
Rosette leaves	wild-type	wild-type
Flower shape	affected	wild-type
Silique length	85%	96%
Degenerated Ovules	yes	no
Ovule shape	protrusions	wild-type

In conclusion, the comparative analysis of *ucn-1* and *ucn-2* shows that, in addition to the flowers and ovules, multiple plant organs that are impaired. I was able to demonstrate that neither *ucn-1* nor *ucn-2* carries a real null-allele. I was further able to verify former results that ovules and flowers are affected in *ucn-1* but not in *ucn-2*. Moreover, I demonstrated that in *ucn-1* additional plant parts are affected, namely seeds, germination rate, main root, and silique length. In addition, the *ucn-1* mutant displays rapid flowering. I also found affected plant organs in *ucn-2*. The main roots and the siliques are a little shorter than the wild-type organs. In addition, the seed size of *ucn-2* seeds is enhanced compared to Col-0 seeds (see table 3.2.1). The affected plant organs coincide with the spatial expression pattern found before.

3.3 Analysis of heterozygous *ucn-1* and *ucn-2* mutants

In an earlier work it was demonstrated that UCN can phosphorylate ABERRANT TESTA-SHAPE (ATS) *in-vitro*. This phosphorylation is absent if *ucn-1* protein is used instead of UCN [91]. Furthermore, *sk21-D*, an over-activation line of *ATS*, also shows protrusions on the integuments. These outgrowths are enhanced in *ucn-1 sk21-D* double mutants. In addition, a homo-heterozygous mutant *ucn-1/- sk21-D/+* is thought to titrate out UCN and therefore also shows small protrusions [92]. It was thus concluded that UCN deactivates *ATS* by phosphorylation to suppress aberrant cell division on integuments. This also suggests that the planar growth of the integuments is a matter of the homeostatic concentration of UCN and *ATS* [91, 92]. I demonstrated above that *UCN* might also play a role in additional processes of the plant due to the multiple affected organs in *ucn-1* and *ucn-2*, respectively. A dosage effect as shown for *ATS-UCN* raises the question if UCN can also be titrated out in the other processes it is involved in. Therefore, I generated heterozygous *ucn-1* and *ucn-2* mutants. If one *UCN* allele is not titrated out in the processes it is putatively involved in, the heterozygous mutants should behave like the wild-type.

The analysis of the seed size revealed that the F_1 seeds of *Ler* x *ucn-1* have a bigger 2D-seed area than *Ler* seeds. In average, I measured a 2D-seed area of $108868\mu\text{m}^2$ ($n = 105$) for seeds of *Ler* x *ucn-1*, while I measured an average 2D-seed area of $89396\mu\text{m}^2$ ($n = 77$) for seeds of *Ler* ($p = 1,61543 * 10^{-18}$) (see figure 3.3.2A). Since the integuments of these seeds are built from maternal wild-type tissue, this result indicates that the paternal allele of *ucn-1* might also influence the seed size. If I used *ucn-1* as maternal (*ucn-1* x *Ler*) crossing partner, I measured an average seed surface of $75010\mu\text{m}^2$ ($n = 82$). This size is close to the seed size of homozygous *ucn-1* plants, for which I measured an average 2D-seed area of $72651\mu\text{m}^2$ ($n = 64$) ($p = 0,3678$) (see figure 3.3.2A). Therefore, the seeds of *ucn-1* x *Ler* are also smaller than *Ler* seeds. Thus, in *ucn-1* the maternal effect on seed size coming from the integuments seem to override the paternal effect coming from the endosperm. I observed a similar effect for the *ucn-2* crossing with *Col-0*. In average, I measured a 2D seed area of $97133\mu\text{m}^2$ for seeds of *ucn-2* x *Col-0* ($n = 317$). For the seeds of *Col-0*, I measured an average 2D seed area of $74290\mu\text{m}^2$ ($n = 82$). Therefore, the seeds are bigger than *Col-0* seeds ($p = 1,5 * 10^{-27}$) (see figure 3.3.2E). If I used *Col-0* as a maternal crossing partner (*Col-0* x *ucn-2*; $n = 350$), the average 2D seed area I measured is $91323\mu\text{m}^2$ and therefore also bigger than *Col-0* seeds ($p = 1,5 * 10^{-19}$). For the average 2D seed area of homozygous *ucn-2* ($n = 68$) plants, I measured $101009\mu\text{m}^2$ ($p = 9,5 * 10^{-29}$) (see figure 3.3.2E). This demonstrates that also in

ucn-2 the paternal loss-of-function allele affects the seed size. It further suggests a role for *UCN* for seed size determination from the paternal side.

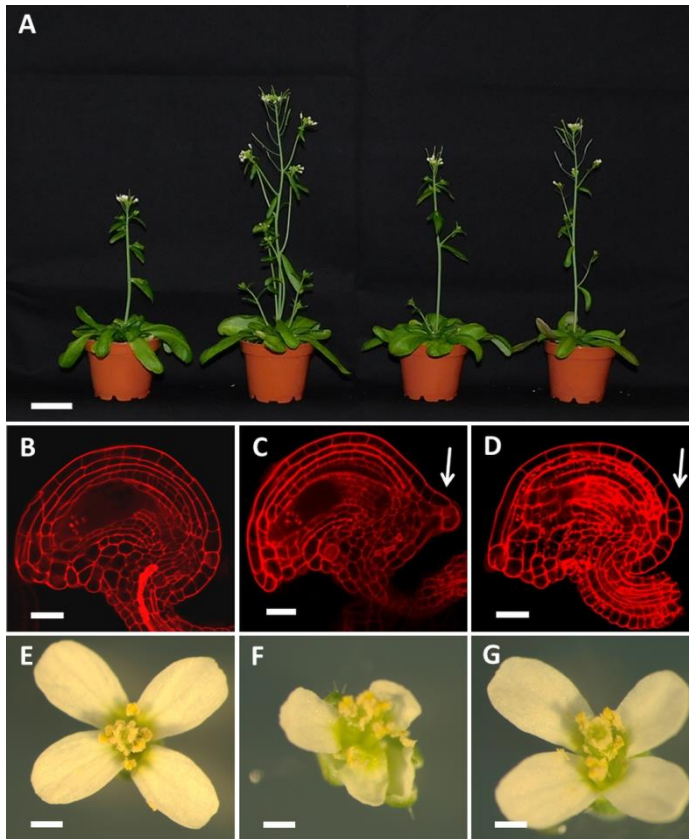


Figure 3.3.1: Phenotypal analysis of heterozygous *ucn-1* plants.

(A) Heterozygous *ucn-1* plants still flower early. Figure shows (from left to right) *Ler*, *ucn-1*, *Ler* x *ucn-1* (F_1), and *ucn-1* x *Ler* (F_1) plants, 37dag. (B) to (D) Ovules of heterozygous *ucn-1* plants (D) still have small protrusions (indicated with arrow), although these are much weaker than protrusions of *ucn-1* (C). *Ler* shows no protrusions (B). (E) to (G) Flowers of heterozygous *ucn-1* plants (G) regained their shape and therefore look like wild-type flowers (E) again. Compare to flower of *ucn-1* (F). Scale bars: A: 3cm; B to D: 20 μ m; E to G: 500 μ m.

When I analyzed the germination rate, 194 out of 288 seeds from *ucn-1* x *Ler* germinated while 284 out of 288 seeds of *Ler* x *ucn-1* germinated. Therefore, the germination rate of *Ler* x *ucn-1* (98,6%) is just as good as the wild-type germination rate (98,3%) ($p = 0,4144$) while the germination rate of *ucn-1* x *Ler* (67,4%) is very close to the germination rate of *ucn-1* (70,8%) ($p = 0,3844$) (see figure 3.3.2B). This indicates that the lower germination rate is inherited when *ucn-1* is used as a maternal crossing partner. For the *ucn-2* crossings I measured a wild-type germination rate independent of the crossing direction (see figure 3.3.2F). This result indicates that the loss-of-function of *UCN* in Col-0 does not influence germination rate.

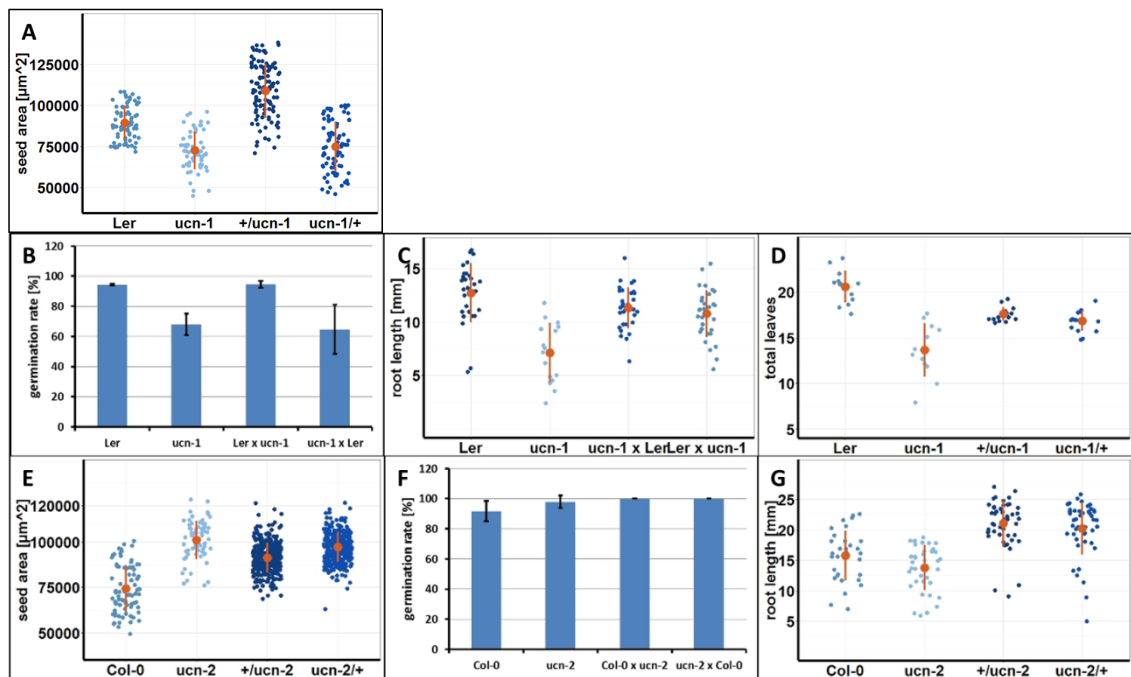


Figure 3.3.2: Analysis of the characteristics of heterozygous *ucn-1* and *ucn-2* mutants.

(A) Seed size of heterozygous *ucn-1* mutants (F_1). (B) Germination rate of heterozygous *ucn-1* mutants (F_1). (C) Root length of heterozygous *ucn-1* mutants (F_1). (D) Flowering time of heterozygous *ucn-1* mutants (F_1). (E) Seed size of heterozygous *ucn-2* mutants (F_1). (F) Germination rate of heterozygous *ucn-2* mutants (F_1). (G) Root length of heterozygous *ucn-2* mutants (F_1). All seedlings were grown under LD conditions. $+/ucn-1 = Ler \times ucn-1$, $ucn-1/+ = ucn-1 \times Ler$, $+/ucn-2 = Col-0 \times ucn-2$, $ucn-2/+ = ucn-2 \times Col-0$. Blue dots represent samples, brown dots with lines represent mean values with 1x standard deviation.

I further analyzed the root length of the main root of five days old seedlings of heterozygous *ucn-1* and *ucn-2*. In average, I measured a mean main root length of 11,3mm ($p = 0,0273$) for *ucn-1* x *Ler* ($n = 33$). For *Ler* x *ucn-1* ($n = 34$) I measured a mean main root length of 10,7mm ($p = 0,0036$). The differences between the root length of the two crossing directions is not significant ($p = 0,2797$). In contrast, I measured an average main root length of 12,7mm for *Ler* ($n = 29$) and an average main root length of 7,1mm ($p = 3,24 \times 10^{-7}$) for *ucn-1*. The result shows that heterozygous *ucn-1* mutants do not regain their wild-type root length (see figure 3.3.2C). Surprisingly, when I analyzed the main root length of heterozygous *ucn-2* seedlings, I found that these seedlings show a longer main root than the wild-type. I measured an average main root length of 20,6mm for five days old seedlings of *Col-0* x *ucn-2* ($n = 47$) ($p = 1,7 \times 10^{-7}$), while I measured an average main root length of 20,2mm for five days old seedlings of *ucn-2* x *Col-0* ($n = 48$) ($p = 1,1 \times 10^{-5}$). Again, the difference between the main root lengths of the different crossing directions is not significant ($p = 0,3278$). For the control plants I measured a mean main root length of 15,8mm ($n = 33$) for *Col-0* and 13,8mm for *ucn-2* ($n = 37$) (see figure 3.3.2G). Therefore, the roots of heterozygous *ucn-2* seedlings are longer than the roots of wild-type seedlings. The

results indicate that the heterozygous loss-of-function lines do not re-gain their wild-type root length.

The analysis of the flowering time of heterozygous *ucn-1* revealed that under LD conditions, the F₁ generation of *Ler* x *ucn-1* (n = 15) and *ucn-1* x *Ler* (n = 15) starts flowering with in mean 17,6 total leaves ($p = 1,6119 * 10^{-5}$) and 16,9 total leaves ($p = 8,72235 * 10^{-7}$), respectively. The wild-type *Ler* (n = 14) starts flowering in mean with 20,6 total leaves and *ucn-1* (n = 12) starts flowering in mean with 13,7 total leaves ($p = 1,47625 * 10^{-6}$). This shows that one dysfunctional *ucn* allele also affects flowering time, although not as severe as in homozygous *ucn-1* mutants. Again, this effect is independent from the crossing direction (see figure 3.3.1A and 3.3.2D). Since *ucn-2* does not show a defect in flowering time determination, the heterozygous *ucn-2* lines were not tested for this characteristic.

The results I gained so far do not support the idea of a recessive *ucn-1* allele otherwise the heterozygous lines would not differ from the wild-type. Therefore, I also analyzed the ovules and the flowers of these lines. In contrast to former information, I discovered ovules with aberrant cell division in the integuments. Nevertheless, the protrusions I observed were smaller than the protrusions of homozygous *ucn-1* mutants (see figure 3.3.1B to D). However, this demonstrates that also the integuments are impaired in a heterozygous *ucn-1* line. In contrast, the flowers of heterozygous *ucn-1* plants displayed the wild-type shape (see figure 3.3.1E to G).

Table 3.3.1: Summarized results of the analysis of heterozygous *ucn-1* and *ucn-2* plants compared to the results gained for homozygous *ucn-1* and *ucn-2* plants.

Analysis was done regarding seed size (2D seed area), germination rate, root length of the main root, flowering time (FT) in LD, and flower and ovule shape. Values are relative to the corresponding wild-types.

Characteristic	<i>ucn-1</i>	<i>ucn-1</i> x <i>Ler</i>	<i>Ler</i> x <i>ucn-1</i>	<i>ucn-2</i>	<i>ucn-2</i> x <i>Col-0</i>	<i>Col-0</i> x <i>ucn-2</i>
Seed size	82%	84%	122%	123%	131%	123%
Germination rate	72%	67,4%	wild-type	wild-type	wild-type	wild-type
Root length	56%	89%	84%	87%	128%	130%
FT (LD)	75%	82%	85%	wild-type	not tested	not tested
Flower shape	affected	wild-type	wild-type	wild-type	wild-type	wild-type
Ovule shape	protrusions	mild protrusions	mild protrusions	not tested	not tested	not tested

In conclusion, the results I gained for heterozygous *ucn-1* plants suggest that *ucn-1* is not a recessive allele. For heterozygous *ucn-1* mutants, the only characteristic that shows a wild-type phenotype is the flower. The other characteristics of *ucn-1* that I described before are still affected in heterozygous mutants, although not as severe as in homozygous *ucn-1*

plants. For *ucn-2* I was able to demonstrate that the root of heterozygous seedlings is also affected, although it grows longer than the wild-type roots. Other plant organs were not investigated. I further demonstrated that *UCN* affects seed size not exclusively from the maternal side, but also from the paternal. This was displayed by both loss-of-function lines (see table 3.3.1).

3.4 The flowering phenotype of a segregating F₂ population of *ucn-1*

The phenotypes I gained for heterozygous *ucn-1* plants contradict the statement that *ucn-1* is a recessive allele. It further raises the question if the phenotypes in heterozygous *ucn-1* plants suffer from a dominant *ucn-1* allele or if *ucn-1* affects the plant epigenetically. If so, it would also result in phenotypically affected heterozygous *ucn-1* plants. The difference would be that the origin of the effect comes from a modified epigenome not the genome. To address this question a segregating F₂ population of *ucn-1* was investigated regarding flowering time. If the *ucn-1* allele is solely responsible for the effect on flowering time, the segregating F₂ population is expected to split up into very early flowering homozygous *ucn-1* plants, less early flowering heterozygous *ucn-1* plants, and wild-type flowering plants that carry no *ucn-1* allele any more (further called *Ler/+* to distinguish them from “original” *Ler* wild-type plants) (see also table 3.8.1 for punnett square). In case of an epigenetic modification, this *Ler/+* offspring would still be impaired.

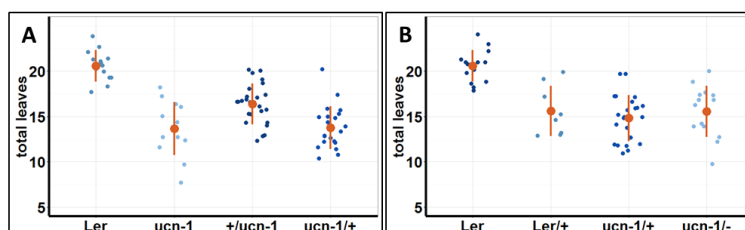


Figure 3.4.1: Flowering time of a segregating F₂ population of *ucn-1* grown under LD conditions.

(A) Flowering time of a segregating F₂ population of *ucn-1*, total result. (B) Flowering time of a segregating F₂ population of *ucn-1* after genotyping the segregating plants. *Ler* = wild-type, *ucn-1* = homozygous *ucn-1*, *+/ucn-1* = F₂ offspring of *Ler* x *ucn-1*, *ucn-1/+* = F₂ offspring of *ucn-1* x *Ler*, *Ler/+* = wild-type offspring of *Ler* x *ucn-1* and *ucn-1* x *Ler*, *ucn-1/+* = heterozygous *ucn-1* offspring of *Ler* x *ucn-1* and *ucn-1* x *Ler*, *ucn-1/-* = homozygous *ucn-1* offspring of *Ler* x *ucn-1* and *ucn-1* x *Ler*. Blue dots represent samples, brown dots with lines represent mean values with 1x standard deviation.

Interestingly, the F₂ generations did not segregate into the expected groups (see figure 3.4.1A). Instead, the F₂ generation of *ucn-1* x *Ler* (n = 21) starts flowering with an average number of 13,8 total leaves ($p = 2,77 \cdot 10^{-11}$) while the F₂ generation of *Ler* x *ucn-1* (n = 25) starts flowering with an average number of 16,4 total leaves ($p = 2,66 \cdot 10^{-7}$). Therefore, at least in average, the F₂ generation starts flowering earlier than the wild-type

(n = 14) that starts flowering with an average of 20,6 total leaves and only slightly later than *ucn-1* (n = 12) that starts flowering with an average of 13,7 total leaves in this experiment.

For a more exact analysis of the flowering time of the F₂ generation, I genotyped the offspring. The result reveals that there really is no segregation regarding flowering time (see figure 3.4.1B). In average, the *Ler/+* plants (n = 8) of the segregating F₂ generation started flowering with 15,6 total leaves ($p = 0,0009896$). The homozygous *ucn-1* mutants (n = 14) of this generation started flowering with in average 17 total leaves ($p = 1,19311 * 10^{-5}$). The segregating heterozygous *ucn-1* plants (n = 24) started flowering with an average number of 14,8 total leaves ($p = 1,03338 * 10^{-9}$). These results indicate that the offspring of a heterozygous *ucn-1* population does not regain its wild-type flowering time. They further suggest that, at least partially, the early flowering is caused by epigenetic effects.

In summary, *Ler/+* plants with a wild-type genome that segregate out of a selfed heterozygous *ucn-1* line still show rapid flowering. The result therefore suggests that the flowering time deregulation can also be inherited epigenetically, independent of the *ucn-1* allele itself.

3.5 Influence of the length of day on *ucn-1* and *ucn-2*

The determination of flowering time is strongly regulated in *Arabidopsis thaliana*. It is influenced by extrinsic and intrinsic signals the plant receives [102]. One signal is the length of day-light. A long day (LD; 16 hours light per 24 hours) promotes flowering while a short day (SD; 8 hours light per 24 hours) represses it. However, the two accessions *Ler* and *Col-0* also start flowering when grown under SD conditions, although much later than under LD conditions. The reason for the flowering in the unfavorable SD condition is that intrinsic signals promoting flowering override the repression. It was shown that the pathways responsible for the flowering in SD are different from the pathways that promote flowering in LD [31, 32]. Therefore, to shed more light on the question why *ucn-1* flowers early under LD conditions and why *ucn-2* does not show a flowering deregulation, I grew the loss-of-function lines under SD conditions. If involved in flowering activation or repression depending on the length of light treatment, the flowering time of *ucn-1* and *ucn-2*, respectively should change.

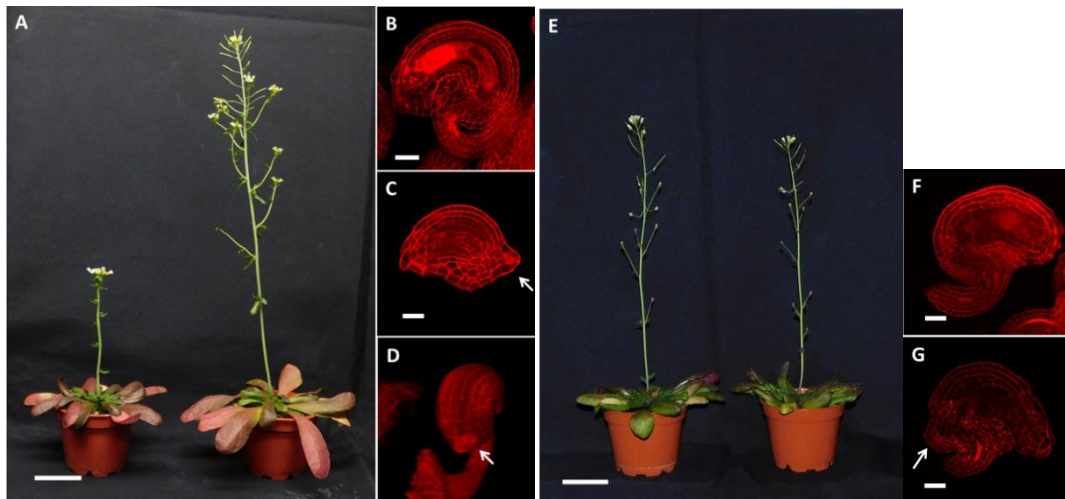


Figure 3.5.1: Result of the phenotypic analysis of *ucn-1* and *ucn-2* grown in SD.

(A) Like in LD, *ucn-1* (right plant) flowers earlier than *Ler* (left plant) when grown in SD. (B) to (D) The protrusions of *ucn-1* ovules (C and D, arrow) get stronger compared to *Ler* (B). For a better visualization of the protrusion visible in (C), a 3D reconstruction was done using Fiji (D). The protrusion is indicated with an arrow. (E) The flowering time of *ucn-2* (right plant) is still the same like the flowering time of *Col-0* (left plant) when grown in SD. (F) and (G) Ovules of *ucn-2* (G) now also show protrusions (indicated with arrow) when compared to *Col-0* ovules (F). Scale bars: A and E: 3cm; B, C, F, and G: 20 μ m.

When growing *ucn-1* and *ucn-2* under SD conditions, *ucn-1* starts flowering with in average 43,1 total leaves. The control plant *Ler* (n = 20) starts flowering with in average 53,1 total leaves ($p = 7,7 * 10^{-15}$) (see figure 3.5.1A and 3.5.2A). The *ucn-2* mutant (n = 29) starts flowering with in average 62,5 total leaves while *Col-0* (n = 21) starts flowering with in average 61,8 total leaves ($p = 0,3372$). This indicates that *ucn-2* does not change its flowering time (see figure 3.5.1E and 3.5.2B). The results therefore indicate that the early flowering of *ucn-1* and the wild-type flowering of *ucn-2* is independent from the length of the light treatment.

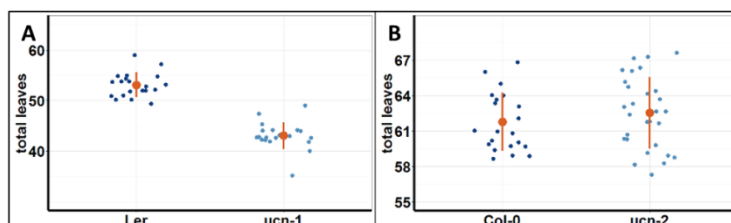


Figure 3.5.2: Determination of the flowering time of *ucn-1* and *ucn-2* in SD.

(A) Flowering time of *ucn-1* under SD conditions. (B) Flowering time of *ucn-2* under SD conditions. Blue dots represent samples, brown dot with line represents average with 1x standard deviation.

I also checked if the growth under SD conditions influences the ovule phenotypes of *ucn-1* as well as *ucn-2*. The analysis of the ovules of the mutant plants shows a surprising result. While *ucn-1* ovules show no differences (see figure 3.5.1B to D), *ucn-2* ovules do. The integuments of plants grown in SD now show *ucn-1* like protrusions (see figure 3.5.1F and G). This result suggests that the length of the light treatment has an effect on the ovule shape of *ucn-2*.

Table 3.5.1: Comparison of the flowering time and the ovule shape of *ucn-1* and *ucn-2* grown under long-day (LD) and short-day (SD) conditions.

Numbers are given in relation to the corresponding wild-type.

Characteristic	<i>ucn-1</i> (LD)	<i>ucn-1</i> (SD)	<i>ucn-2</i> (LD)	<i>ucn-2</i> (SD)
Flowering time	75%	77%	wild-type	wild-type
Ovules	protrusions	protrusions	wild-type	protrusions

In conclusion, the day-length has no influence on the flowering time of *ucn-1* or *ucn-2* plants. However, when grown under SD conditions, *ucn-2* displays *ucn-1* like protrusions on its ovules (see table 3.5.1).

3.6 Overexpression of *UCN*

I was able to show that neither *ucn-1* nor *ucn-2* is a real null allele. Both alleles are still expressed. Although this expression is lower than the wild-type expression, there is a chance that the transcribed mRNA also is translated into a truncated protein. To better understand the function of *UCN*, I generated gain-of-function lines in *Ler* and *Col-0*. Therefore, I transformed the overexpression construct pUBQ::*UCN* into the wild-types. For the subsequent investigations I chose three independent T₁ lines from each transformation. I selfed them until I received homozygous T₃ lines. The plants with the *UCN* overexpression construct in *Ler* will further be called LUox (for **L**er **U**CN **o**ver**e**xpressed) and CUox (for **C**ol-0 **U**CN **o**ver**e**xpressed). As above, the lines were analyzed phenotypically. Ideally, the gain-of-function lines show the opposite results of the loss-of-function lines. This behavior would suggest a direct involvement of *UCN* in the processes related to the impaired organ.

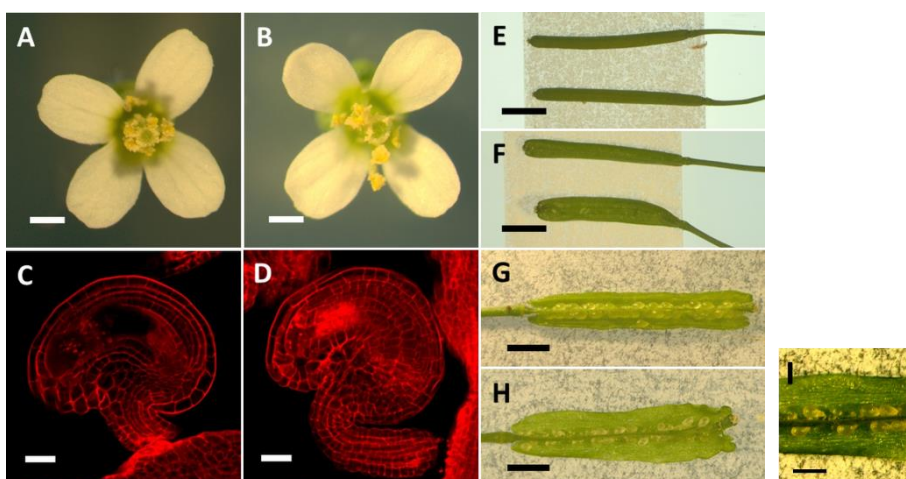


Figure 3.6.1: Phenotypic analysis of the reproductive organs of LUox.

(A) to (D) Flowers and ovules of LUox (B and D) are inconspicuous compared to wild-type flowers (A) and ovules (C). (E) and (F) Siliques of LUox (F) can contain more than two fused carpels (lower silique in F) than wild-type siliques (E). (G) and (H) LUox siliques also contain degenerated ovules (H) in contrast to *Ler* siliques (G). (I) Detail of H, contrast enhanced. Scale bars: A and B: 500µm; C and D: 20µm; E to H: 2mm; I = 1mm

The analysis of the flowers of the gain-of-function lines LUox and CUox revealed no specialties (see figure 3.6.1A and B and figure 3.6.2A and B). This also holds true for the ovules (see figure 3.6.1C and D and figure 3.6.2C and D) and the germination rate (see figure 3.6.5B and 3.6.5H).

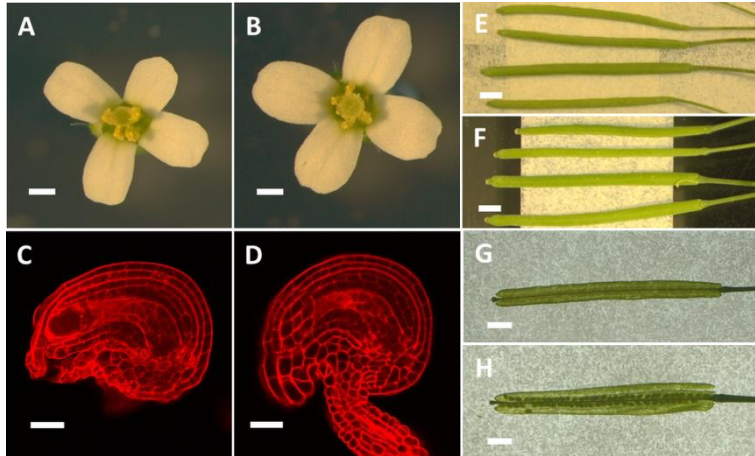


Figure 3.6.2: Reproductive plant parts of CUox compared to Col-0.

(A) and (B) Flowers of CUox (B) do not differ from Col-0 flowers (A). (C) and (D) Ovules of CUox (D) are also inconspicuous when compared to ovules of Col-0 (C). (E) and (F) Siliques of CUox (E) also show no special features compared to siliques of Col-0 (F). Scale bars: A, B and E, F: 2mm; C and D: 20 μ m.

The analysis of the 2D seed area revealed that LUox produces slightly bigger seeds than the wild-type (see figure 3.6.5A). The seeds ($n = 66$) have a mean surface area of $90874\mu\text{m}^2$ while the seeds of *Ler* ($n = 103$) have an average 2D surface of $86761\mu\text{m}^2$ ($p = 0,0169$). The determination of the 2D seed area of CUox revealed that in average, the seed surface of CUox is $67645\mu\text{m}^2$ ($n = 173$) while the seed surface of Col-0 is in average $78127\mu\text{m}^2$ ($n = 93$) ($p = 9,36 * 10^{-10}$) (see figure 3.6.5G). This indicates that, regarding seed size, the gain-of-function lines show the opposite phenotype than the loss-of-function lines.

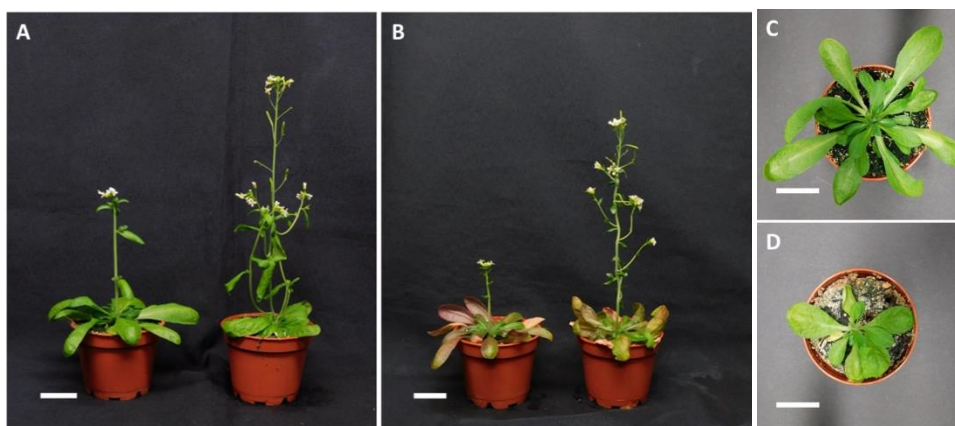


Figure 3.6.3: *Ler* and LUox grown under LD (A) and SD (B) conditions.

(A) and (B) Compared to *Ler* (left plants), LUox shows a compact overall stature when grown under LD (A) or SD (B) conditions. In both conditions, LUox (plants on the right) flowers earlier than *Ler*. In addition, LUox grows a zig-zag formed stem when grown in SD (B). (C) and (D) When grown under LD conditions, the rosette of LUox (D) is much smaller than the rosette of *Ler* (C) and its leaves show a more roundish shape than the lanceolatic of the wild-type leaves. Scale bars: 2cm.

The investigation of the root length of five days old seedlings revealed that both gain-of-function lines grow smaller roots than the corresponding wild-types. LUox grows a main root of an average length of 6,1mm (n = 34). The main root of *Ler* (n = 22) grows an average length of 11,5mm ($p = 1,92948 * 10^{-6}$) (see figure 3.6.5C). CUox grows a main root of an average length of 4,2mm (n = 53). In the same time, Col-0 (n = 60) grows a main root of an average length of 8,9mm ($p = 1,43717 * 10^{-11}$) (see figure 3.6.5I). This observation indicates that the gain-of-function of *UCN* impairs root growth even more than the loss-of-function.

The characterization of the flowering time revealed an early flowering for pUBQ::*UCN* in *Ler* and a late flowering for pUBQ::*UCN* in Col-0. LUox (n = 17) starts flowering with an average of 9,4 total leaves compared to the wild-type (n = 20) that starts flowering with in average 17 total leaves ($p = 3,4442 * 10^{-20}$) or *ucn-1* (n = 19), which starts flowering with in average 13,6 total leaves ($p = 1,66027 * 10^{-10}$) (see figure 3.6.3A and 3.6.5D). In contrast, CUox (n = 13) starts flowering with in average 15,6 total leaves compared to Col-0 which starts flowering with in average 12,6 total leaves ($p = 0,01194$) (see figure 3.6.4A and 3.6.5J). This result indicates that a gain-of-function of *UCN* in *Ler* accelerates flowering while it delays it in Col-0.

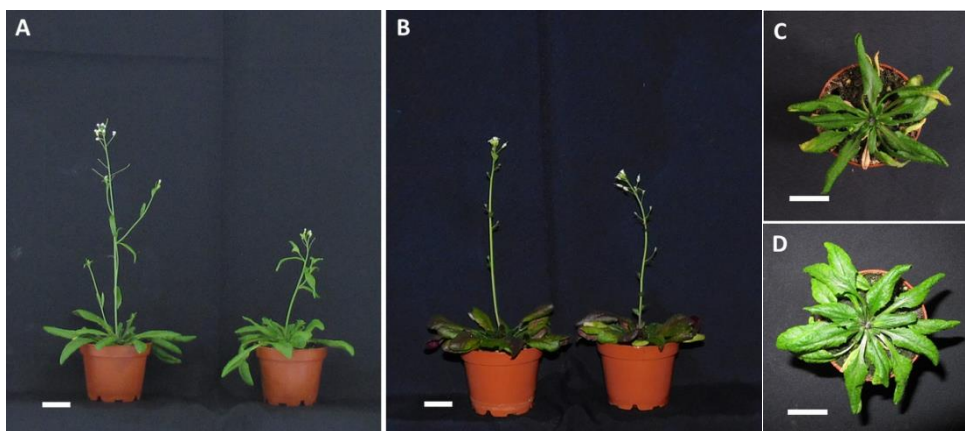


Figure 3.6.4: Col-0 and CUox grown under LD (A) and SD (B) conditions.

(A) and (B) In contrast to LUox, the overall phenotype of CUox is inconspicuous compared to Col-0. When grown under LD conditions (A), CUox (right plant) flowers later than Col-0 (left plant). When grown under SD conditions (B), CUox (right plant) flowers the same time as Col-0 (left plant). (C) and (D) Compared to a wild-type rosette (C), the rosette of CUox (D) shows no special features. Scale bars: 2cm.

The analysis of the siliques revealed that the siliques of LUox are inconspicuous in length (see figure 3.6.5F) but they show a very striking phenotype in their shape. Instead of constantly two fused carpels LUox shows a lot of pistils with up to four fused carpels (see figure 3.6.1E and F). This supernumerous number in organs was restricted to the innermost whorl of the flower. A look into the carpels revealed that they contain sterile ovules (see figure 3.6.1G and H). Like in the siliques of *ucn-1*, the numbers of degenerated ovules vary a

lot from silique to silique and also from plant to plant. In contrast to LUox, the siliques of CUox show a slight increase in their length (see figure 3.6.5L). In average, the wild-type ($n = 93$) grows siliques of 16,4mm length while CUox ($n = 104$) grows siliques of 16,9mm length in average ($p = 0,001917$). However, multiple fused carpels with more than two like on LUox cannot be found (see figure 3.6.2E and F). Furthermore, no lethality was observed (see figure 3.6.2G and H).

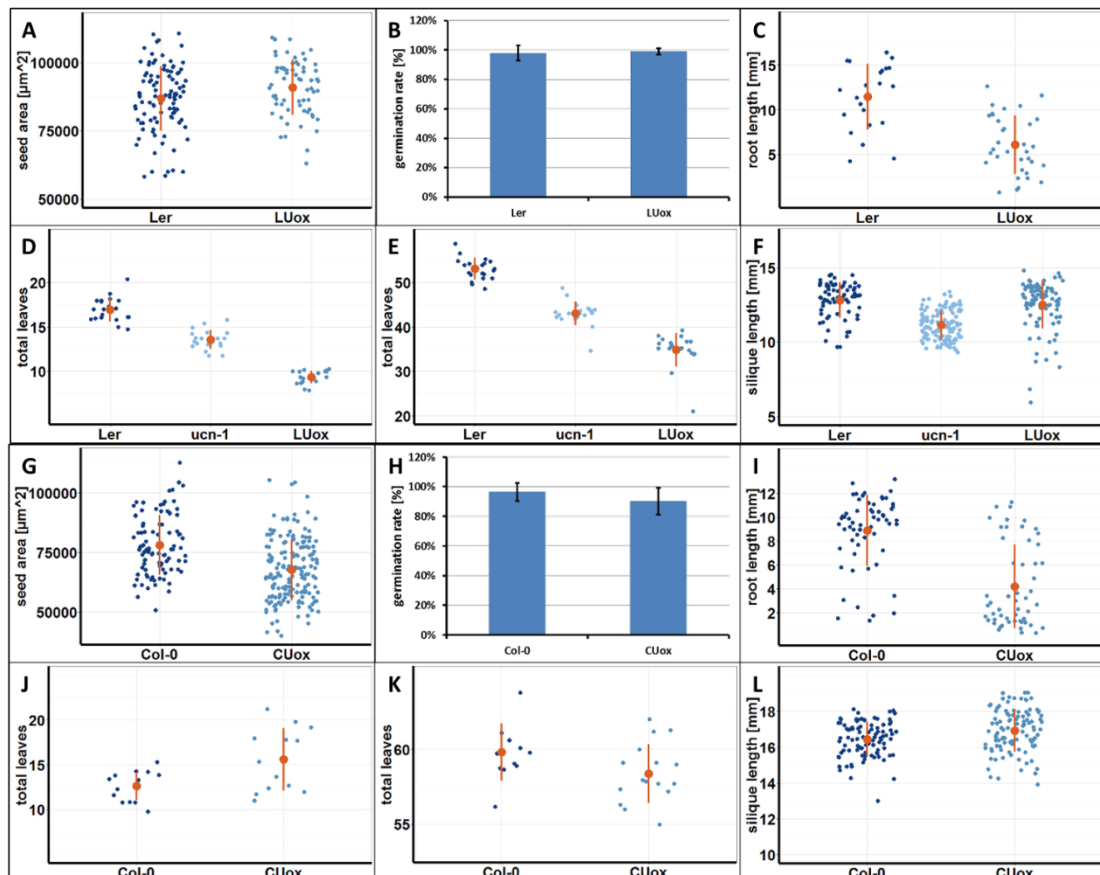


Figure 3.6.5: Analysis of the characteristics of the *UCN* overexpressor lines LUox (upper two rows) and CUox (lower two rows).

(A) Seed size of LUox lines. (B) Germination rate of LUox lines. (C) Root length of LUox lines, 5dag. (D) Flowering time of LUox lines grown in LD. (E) Flowering time of LUox lines grown in SD. (F) Silique length of LUox lines. (G) 2D seed area of CUox. (H) Germination rate of CUox. (I) Root length of CUox, 5dag. (J) Flowering time of CUox in LD conditions. (K) Flowering time of CUox in SD conditions. (L) Silique length of CUox. Blue dots represent samples, brown dots with lines represent average with 1x standard deviation.

In addition to the above named features, LUox itself shows a very striking plant phenotype. The leaves of the T-lines are round with less long petioles and the leaf blade is more expanded than the leaf blade of *Ler* (see figure 3.6.3C and D). This leaf shape makes the whole rosette smaller than wild-type rosettes. The overall plant also grows more compact than the wild-type, giving it kind of bushy look (see figure 3.6.3A). However, the number of lateral organs (lateral stems, 2ndary stems, cauline leaves, etc.) of LUox is the same number as for *Ler*. These characteristics were not observed on CUox (see figure 3.6.4A, C and D).

To check if the flowering time deregulations of LUox and CUox are also independent of the length of the day, the gain-of-function lines were also grown under SD conditions. In average, LUox starts flowering with 34,9 total leaves ($n = 20$) ($p = 1,79978 * 10^{-18}$) whereas *Ler* starts flowering with in average of 53,1 total leaves ($n = 20$). This acceleration in flowering is still greater than in *ucn-1*, which starts flowering with 43,1 total leaves ($n = 20$) when grown in SD ($p = 7,70116 * 10^{-15}$) (see figure 3.6.3B and 3.6.5E). Therefore, the early flowering is again not dependent on the length of the light treatment. In contrast to LUox, CUox starts flowering with in average 58,4 total leaves until the first flower opens while Col-0 grows in average 59,8 total leaves ($p = 0,0721$) until flowering (see figure 3.6.4B and 3.6.5K). This indicates that CUox only flowers late in LD but not in SD.

It is noteworthy that LUox, when grown under SD conditions, shows stems that grew in a zig-zag shape (see figure 3.6.3B). I observed this phenotype additionally to the smaller stature and the striking rosette leaf form already observed under LD conditions. In contrast, CUox shows no additional features when grown under SD conditions (see figure 3.6.4B).

Table 3.6.1: Conclusion of the analysis of the UCN gain-of-function lines LUox and CUox compared to their corresponding loss-of-function lines *ucn-1* and *ucn-2*.

Plants were analyzed for Flower and ovule shape, germination rate, 2D seed area (seed size), length of the root of five day old seedlings (root length), flowering time (FT) in LD and SD, silique length and shape, ovule lethality, and plant/leaf shape. All numbers are given in relation to the corresponding wild-type.

Characteristic	<i>ucn-1</i>	LUox	<i>ucn-2</i>	CUox
Ovule shape (LD)	protrusions	wild-type	wild-type	wild-type
Flower shape	affected	wild-type	wild-type	wild-type
Germination rate	72%	wild-type	wild-type	wild-type
Seed size	82%	105%	123%	85%
Root length	64%	53%	87%	47%
FT (LD)	80%	55%	wild-type	124%
FT (SD)	81%	66%	wild-type	wild-type
Silique length	85%	wild-type	96%	97%
Silique shape	wild-type	>2 fused carpels	wild-type	wild-type
Ovule lethality	yes	yes	no	no
Plant/leaf shape	wild-type	compressed plant stature, round leaves	wild-type	wild-type

In conclusion, the gain-of-function lines only show an opposite behavior to the loss-of-function lines regarding the seed size. In *Ler* background, LUox shows a slight increase in seed size while *ucn-1* produces smaller seeds. In Col-0 background, CUox produces smaller seeds than the wild-type while *ucn-2* produces bigger seeds. The root length of both gain-of-function lines is even smaller than the root length of the loss-of-function lines. The flowering

time of LUox is even more rapid than in *ucn-1* while CUox shows late flowering. In SD, the late flowering is neutralized, while the length of day shows no effect on the rapid flowering of LUox. CUox also grows slightly smaller siliques like *ucn-2* while LUox shows no effect on silique length but on the number of fused carpels per pistil. Furthermore, LUox shows additional phenotypes, like roundish rosette leaves and a zig-zag shape of the stem when grown in SD. In summary, the *Ler* background is again much more susceptible than the Col-0 background (see table 3.6.1).

3.7 Overexpression of *ucn-1*

With heterozygous *ucn-1* lines I was able to demonstrate that *UCN* is likely not a recessive allele. This raises the question what is responsible for the dominance. It could come from a haplo-insufficiency, the need for both wild-type alleles for proper functioning. Another explanation is a dominant-negative behavior of *ucn-1*. Here, the availability of *ucn-1* negatively influences the processes *UCN* is involved in. To address the question, I overexpressed *ucn-1* in the wild-types *Ler* and Col-0 using a pUBQ::*ucn-1* construct. For each *ucn-1* gain-of-function line I analyzed three independent homozygous T₃ lines. For further reading I call the overexpression of *ucn-1* in *Ler* L1ox (for **Ler *ucn-1* overexpressed**) and the overexpression in Col-0 C1ox (for **Col-0 *ucn-1* overexpressed**). In case of a haplo-insufficiency this should not have an impact on the plants. In case of a dominant-negative behavior, I would receive a phenotype different from wild-type.

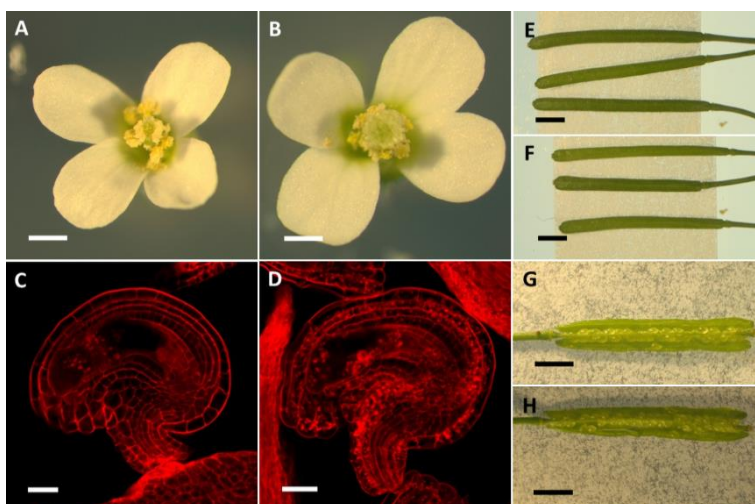


Figure 3.7.1: Phenotypical analysis of the reproductive organs of L1ox.

The overexpression of *ucn-1* in *Ler* (= L1ox) does not influence the overall shape of the reproductive organs. (A) to (D) The flower of L1ox (B) as well as the ovules of L1ox (D) look like wild-type flowers (A) and ovules (C), respectively. (E) to (H) The same is true for the siliques of L1ox (F) which looks like wild-type siliques (E). A look inside the siliques of L1ox (H) shows that there are no degenerated ovules when compared to wild-type siliques (G). Scale bars: A and B: 500µm; C and D: 20µm; E to H: 2mm.

Flowers as well as ovules of both *ucn-1* gain-of-function lines are inconspicuous (see figure 3.7.1A to D and 3.7.2A to D). Also germination rate, silique length and shape, ovule survival, and rosette leaves are inconspicuous (see figure 3.7.1E to H, 3.7.2E to H, 3.7.3B, F, H, and L, 3.7.4C and D, and 3.7.5C and D).

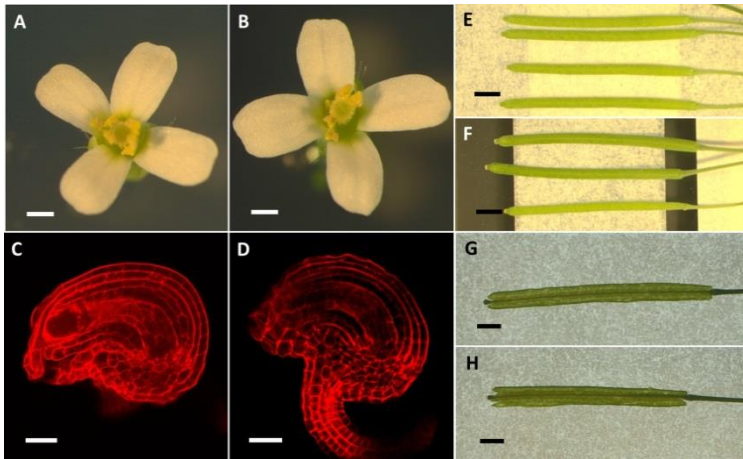


Figure 3.7.2: Phenotypical analysis of the reproductive organs of C1ox.

(A) to (D) Flowers and ovules of C1ox (B and D) do not show any special features when compared to flowers and ovules of Col-0 (A and C). (E) to (H) The silique shape of C1ox (F) does not differ from the Col-0 silique shape (E). The overexpression of *ucn-1* also has no influence on the ovules. The siliques of C1ox do not bear any degenerated ovules (H) just like wild-type siliques (G). Scale bars: A and B: 500µm; C and D: 20µm; E to H: 2mm.

The analysis of the 2D seed area of L1ox revealed an average area of 77464µm² (n = 159) while wild-type seeds (n = 103) have an area of 86761µm² (p = 1,8 * 10⁻⁹) (see figure 3.7.3A). Seeds of C1ox (n = 104) have an average 2D seed area of 90509µm², while seeds of Col-0 (n = 93) show an average 2D seed surface of 78127µm² (p = 1,2 * 10⁻⁹) (see figure 3.7.3G). The result therefore indicates that the overexpression of *ucn-1* increase the seed size in Col-0 while it decreases the seed size in *Ler*.

The investigation of the main root length of five day old seedlings revealed that the overexpression of *ucn-1* also has an impact here. In average, L1ox seedlings (n = 32) grow a root of 7,0mm length while *Ler* seedlings (n = 22) grow a main root that is in average 11,5mm long (p = 4,82 * 10⁻⁵) (see figure 3.7.3C). Seedlings of C1ox (n = 56) grow a 10,2mm long main root while Col-0 (n = 53) grows a main root which is in average 11,1mm long (p = 0,02025) (see figure 3.7.3I). The result indicates a negative influence of the overexpression of *ucn-1* on root size in both accessions, although the negative influence is much stronger in *Ler* than in Col-0.

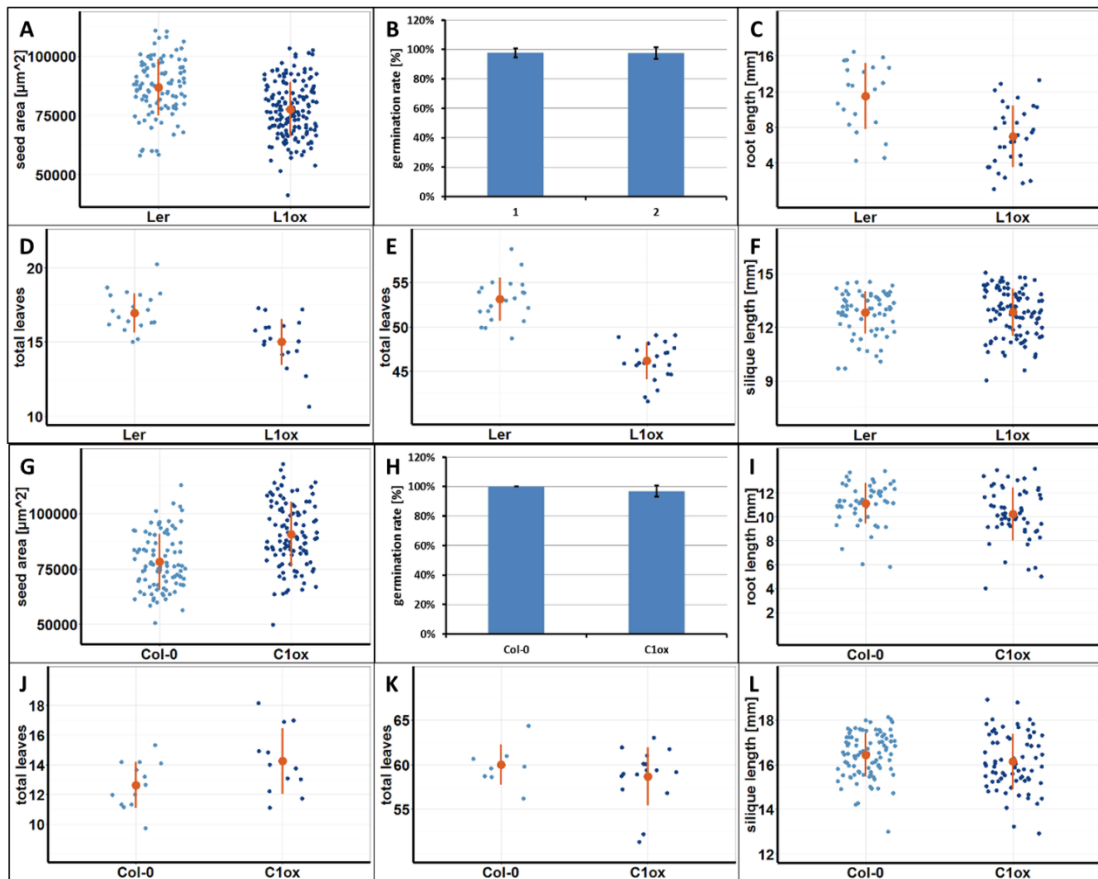


Figure 3.7.3: Analysis of the characteristics of *Ler* and *Col-0* overexpressing *ucn-1*.

(A) 2D seed area of L1ox compared to *Ler*. (B) Germination rate of L1ox does not differ from wild-type. (C) The average root length of L1ox is smaller than the average root length of *Ler*. (D) L1ox flowers earlier than *Ler* when grown in LD conditions. (E) L1ox still flowers early when grown in SD conditions. (F) The overexpression of *ucn-1* has no influence on silique length. (G) 2D seed area of C1ox compared to *Col-0* seeds. (H) Germination rate of C1ox does not differ from *Col-0*. (I) The average root length of C1ox is almost the same as *Col-0*. (J) In LD conditions C1ox flowers a little later than the wild-type. (K) Flowering time of C1ox when grown in SD. (L) The overexpression of *ucn-1* has no influence on silique length. Each blue dot represents one sample, brown dots and lines represent average with 1x standard deviation.

The analysis of the flowering time under LD conditions revealed that L1ox ($n = 19$) flowers with in average 15 total leaves while *Ler* ($n = 20$) flowers with in mean 17 total leaves ($p = 0,0001715$) (see figure 3.7.3D and 3.7.4A). In contrast, under LD conditions C1ox ($n = 12$) starts flowering with in average 14,3 total leaves while *Col-0* ($n = 13$) starts flowering with in average 12,6 total leaves ($p = 0,04749$) (see figure 3.7.3J and 3.7.5A). These results indicate that the flowering time is also affected by the overexpression of *ucn-1*. In both cases, the flowering time deregulation is a weaker phenocopy of corresponding *UCN* overexpression lines.

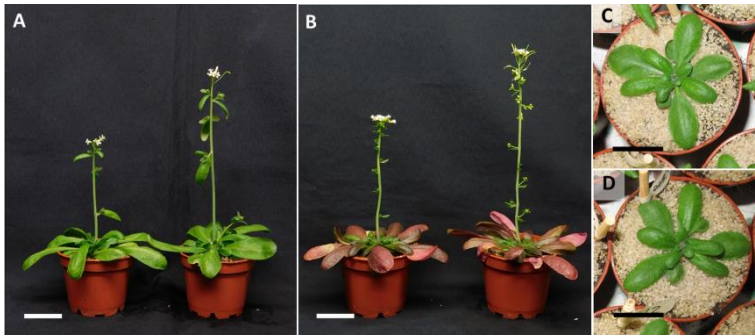


Figure 3.7.4: L1ox grown in LD (A, C, and D) and SD (B).

(A) and (B) L1ox (right plants) flowers earlier than *Ler* (left plants) independent of the length of the day (A: LD; B: SD). (C) and (D) In contrast to LUox, the rosette of L1ox (D) is inconspicuous compared to *Ler* (C). Scale bars: A and B: 3cm; C and D: 2cm.

When grown under SD conditions, L1ox ($n = 22$) starts flowering with in average 46,2 total leaves while *Ler* ($n = 20$) starts flowering with in average 53,1 total leaves ($p = 6,13 \cdot 10^{-12}$) (see figure 3.7.3E and 3.7.4B). In contrast, C1ox starts flowering with in average 58,7 total leaves ($n = 16$) and is therefore not significantly different from the wild-type that grows 60 total leaves ($n = 8$) until flowering ($p = 0,264999$) (see figure 3.7.3K and 3.7.5B). Hence, the flowering deregulation caused by *ucn-1* overexpression in *Ler* is again independent from the length of day while the delay in flowering caused by *ucn-1* overexpression in Col-0 accession is again rescued under SD conditions.

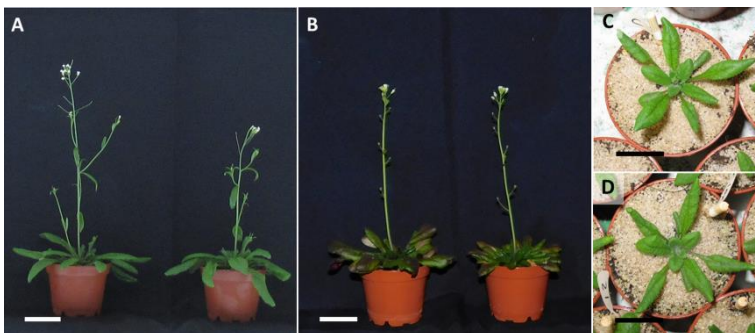


Figure 3.7.5: Phenotypical analysis of C1ox (right plants) compared to Col-0 (left plants).

(A) C1ox flowers late when grown in LD (right plant). (B) This late flowering disappears when growing the plant in SD (right plant). (C) and (D) The rosettes of C1ox (D) are inconspicuous compared to Col-0 (C). Scale bars: A and B: 3cm; C and D: 2cm.

In conclusion, the results clearly show a negative influence of the overexpression of *ucn-1*. Thereby, the plant organs that are impaired are the same like in LUox or CUox, although in a weaker extend. The flowering time phenocopies the corresponding *UCN* gain-of-function lines, too. Pistils with multiple fused carpels like on LUox are not found on L1ox. Also the zig-zag shape of the stem is not observed when grown under SD conditions. The seed size of the *ucn-1* gain-of-function lines shows the behavior of the loss-of-function lines, although in a weaker fashion (see table 3.7.1). Again, the overexpression impairs *Ler* stronger than Col-0.

Table 3.7.1: Summary of the analysis of the *ucn-1* gain-of-function lines L1ox and C1ox compared to the UCN gain-of-function lines.

Plants were analyzed for Flower and ovule shape, germination rate, 2D seed area (seed size), length of the root of five day old seedlings (root length), flowering time (FT) in LD and SD, silique length and shape, and ovule lethality. All numbers are given in relation to the corresponding wild-type.

Characteristic	LUox	L1ox	CUox	C1ox
Flower shape	wild-type	wild-type	wild-type	wild-type
Ovule shape	wild-type	wild-type	wild-type	wild-type
Germination rate	wild-type	wild-type	wild-type	wild-type
Seed size	105%	89%	85%	116%
Root length	53%	61%	47%	92%
FT (LD)	55%	88%	124%	113%
FT (SD)	66%	87%	wild-type	wild-type
Silique length	wild-type	wild-type	97%	wild-type
Silique shape	>2 carpels fused	wild-type	wild-type	wild-type
Degenerated ovules	yes	no	no	no

3.8 Some features of the plants are inherited epigenetically

I demonstrated that all plants of a segregating F_2 generation of a crossing of *ucn-1* and *Ler* flower early independent of the *ucn-1* allele (see above). Hence, also the plants homozygous for wild-type *UCN* (*Ler/+*; see table 3.8.1) do not regain their flowering time. This suggests a role for *UCN* in an epigenetic process which is then inherited independently from the *ucn-1* allele. I observed a similar effect when I analyzed the segregating T_2 generations of the overexpression lines LUox, CUox, but also L1ox and C1ox. Thus, all plants independent of the T-DNA showed a similar phenotype. To gain more information about that phenomenon and where it is involved in, the wild-type offspring of the different T_2 generations (see table 3.8.2) was also analyzed. To distinguish the offspring lines from the “real” wild-types *Ler*, the abbreviation EMO will be used for epigenetically manipulated organism. Therefore, an EMO line is the wild-type offspring of a heterozygous T-DNA line. To distinguish between the EMO lines from LUox, CUox, L1ox, and C1ox, EMOs in *Ler* background were further called EFL (for early flowering *Ler*, the offspring of LUox) and EFL1 (for early flowering *Ler* coming from *ucn-1* overexpression, the offspring L1ox). The EMO lines in Col-0 background are named EFC (for early flowering Col-0, the offspring of CUox) and EFC1 (for early flowering Col-0 coming from *ucn-1* overexpression, the offspring of C1ox), according to the naming of the EMO lines in *Ler* background (see also table 3.8.3).

Table 3.8.1: Punnett square for the segregation of a heterozygous *ucn-1* parental line.

maternal/paternal	<i>UCN</i>	<i>ucn-1</i>
<i>UCN</i>	<i>UCN/UCN</i> (= <i>Ler/+</i>)	<i>UCN/ucn-1</i> (= het. <i>ucn-1</i>)
<i>ucn-1</i>	<i>ucn-1/UCN</i> (= het. <i>ucn-1</i>)	<i>ucn-1/ucn-1</i> (= <i>ucn-1</i>)

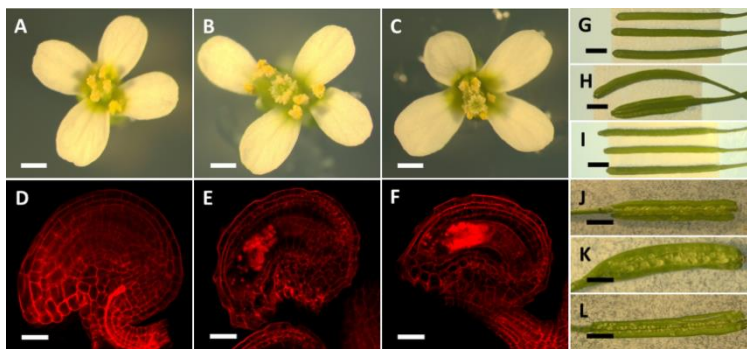
Table 3.8.2: Punnett square for the segregation of a heterozygous T-DNA parental line.

maternal/paternal	T-DNA	wild-type (WT)
T-DNA	T-DNA/T-DNA (= hom. T-line)	T-DNA/WT (=het. T-line)
wild-type (WT)	WT/T-DNA (=het. T-line)	WT/WT (=EMO)

Table 3.8.3: *UCN* and *ucn-1* gain-of-function lines and the corresponding EMO lines.

T-DNA line	corresponding EMO line
LUox	EFL
L1ox	EFL1
CUox	EFC
C1ox	EFC1

Flowers, ovules, germination rate and the 2D seed area of the EMO lines are inconspicuous (see figure 3.8.1A to F, 3.8.2A to F, 3.8.3A, B, G, and H).

**Figure 3.8.1: Phenotypical analysis of the reproductive organs of EFL and EFL1.**

(A) to (C) Flowers of *Ler* (A), EFL (B), and EFL1 (C). No differences can be observed. (D) to (F) Ovules of *Ler* (D), EFL (E), and EFL1 (F). Both EMOs do not show irregular cell division in the integuments. (G) to (I) Siliques of *Ler* (G), EFL (H), and EFL1 (I). The siliques of EFL1 are inconspicuous as the siliques of L1ox were while siliques of EFL show multiple fused carpels (see H, lower silique, 4 fused carpels). (J) to (L) Open siliques of *Ler* (J), EFL (K), and EFL1 (L). No EMO shows ovule lethality. Scale bars: A to C: 500 μ m; D to F: 20 μ m; G to L: 2mm.

The analysis of the root length of the main root of five day old EFL ($n = 13$) seedlings revealed an average length of 4,4mm ($p = 1,44 * 10^{-7}$) while seedlings of EFL1 ($n = 36$) have an average root length of 8,5mm ($p = 0,00876$) five days after germination (see figure 3.8.3C). In case of five day old EFC seedlings ($n = 36$), I measured an average root length of 8,9mm ($p = 0,0284$). Five day old seedlings of EFC1 ($n = 58$) grow an average root length of

8,0mm ($p = 3,23 * 10^{-8}$) (see figure 3.8.3I). Thus, all EMO lines grow smaller roots than their corresponding wild-types *Ler* ($n = 23$; 10,3mm) and *Col-0* ($n = 53$; 9,8mm), although the root length of EFC is much longer than the root length of CUox.

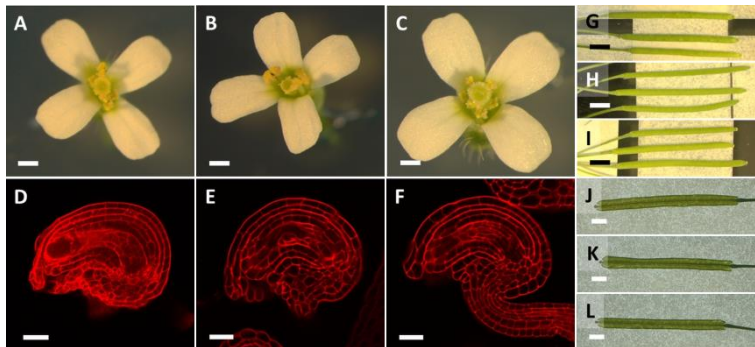


Figure 3.8.2: Phenotypic analysis of the reproductive plant parts of EFC and EFC1.

(A) to (C) Flowers of EFC (B) and EFC1 (C) are inconspicuous (compare to *Col-0* (A)). (D) to (F) Ovules of EFC (E) and EFC1 (F) are not differing from *Col-0* ovules either (D). (G) to (L) Siliques of *Col-0* (G/J), EFC (H/K), and EFC1 (I/L). The silique shape of EFC (H) and EFC1 (I) show wild-type shape (G). They also bear no degenerated ovules (compare J (*Col-0*) to K (EFC) and L (EFC1)). Scale bars: A to C: 500 μ m; D to F: 20 μ m; G to I: 3mm; J to L: 2mm.

The analysis of the flowering time under LD conditions revealed that EFL ($n = 17$) starts flowering with in average 10,4 total leaves while *Ler* ($n = 20$) starts flowering with 17,0 total leaves ($p = 1,29 * 10^{-18}$). With a total leaves number of in average 15,3 total leaves, EFL1 ($n = 20$) also flowers early ($p = 0,00999$) (see figure 3.8.3D and 3.8.5A and D). Therefore, EFL grew a few more leaves than LUox which grows in average 9,4 total leaves until flowering (see above). Compared to *ucn-1* which grows in average 13,6 total leaves (see above) the acceleration of flowering is still much stronger. In average, EFL1 grows 15,3 total leaves ($n = 20$) until flowering, which does not differ significantly from the average of 15 total leaves of L1ox (see above). The analysis of the EMO lines in *Col-0* background revealed that in average, EFC ($n = 12$) grows 17,3 total leaves until flowering ($p = 0,0006353$) while EFC1 ($n = 12$) grows 16,4 total leaves (see figure 3.8.3J and 3.8.6A and E). In both cases, this is more than the 15,1 total leaves that *Col-0* ($n = 11$) grows in average until flowering ($p = 0,02270$). The number of leaves the EMO lines grow is therefore very close to its T-DNA carrying ancestors ($p_{\text{CUox-EFC}} = 0,6530$, $p_{\text{C10x-EFC1}} = 0,3757$). The results indicate that the deregulation of flowering time not only depends on the overexpression of *UCN* or *ucn-1*, but is also inherited epigenetically.

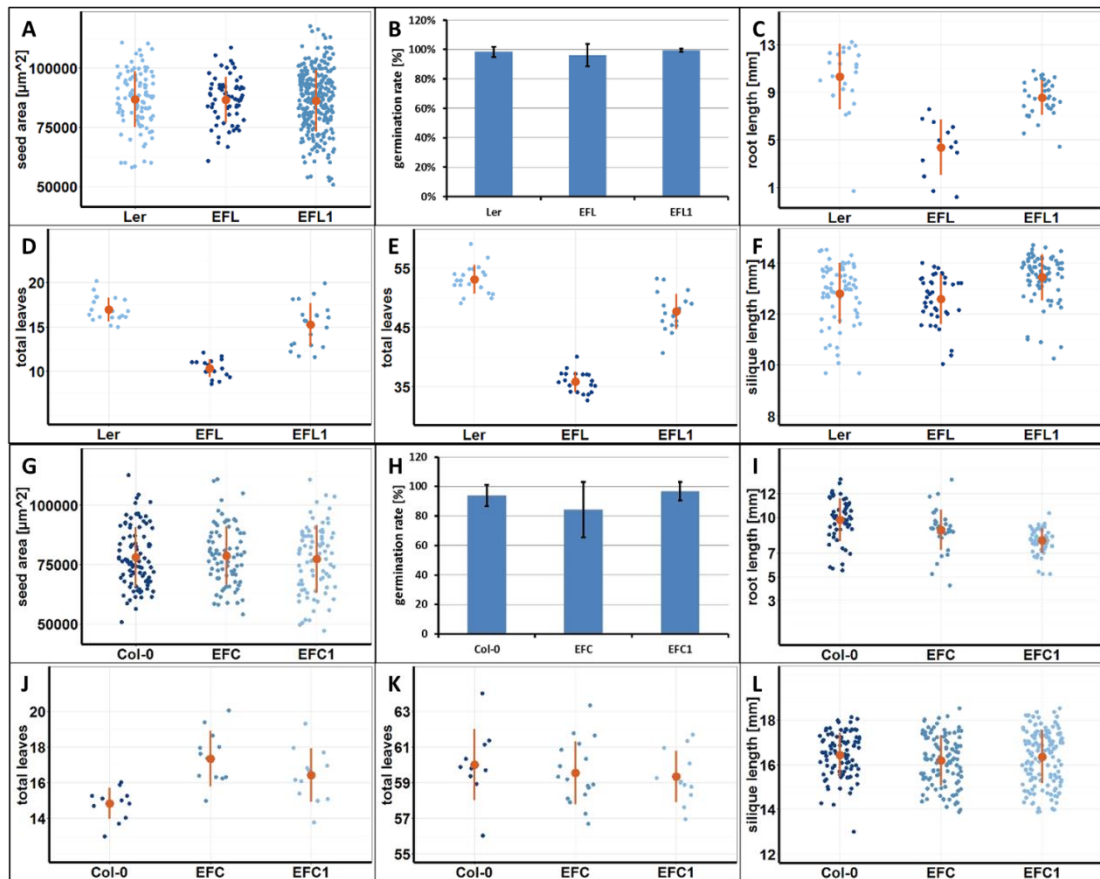


Figure 3.8.3: Analysis of the characteristics of the two EMO lines EFL and EFL1.

(A) 2D seed area of EFL and EFL1 compared to Ler. (B) Germination rate of EFL and EFL1 compared to Ler. (C) Root length of EFL and EFL1 compared to Ler. (D) Flowering time of EFL and EFL1 in LD conditions. (E) Flowering time of EFL and EFL1 when grown in SD. (F) Silique length of EFL and EFL1 compared to Ler. (G) 2D seed area of seeds from EFC and EFC1. (H) The germination rate of EFC and EFC1 do not differ from the germination rate of Col-0. (I) Root length of EFC and EFC1. (J) Flowering time of EFC and EFC1 when grown in LD. (K) Flowering time of EFC and EFC1 when grown in SD. (L) Silique length of EFC and EFC1. Each blue dot represents one sample, brown dots with lines represent average with 1x standard deviation.

Further, I analyzed the silique length of the EMO lines. Siliques of EFL show the wild-type length. Surprisingly, this was not the case for EFL1 siliques ($n = 79$). Here, fully developed siliques have an average length of 13,4mm, which is significantly longer than wild-type siliques (12,8mm) ($p = 0,00052734$) (see figure 3.8.3F). The siliques of EFC and EFC1 show wild-type length (see figure 3.8.3L). Therefore, only siliques of EFL1 show a very slight increase of 5% in their length. A much more striking feature is found for the silique shape of EFL. Like already observed for LUox, the siliques of EFL still consist of more than two fused carpels (see figure 3.8.1G to I). In addition, sterility is also still observed (see figure 3.8.1J to L). This indicates that the silique shape of LUox is inherited epigenetically. Furthermore, the ovules do not regain their viability and still degenerate. The rosette size and the leaf shape of EFL are also phenocopying the overexpression line LUox, although in a weaker fashion (see figure 3.8.4C). Leaves of EFL are more lanceolatic but still do not regain

their full size. This suggests that *UCN* is involved in epigenetic processes that influence plant organ shape.

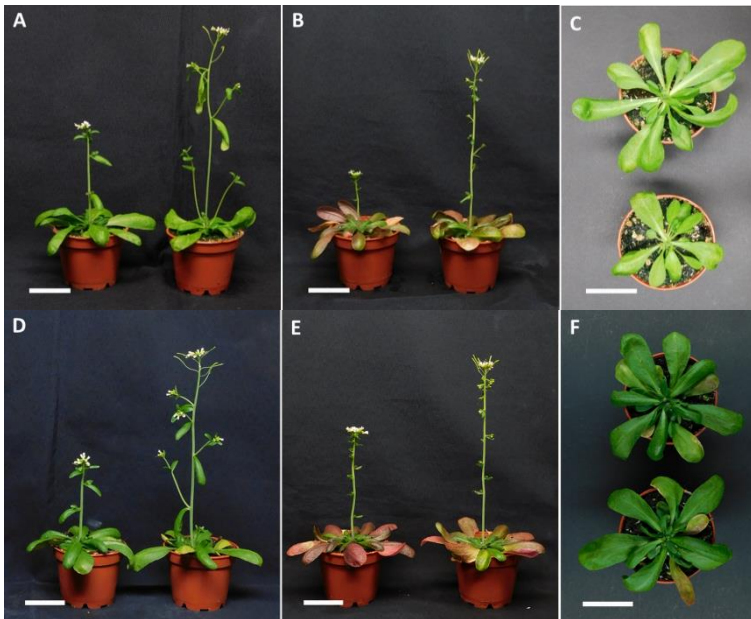


Figure 3.8.4: Result of the phenoptical analysis of EFL (A to C) and EFL1 (D to F).

(A) and (D) When grown in LD, EFL (A; right plant) as well as EFL1 (D; right plant) are flowering earlier than *Ler* (A and D; left plants). (B) and (E) When grown in SD, EFL (B; right plant) and EFL1 (E; right plant) are flowering earlier than the wild-type (B and E; left plants). (C) and (F) The rosette of EFL (C; lower plant, 23dag, stem removed) does not have the striking phenotype of *LUox* when compared to *Ler* (C; upper plant, 23dag, stem removed). The rosette of EFL1 (F; lower plant, 23dag, stem removed) looks like the wild-type rosette (F; upper plant, 23dag, stem removed). Scale bars: 3cm.

Since the flowering time of the overexpressor lines in LD conditions is epigenetically inherited to the EMO lines, it was also analyzed how they behave when grown under SD conditions. The analysis revealed that EFL ($n = 20$) starts flowering with in average 35,8 total leaves. This is much earlier than the wild-type ($n = 20$) that starts flowering with in average 53,1 total leaves ($p = 5,11 * 10^{-24}$). When EFL1 ($n = 20$) is grown under SD conditions, it starts flowering with in average 47,7 total leaves which is also earlier than the wild-type ($p = 2,6 * 10^{-7}$) (see figure 3.8.3E and 3.8.4B and E). The EMO lines with *Col-0* background again lose their delay in flowering (see figure 3.8.3K and 3.8.5B and F). The results indicate that the EMO lines phenocopy the flowering time deregulation of their T-DNA carrying parental lines.

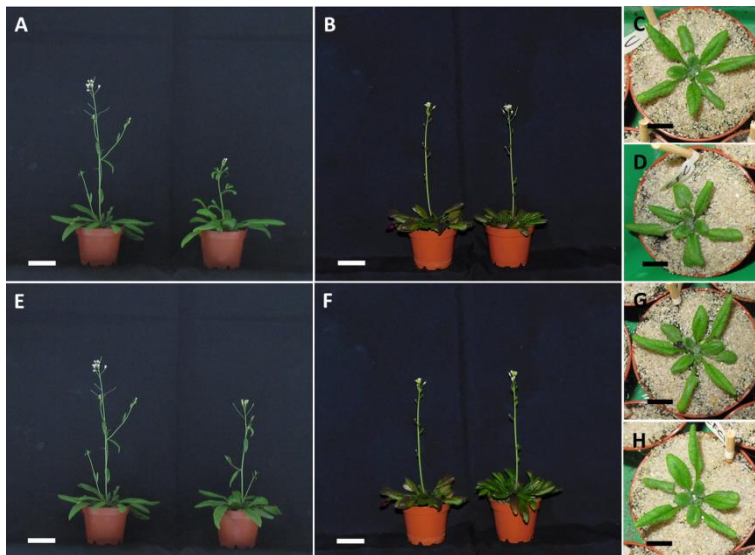


Figure 3.8.5: Result of the phenotypical analysis of EFC and EFC1.

(A), (B), (E), and (F) Plants of EFC and EFC1 grown in LD (A and E) and SD (B and F). In LD, EFC (A; right plant) and EFC1 (E; right plant) flower later than Col-0 (A and E; left plants). Under SD conditions, EFC (B; right plant) and EFC1 (F; right plant) flower with Col-0 (B and F; left plants). The rosettes of EFC (D) and EFC1 (H) do not show any features when compared to the wild-type (C and G). Scale bars: A, B, E, and F: 3cm; C, D, G, and H: 1cm.

In conclusion, the results demonstrate that an epigenetic inheritance of some features as observed for the offspring of heterozygous *ucn-1* plants can also be generated through the overexpression of *UCN* or *ucn-1*. An epigenetic inheritance of features observed for the overexpression lines is found for multiple plant organs (see table 3.8.4). The seed size on the other hand and, in case of EFC, the silique length is not inherited epigenetically.

Table 3.8.4: Summary of the analysis of the EMO offspring of the gain-of-function lines L1ox and C1ox compared to their T-DNA carrying ancestors.

Only affected plant organs are listed. Seed size = 2D seed area, Root length = main root length of five days old seedlings, FT = flowering time in long day (LD) and short day (SD). Numbers are in relation to the corresponding wild-types.

Characteristic	LUox	EFL	L1ox	EFL1	CUox	EFC	C1ox	EFC1
Seed size	105%	wild-type	89%	wild-type	85%	wild-type	116%	wild-type
Root length	53%	43%	61%	83%	47%	91%	92%	82%
FT (LD)	55%	61%	88%	90%	124%	115%	113%	109%
FT (SD)	66%	67%	87%	90%	wild-type	wild-type	wild-type	wild-type
Silique length	wild-type	wild-type	wild-type	105%	97%	wild-type	wild-type	wild-type
Silique shape	>2 fused carpels	>2 fused carpels	wild-type	wild-type	wild-type	wild-type	wild-type	wild-type

3.9 *UCN* is putatively involved in processes that affect flowering

The determination of flowering time is strongly regulated. Multiple processes are involved in this regulation. It comprises the processing of extrinsic signals, such as temperature and day-length and also intrinsic signals, such as plant age [1]. The transition to flowering is not only regulated genetically but also comes along with a chromatin change [103]. Therefore, not only the early flowering but also the epigenetic inheritance of this feature of *ucn-1* might indicate an involvement of *UCN* in flowering time determination. Thereby, a direct involvement in flowering transition in the SAM is unlikely, since *UCN* shows no expression in the meristem itself. This does not exclude a role for *UCN* in the promotion of flowering. Therefore, to address the question if *UCN* is involved in the process of flowering promotion, I further investigated the deregulation of the flowering time.

3.9.1 *UCN* interacts with *ATXR7* in yeast

With an Y2H screen that was previously performed to find proteins that interact with *UCN*, amongst others *ATXR7* was found as a candidate protein (unpublished data). Since *ATXR7* is known for being involved in flowering time regulation and *ucn-1* and also the *UCN* overexpression lines show deregulations in flowering time, the *UCN-ATXR7* relation was further investigated. To confirm the physical *UCN-ATXR7* interaction in yeast *ATXR7* (full CDS and in fragments) was tested for interaction with *UCN*. The fragmented *ATXR7* was used to avoid eventual auto-activation of the system, since *ATXR7* can interact with DNA which might result in an activation of the system and therefore a false positive result.

After mating, all SD-LW plates show growth (see figure 3.9.1, (A) to (G)) indicating that the mating worked out and the grown colonies carry both plasmids (AD and BD). On SD-LWH, growth is observed for colonies with the plasmid combinations #23, #25, #26, #36, #39 to #44, #71, #72, #81, and #93 to #105 (see figure 3.9.1(H) to (N); see also table S1 and S2 for combinations).

Combinations #23 and #81 are the positive controls with the combination *UCN-PDK1.2* while combination #1 is the negative control with two empty vectors. The growth of the positive controls in combination with the absence of growth in combination #1 promotes the functionality of the Y2H system.

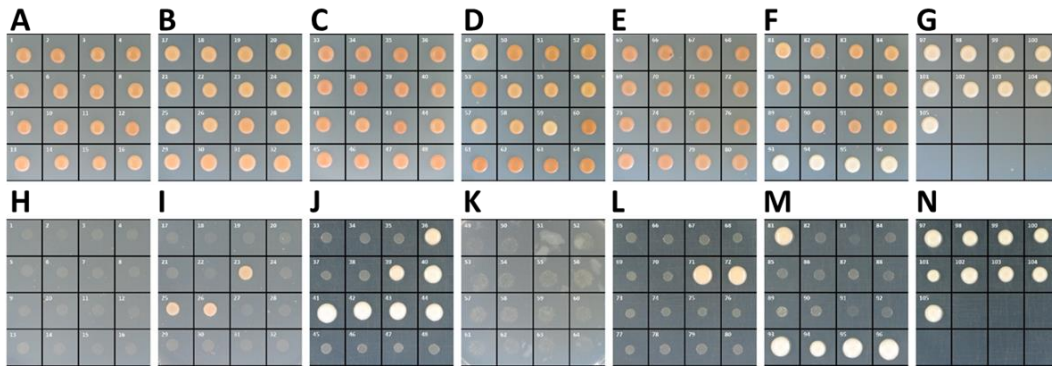


Figure 3.9.1: Y2H results after mating the colonies with the plasmid combinations of interest.

(A) to (G) SD-LW plates to verify the mating result: (A) Combinations #1 to #16, (B) Combinations #17 to #32, (C) Combinations #33 to #48, (D) Combinations #49 to #64, (E) Combinations #65 to #80, (F) Combinations #81 to #96, (G) Combinations #97 to #105. All combinations carry both plasmids (AD and BD) to check for possible interactions. (H) to (N) SD-LWH plates with interacting combinations (Combinations have the same order as in (A) to (G)). The following combinations show protein interaction: #23 (AD::*ATXR7* [frag. 7] and BD::*UCN*), #25 (AD::*PDK1.2* and BD::*UCN* (positive control)), #26 (AD::*ATXR7* [full protein] and BD::*UCN*), #36 (AD::*ATXR7* [frag. 7] and BD::*ucn-1*), #39 (AD::*ATXR7* [full protein] and BD::*ucn-1*), #40 to #44 (auto-activation: BD::*ATXR7* [frag. 1] combined with: #40: AD::empty, #41: AD::*UCN*, #42: AD::*ucn-1*, #43: AD::*PDK1.2*, #44: AD::*ATXR7* [full protein]), #71 (AD::*UCN* + BD::*ATXR7* [frag. 7]), #72 (AD::*ucn-1* + BD::*ATXR7* [frag. 7]), #81 (AD::*UCN* and BD::*PDK1.2*), #93 to #105 (auto-activation: BD::*ATXR7* [full protein] combined with: #93: AD::empty, #94: AD::*UCN*, #95: AD::*ucn-1*, #96 to #103: AD::*ATXR7* [fragments], #104: AD::*PDK1.2*, and #105: AD::*ATXR7* [full protein]). For further information see also supplemental information, tables S1 and S2.

The combinations that also show growth are #25, #26, #36, #39, #40, #41, #42, #43, #44, #71, #72, and #93 to #105. In combinations #40 to #44, BD::*ATXR7* (frag. 1) is involved, while in combinations #93 to #105, BD::*ATXR7* (full) is involved. Because of the one-sided activation of the Y2H system (only BD::*ATXR7* + X, not AD::*ATXR7* + X) this is most likely the expected auto-activation.

UCN interacts, regardless of the auto-activation in combinations #41 and #94 and the positive control #25 and #81, with *ATXR7* (frag. 7) in combinations #71 (AD::*UCN* – BD::*ATXR7frag7*), #23 (AD::*ATXR7frag7* – BD::*UCN*), and #26 (AD::*ATXR7full* – BD::*UCN*). The other *ATXR7* fragments show no growth in combination with *UCN*. Interestingly, the combinations that work for *UCN*, also work for *ucn-1*, which shows colony growth for combinations #36 (AD::*ATXR7frag7* – BD::*ucn-1*), #39 (AD::*ATXR7full* – BD::*ucn-1*), and #72 (AD::*UCN* – BD::*ATXR7frag7*). Although *ucn-1* is not interacting with *PDK1* (combinations #38 and #82), it might be able to still interact with *ATXR7*. The result indicates that an *ATXR7-UCN* as well as an *ATXR7-ucn-1* interaction is possible and the interaction domain in *ATXR7* is closely upstream of the SET domain.

3.9.2 *UCN* interacts with *ATXR7* in protoplasts

Since I was able to verify the interaction between *UCN* and *ATXR7* in yeast which is a relatively artificial system and in addition *ATXR7* was used as a fragmented protein, I

performed an additional interaction test using a bimolecular fluorescence complementation (BiFC) system. The BiFC system has the advantage that it is closer to plants than yeast since plant protoplasts are used for the test. In addition, since the system is not based on the interaction between DNA and protein, a full ATXR7 protein was used.

For the combinations pUC-SPYNE::*ATXR7* + pUC-SPYCE::*UCN* as well as vice versa (pUC-SPYNE::*UCN* + pUC-SPYCE::*ATXR7*) a nuclear signal can be observed (see figure 3.9.2A). The signal suggests that UCN and ATXR7 physically interact in protoplasts and that the interaction is restricted to the nucleus.

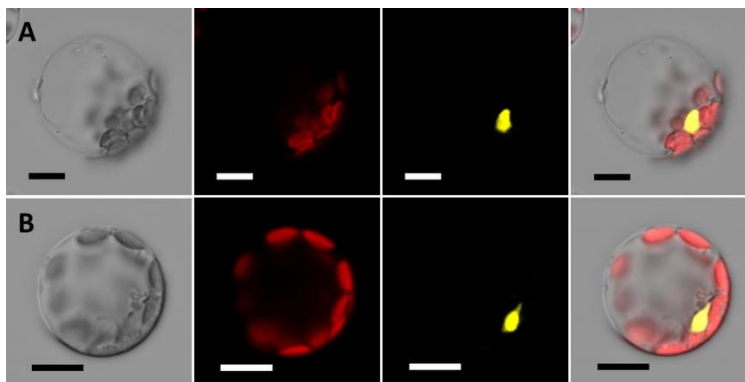


Figure 3.9.2: Result of the investigation of ATXR7-UCN interaction in protoplasts via BiFC.

Upper row: pUC-SPYCE::*ATXR7* + pUC-SPYNE::*UCN*; lower row: pUCN-SPYCE::*ATXR7* + pUC-SPYNE::*ucn-1*. The negative controls (combinations with empty vectors) show no signals (data not shown).

Because *ucn-1* interacted with an ATXR7 fragment in yeast, this interaction was also tested with the BiFC system in protoplasts. A nuclear signal was visible for the combinations pUC-SPYNE::*ATXR7* + pUC-SPYCE::*ucn-1* and pUC-SPYNE::*ucn-1* + pUC-SPYCE::*ATXR7* (see figure 3.9.2B). This result suggests that ATXR7 not only interacts with UCN but also with *ucn-1* in protoplasts. The ATXR7-*ucn-1* interaction is also restricted to the nucleus.

3.10 Testing the influence of ATXR7 on UCN and vice versa

To further test the relationship of ATXR7 on UCN and vice versa, I used the *atxr-1* single mutant. This mutant carries a loss-of-function mutation in *ATXR7* in the Col-0 background. ATXR7 is a trithorax-like protein that modifies chromatin structure by methylation of H3K4 and H3K36 [74]. It therefore enhances the expression of its targets. It was shown that *atxr7-1* flowers earlier than Col-0. The reason was claimed that genes repressing flowering are targets of ATXR7 [75]. In *atxr7-1*, these genes are not expressed properly and therefore, the repression of flowering is impaired. However, the focus of the

atxr7-1 investigation was set on flowering time. Therefore, I re-examined the mutant regarding the plant organs that are affected in the *UCN* loss- and gain-of-function lines.

3.10.1 Phenotypical characterization of *atxr7-1*

The *atxr7-1* mutant was described earlier, often regarding flowering time regulation [74, 75]. Here, I will re-examine the mutant regarding the features I found for *ucn-1* and *ucn-2*. Similarities in the phenotypes could indicate that *ATXR7* and *UCN* are involved in the same processes.

Flowers, ovules (including viability), germination rate, main root length, and siliques length and shape of *atxr7-1* were inconspicuous (see figure 3.10.1, 3.10.2B, C, and F, and 3.10.3C and D).

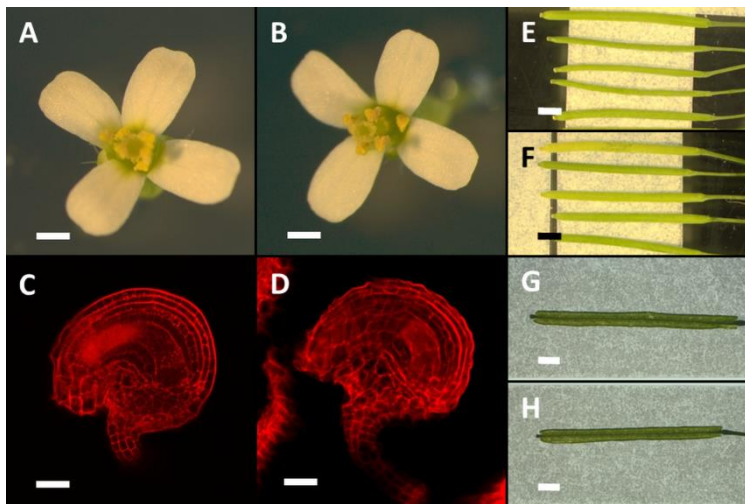


Figure 3.10.1: Result of the phenotypical characterization of the reproductive plant parts of *atxr7-1*. (A) and (B) Flowers of Col-0 (A) and *atxr7-1* (B). (C) and (D) Ovules of Col-0 (C) and *atxr7-1* (D). (E) to (H) Siliques of Col-0 (E) and *atxr7-1* (F). Open siliques of Col-0 (G) and *atxr7-1* (H). No embryo lethality is found. Scale bars: A/B = 500 μ m; C/D = 20 μ m; E to H = 2mm.

The analysis of the 2D seed area revealed that seeds of *atxr7-1* ($n = 96$) have an average surface of 100557 μ m². For Col-0 ($n = 82$), I measured an average 2D seed area of 74290 μ m² ($p = 2,97 * 10^{-29}$). Therefore, the average seed surface of *atxr7-1* is very close to the average seed area of *ucn-2* (100348 μ m², $p_{atxr7-1} = 0,9063$) (see figure 3.10.2A). This indicates that the loss-of-function of *ATXR7* has the same effect on seed size like the loss-of-function of *UCN*.

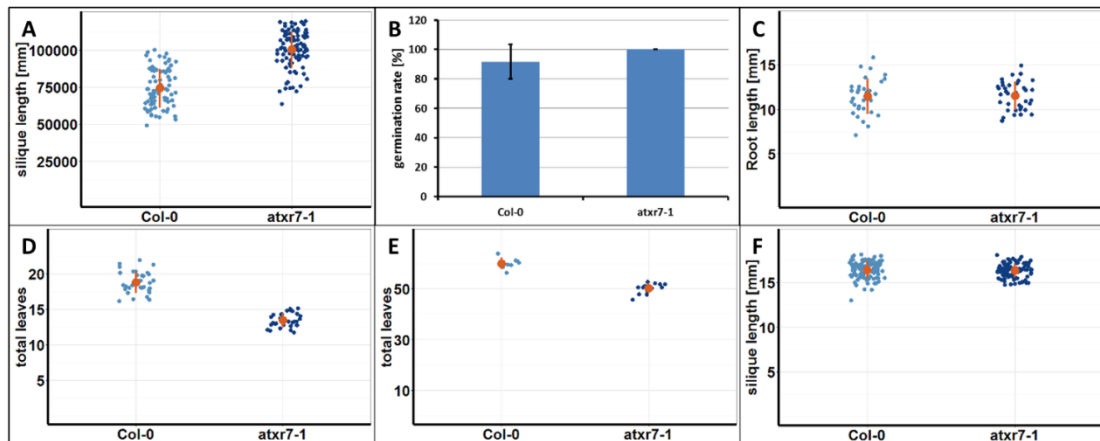


Figure 3.10.2: Analysis of the characteristics of *atxr7-1*.

(A) 2D seed area of *atxr7-1*. (B) Germination rate of *atxr7-1*. (C) Root length of *atxr7-1*. (D) Flowering time of *atxr7-1* in LD conditions. (E) Flowering time of *atxr7-1* in SD conditions. (F) Silique length of *atxr7-1*. Each blue dot represents one sample, brown dots with lines represent average with 1x standard deviation.

The flowering time of *atxr7-1* was also characterized. Here, former results were verified [74]. Under LD conditions, the *atxr7-1* mutant ($n = 30$) grows in average 13,4 total leaves ($p = 7,49 * 10^{-23}$). This is less total leaves than Col-0 ($n = 33$), which grows 18,8 total leaves until flowering (see figure 3.10.2D and 3.10.3A). This confirms former results that *atxr7-1* flowers early when grown under LD conditions.

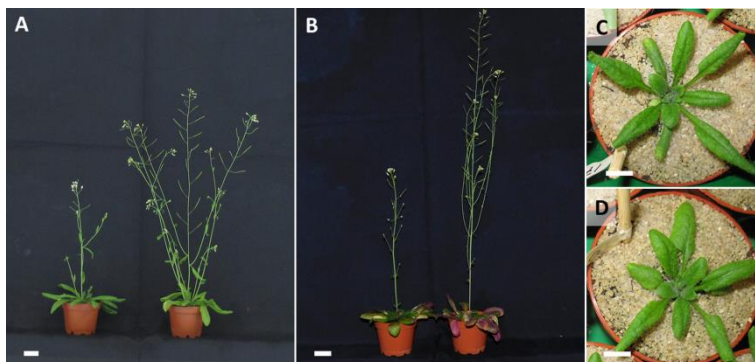


Figure 3.10.3: Phenotypal analysis of *atxr7-1*.

(A) and (B) Independent from LD (A) or SD (B) the *atxr7-1* mutant flowers early (A and B; right plants) compared to Col-0 (A and B; left plants). (C) and (D) The rosette of the *atxr7-1* mutant (C) also has no significant characteristics (compare to Col-0, (D)). Scale bars: A/B = 2cm, C/D = 1cm.

To analyze if the early flowering is independent of day-length, I also analyzed it under SD conditions. Here, *atxr7-1* ($n = 14$) grows in average 50,3 total leaves until flowering while Col-0 ($n = 8$) grows in average 60 total leaves ($p = 1,62 * 10^{-7}$) (see figure 3.10.2E and 3.10.3B). The result indicates that the early flowering of *atxr7-1* is independent of the length of day.

Table 3.10.1: Comparison between *atxr7-1*, *ucn-1*, and *ucn-2*.

Only affected plant organs are listed. Seed size = 2D seed area, Root length = main root length of five day old seedlings, FT = flowering time under long day (LD) and short day (SD) conditions. Numbers are given in relation to the corresponding wild-types.

Characteristic	<i>atxr7-1</i>	<i>ucn-1</i>	<i>ucn-2</i>
Flower shape	wild-type	affected	wild-type
Ovule shape	wild-type	protrusions	wild-type
Seed size	135%	82%	135%
Germination rate	wild-type	72%	wild-type
Root length	wild-type	56%	87%
FT (LD)	71%	75%	wild-type
FT (SD)	84%	77%	wild-type
Silique length	wild-type	85%	96%
Silique shape	wild-type	wild-type	wild-type

In conclusion, the *atxr7-1* mutant does not show a wide range of features. In addition to the early flowering, I only found an enhanced seed size (see table 3.10.1). Anyway, it should be mentioned that the seed size coincides with the seed size of *ucn-2*.

3.10.2 Phenotypical characterization of *atxr7-1 ucn-2*

To further verify the involvement of *ATXR7* and *UCN* in the same processes or maybe even in the same pathways, I generated *atxr7-1 ucn-2* double mutants. Features observed in *atxr7-1* and/or *ucn-2* should not be further enhanced in the double mutant. Therefore, the double mutant was analyzed regarding the common features analyzed above and compared to the *atxr7-1* and *ucn-2* single mutants.

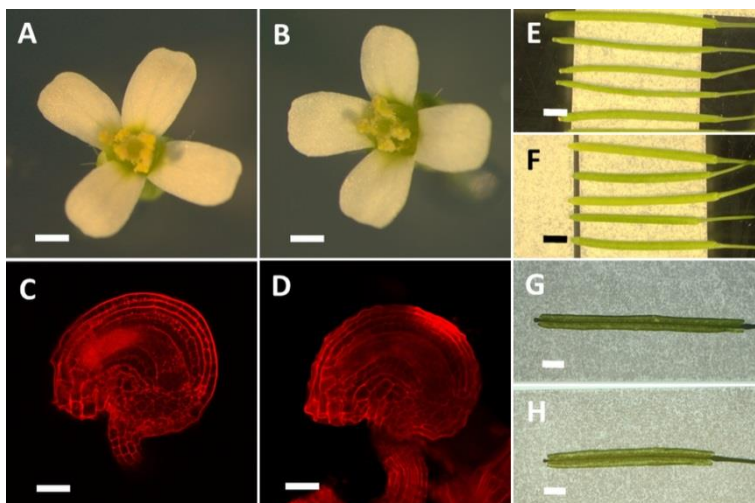


Figure 3.10.4: Result of the phenotypical characterization of the reproductive plant parts of *atxr7-1 ucn-2*.

(A) and (B) Flowers of Ler (A) and *atxr7-1 ucn-2* (B). (C) and (D) Ovules of Ler (C) and *atxr7-1 ucn-2* (D). (E) to (H) Siliques of Ler (E) and *atxr7-1 ucn-2* (F). Open siliques of Ler (G) and *atxr7-1 ucn-2* (H). No embryo lethality is found. Scale bars: A/B = 500µm; C/D = 20µm; E to H = 2mm.

Again, the flowers and ovules did not show any features. The same is true for the other above-ground plant organs (see figure 3.10.4A to D and 3.10.6A and C). This indicates that there are no new features observed in the double mutant when compared to each single mutant. The same holds true for germination rate (see figure 3.10.5B).

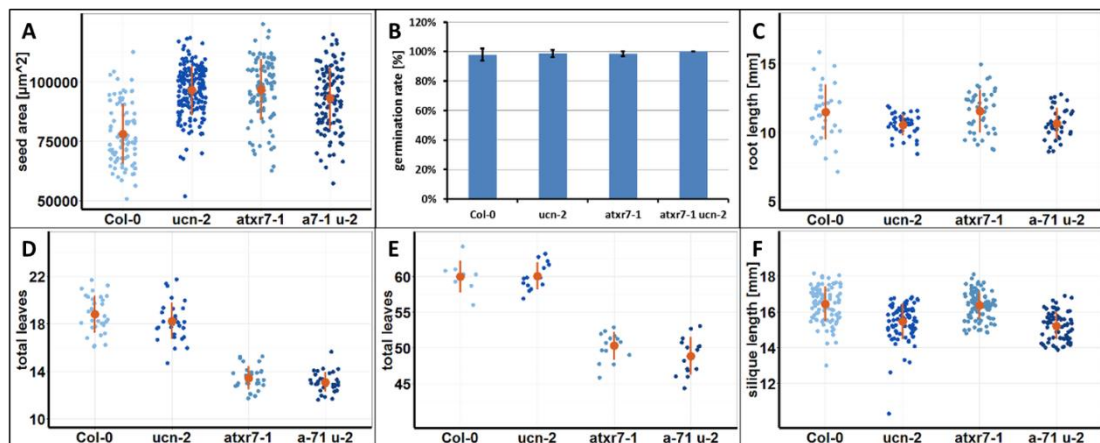


Figure 3.10.5: Analysis of the characteristics of *atxr7-1 ucn-2*.

(A) 2D seed area of *atxr7-1 ucn-2*. (B) Germination rate of *atxr7-1 ucn-2*. (C) Root length of *atxr7-1 ucn-2*. (D) Flowering time of *atxr7-1 ucn-2* in LD conditions. (E) Flowering time of *atxr7-1 ucn-2* in SD conditions. (F) Silique length of *atxr7-1 ucn-2*. Each blue dot represents one sample, brown dots with lines represent average with 1x standard deviation.

The investigation of the 2D seed surface revealed that the double mutant *atxr7-1 ucn-2* produces bigger seeds than the wild-type (see figure 3.10.5A). While the average 2D seed area of Col-0 ($n = 93$) is $78127\mu\text{m}^2$, the average 2D seed surface of *atxr7-1* seeds ($n = 101$) is $96783\mu\text{m}^2$ ($p = 5,8 * 10^{-20}$) and the average 2D seed surface of *ucn-2* ($n = 176$) is $96485\mu\text{m}^2$ ($p = 2,7 * 10^{-24}$). The difference in the 2D seed surface between the two single mutants is not significant ($p = 0,8422$) indicating the same seed size for *atxr7-1* like for *ucn-2*. The seeds of the double mutant ($n = 121$) have in average a 2D seed area of $93186\mu\text{m}^2$ ($p = 2,4 * 10^{-15}$). This is slightly smaller than the 2D seed area of each single mutant ($p_{ucn-2} = 0,0207$, $p_{atxr7-1} = 0,0389$). However, this result suggests that there is no additive or enhancing effect of *atxr7-1* and *ucn-2* regarding seed size.

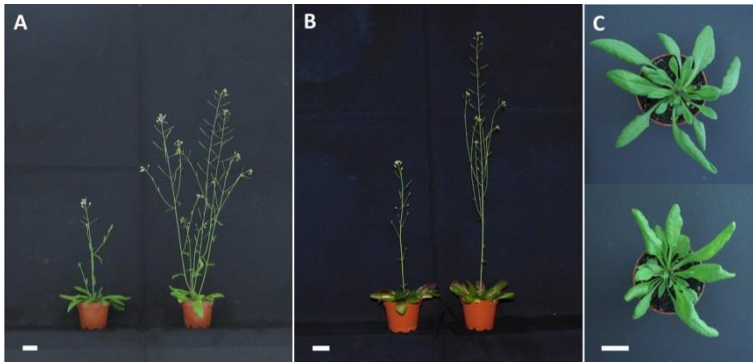


Figure 3.10.6: Phenotypic analysis of *atxr7-1 ucn-2*.

(A) and (B) Independent from LD (A) or SD (B) the *atxr7-1 ucn-2* double mutant flowers early (A and B; right plants) compared to Col-0 (A and B; left plants). (C) The rosette of the double mutant (lower plant, stem removed) also has no significant characteristics (compare to Col-0, upper plant, stem removed). Scale bars = 2cm.

The analysis of the main root length of five day old seedlings revealed that *atxr7-1 ucn-2* double mutants grow in average a 10,6mm ($p = 0,04576$) long root while the wild-type ($n = 32$) grows a root of in average 11,5mm length (see figure 3.10.5C). The result indicates that the double mutants grow a slightly smaller root than the wild-type. Hence, the average root length of the double mutants is close to the average root length of *ucn-2*.

Under LD conditions the flowering time of *atxr7-1 ucn-2* does not differ from the flowering time of *atxr7-1*. Both lines flower earlier than Col-0 ($n = 33$) or *ucn-2* ($n = 30$) which start flowering with in average 18,8 total leaves and 18,2 total leaves, respectively. The single mutant *atxr7-1* ($n = 30$) starts flowering with in average 13,4 total leaves ($p = 7,49 * 10^{-25}$) while the double mutant *atxr7-1 ucn-2* ($n = 33$) starts flowering with in average 13,1 total leaves ($p = 8,18 * 10^{-24}$) (see figure 3.10.5D and 3.10.6A). Thus, the difference between *atxr7-1* and *atxr7-1 ucn-2* is not significant ($p = 0,1423$). This result indicates that *ucn-2* has no influence on the early flowering of *atxr7-1*.

The analysis of the silique length revealed that siliques of *atxr7-1 ucn-2* ($n = 72$) have in average a length of 15,2mm. Therefore, the double mutant has slightly shorter siliques than the wild-type ($n = 93$) which grows in average siliques that are 16,4mm long ($p = 0,08576$) (see figure 3.10.5F). This result is comparable with the result of the root length. The mutation of *atxr7-1* has no influence on the silique size and it is not able to enhance the decrease of silique size of *ucn-2* either. The shape of the siliques was inconspicuous and it does not bear degenerated ovules (see figure 3.10.4E to H).

I also checked if the early flowering of the double mutant is independent from day-length by growing it under SD conditions. In SD the double mutant ($n = 15$) flowers with

in average 48,9 total leaves ($p = 9,05 * 10^{-9}$). This is significantly earlier than the wild-type ($n = 8$) or *ucn-2* ($n = 14$) which starts flowering with in average 60 and 60,1 total leaves, respectively. The *atxr7-1* single mutant ($n = 14$) starts flowering with in average 50,3 total leaves (see figure 3.10.5E and 3.10.6B). Therefore, the difference in early flowering between *atxr7-1* and *atxr7-1 ucn-2* is not significant ($p = 0,1121$). Hence, the early flowering of *atxr7-1* and *atxr7-1 ucn-2*, respectively, is independent of the length of day.

In conclusion, the double mutant *atxr7-1 ucn-2* does not show any new features compared to the single mutants. Furthermore, no features observed for the single mutants *atxr7-1* and *ucn-2* are enhanced or rescued (see table 3.10.2). The results therefore suggest that at least in seed size determination, *ATXR7* and *UCN* act in the same pathway.

Table 3.10.2: Summary of the phenotypical features of *atxr7-1*, *ucn-2*, and the double mutant *atxr7-1 ucn-2*.

Only affected plant organs are listed. Seed size = 2D seed are, Root length = main root length of five day old seedlings, FT = flowering time in long day (LD) and short day (SD) conditions. Numbers are given in relation to the corresponding wild-types.

Characteristic	<i>ucn-2</i>	<i>atxr7-1</i>	<i>atxr7-1 ucn-2</i>
Seed size	123%	124%	119%
Root length	87%	wild-type	92%
FT (LD)	wild-type	71%	70%
FT (SD)	wild-type	84%	82%
Silique length	96%	wild-type	93%

3.11 Overexpressing *ATXR7*

The results above indicate that it is likely that *ATXR7* and *UCN* are involved in the same pathways to determine seed size. Also a common role for flowering time regulation cannot be completely excluded. To gain more insight into the processes where *ATXR7* and/or *UCN* is involved in and also to better understand *ATXR7*, I also generated gain-of-function lines for *ATXR7*. This further has the advantage that a gain-of-function can also be generated in *Ler* background where a loss-of-function line is missing. Thus, the role of *ATXR7* can also be compared between the two accessions *Ler* and *Col-0*. Therefore, a pUBQ::*ATXR7* construct was transformed into *Col-0* and *Ler*, respectively. Three independent T_1 lines were then chosen and inbred until I received homozygous T_3 lines. These lines are further called LAox for Landsberg *ATXR7* overexpressed and CAox for Colombia *ATXR7* overexpressed), respectively.

3.11.1 Overexpression of *ATXR7* in wild-type plants

The gain-of-function lines were first characterized regarding the plant organs as above. If no other plant organs are harmed as found before in the *atxr7-1* mutant this would verify that *ATXR7* is most likely not involved in more processes than seed size development and flowering time determination. I also used these gain-of-function lines to compare the role of *ATXR7* in the two different accessions *Ler* and *Col-0*.

The flowers and ovules of LAox as well as of CAox are inconspicuous (see figure 3.11.1A to D and I to L). The same holds true for the germination rate (see figure 3.11.2B and H).

The analysis of the 2D seed area revealed a background dependent result. The seeds of CAox show a bigger 2D surface than seeds of *Col-0* while seeds of LAox almost have the same size as *Ler* (see figure 3.11.2A and G). Seeds of CAox ($n = 122$) have an average 2D seed area of $110600\mu\text{m}^2$ and are therefore bigger than the seed of *Col-0* ($n = 204$), which is in average $87436\mu\text{m}^2$ ($p = 1,8 * 10^{-38}$) (see figure 3.11.2A). In contrast, seeds of LAox ($n = 126$) have an average seed size of $89469\mu\text{m}^2$, which is pretty close to the average 2D seed area of the $86761\mu\text{m}^2$ that *Ler* ($n = 103$) shows ($p = 0,3238$) (see figure 3.11.2G). The result suggests that the gain-of-function of *ATXR7* is able to influence seed size in *Col-0* but not in *Ler*.

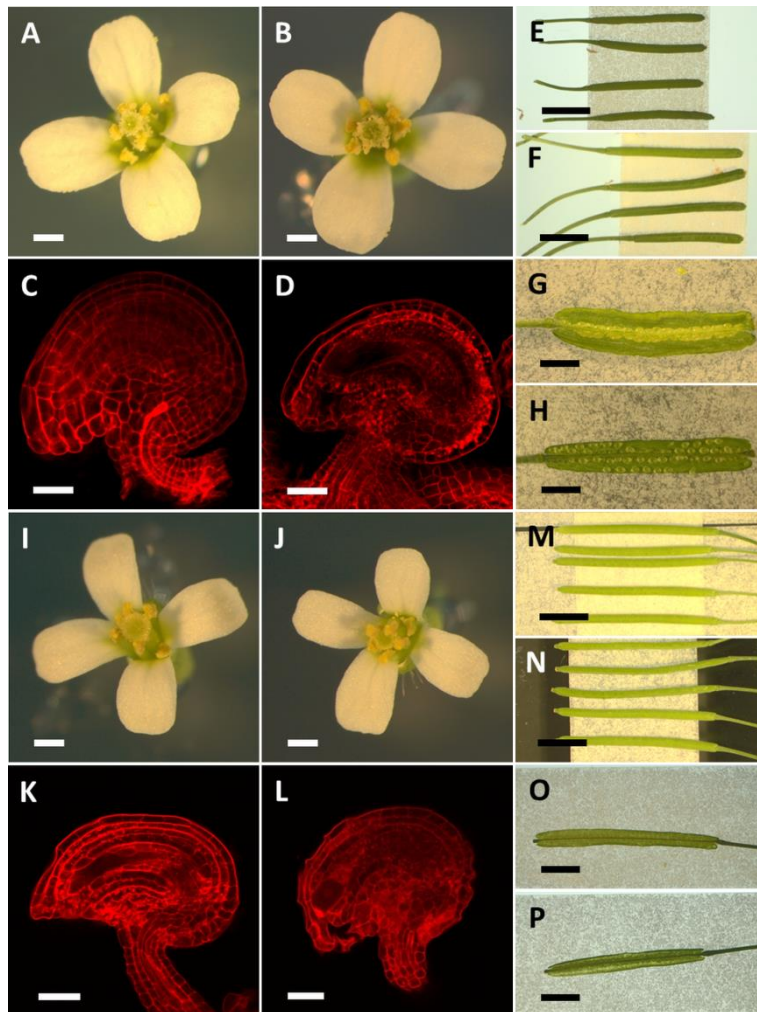


Figure 3.11.1: Analysis of the reproductive organs of LAox (A to H) and CAox (I to P).

(A), (B), (I), and (J) The flowers of LAox (B) and CAox (J) do not differ in shape or organ number from *Ler* (A) or *Col-0* (I). (C), (D), (K), and (L) The ovules of LAox (D) and CAox (L) also show no features compared to *Ler* (C) and *Col-0* (K), respectively. (E) to (H) and (M) to (P) The silique shape of LAox (F) and CAox (N) does also not differ from *Ler* (E) or *Col-0* (M). Embryo lethality cannot be found in siliques of LAox (H) or CAox (P) (compare to *Ler* (G) and *Col-0* (O)). Scale bars: A, B, I, J = 500 μ m; C, D, K, L = 20 μ m; E, F, M, N = 5mm; G, H, O, P = 2mm.

The analysis of the root size revealed no difference between CAox and *Col-0* (see figure 3.11.2C) and a smaller root of LAox compared to *Ler* (see figure 3.11.2I). Five day old seedlings of *Ler* ($n = 23$) grow an average root length of 10,3mm whereas five day old seedlings of LAox ($n = 29$) grow in average a root length of 8,6mm ($p = 0,01917$) and therefore a smaller root (see figure 3.11.2I). This indicates that in case of *Ler*, the gain-of-function of *ATXR7* has a negative influence on root growth while in case of *Col-0* the gain-of-function of *ATXR7* has no influence on root growth.

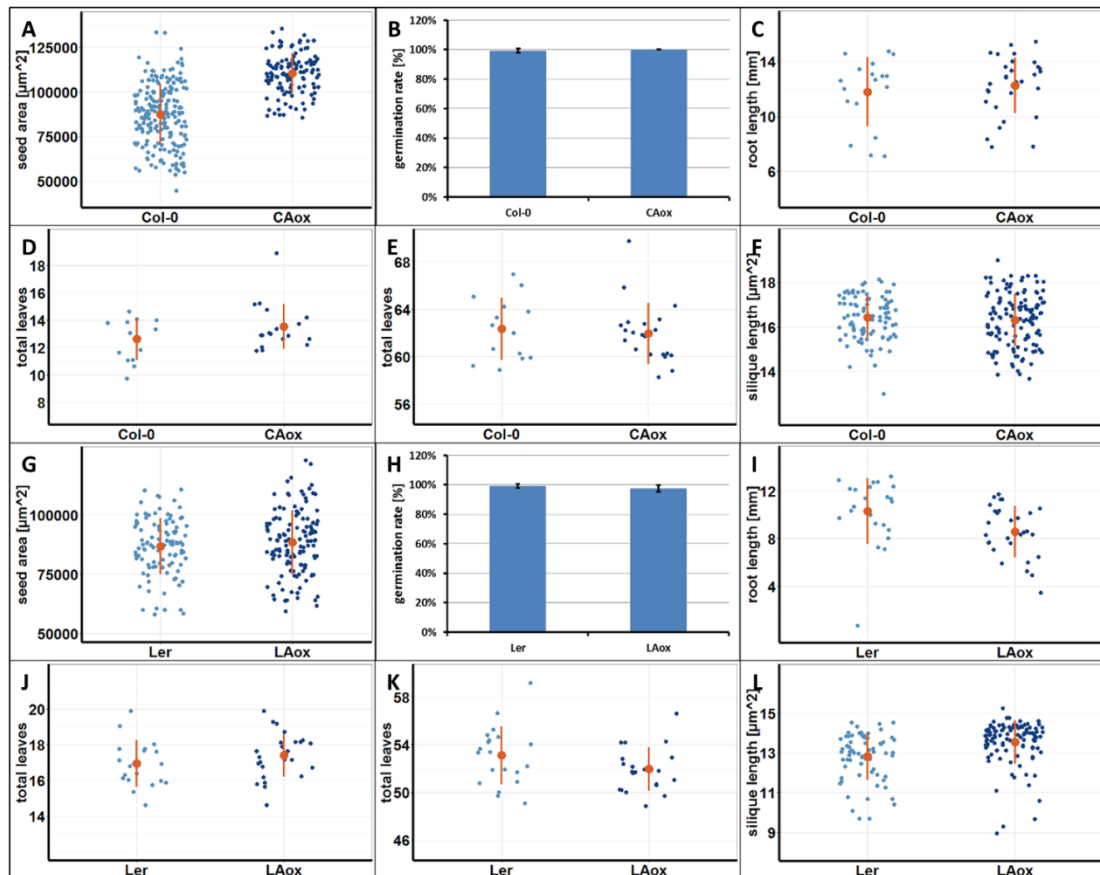


Figure 3.11.2: Analysis of the characteristics of CAox (A to F) and LAox (G to L).

(A) 2D seed area of CAox compared to Col-0. (B) Germination rate of CAox. (C) Root length of CAox seedlings, 5dag. (D) Flowering time of CAox in LD conditions. (E) Flowering time of CAox in SD conditions. (F) Silique length of CAox. (G) 2D seed area of LAox compared to Ler. (H) Germination rate of LAox. (I) Root length of LAox seedlings, 5dag. (J) Flowering time of LAox in LD conditions. (K) Flowering time of LAox when grown in SD. (L) Silique length of LAox. Each blue dot represents one sample, brown dots with lines represent the average with standard deviation.

The analysis of the flowering time under LD conditions revealed that, interestingly, the gain-of-function of *ATXR7* has no influence independent of the background (see figures 3.11.2D and J and 3.11.3A and D). LAox as well as CAox start flowering like the wild-type. This also holds true when grown under SD conditions (see figure 3.11.2E and K and 3.11.3B and E). The result indicates that the gain-of-function of *ATXR7* has, in contrast to the loss-of-function, no influence on flowering time.

The analysis of the silique length showed an influence of the gain-of-function in *Ler* background but not in Col-0 (see figure 3.11.2F and L). LAox ($n = 102$) grows siliques which are in average 13,5mm long. These siliques are bigger than siliques of *Ler* ($n = 68$), that grows siliques that are in average 12,8mm long ($p = 9,99 \cdot 10^{-5}$). Anyway, independent of background the siliques all show wild-type shape and also no degenerated ovules (see figure 3.11.1E to H and M to P). The results indicate that *ATXR7* might have a slight influence on silique length but exclusively in *Ler* background.

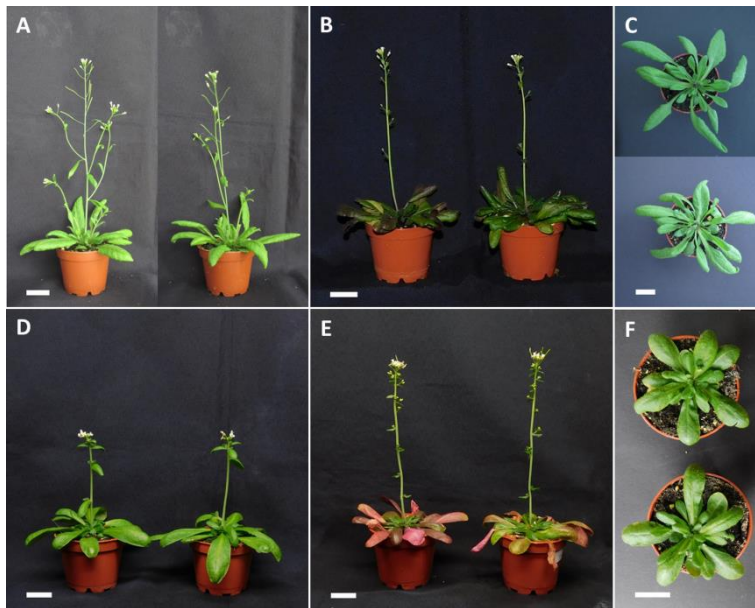


Figure 3.11.3: Phenotypal analysis of CAox and LAox.

(A), (B), (D), and (E) Plants overexpressing *ATXR7* in Col-0 background (A and B, right plants) or *Ler* background (D and E, right plants) flower the same time like the corresponding wild-type (A, B, D, and E; left plants) independent from LD (A and D) or SD (B and E). (C) and (F) The rosettes of plants overexpressing *ATXR7* in Col-0 (C; lower plant) or *Ler* (F; lower plant) also show no special features when compared to Col-0 (C; upper plant) or *Ler* (F; upper plant). Scale bars = 2cm.

In conclusion, the gain-of-function of *ATXR7* only has mild effects on the investigated plant organs and no effect is observed on common organs of both accessions. In case of Col-0, *ATXR7* overexpression only effects seed size, while in *Ler*, root and silique length are affected. Further, no opposite effects were observed compared to *atxr7-1*. This holds also true for the flowering time where the gain-of-function starts flowering like the wild-type (see table 3.11.1).

Table 3.11.1: Comparison of the loss-of-function line *atxr7-1* to its gain-of-function lines LAox and CAox.

Only affected plant organs are listed. Seed size = 2D seed area, Root length = main root length of five day old seedlings, FT = flowering time under long day (LD) and short day (SD) conditions. Numbers are in relation to the corresponding wild-types.

Characteristic	<i>atxr7-1</i>	LAox	CAox
Seed size	124%	wild-type	126%
Root length	wild-type	83%	wild-type
FT (LD)	71%	wild-type	wild-type
FT (SD)	84%	wild-type	wild-type
Silique length	wild-type	105%	wild-type

3.11.2 Overexpressing *ATXR7* and *UCN* in wild-type plants

The double mutant *atxr7-1 ucn-2* indicated that *UCN* and *ATXR7* could be involved in the same processes and pathways, respectively, at least in seed size determination. The

results could not yet be interpreted regarding for example epistasis. In addition, a loss-of-function mutant of *ATXR7* is not available in *Ler* background. Therefore, to get more insight into the relationship of *UCN* and *ATXR7*, I generated double gain-of-function lines. Comparable to the double mutant *atxr7-1 ucn-2* these lines ideally do not add up in the features they are showing. This should shed more light on the question which gene is epistatic to the other.

For the double gain-of-function line I transformed a double overexpression construct pUBQ::*ATXR7* pUBQ::*UCN* into Col-0 (further called CAUox for **Col-0 ATXR7/UCN overexpression** line) and *Ler* (further called LAUox for **Ler ATXR7/UCN overexpression** line). Again, three independent T₁ plants of CAUox were inbred until I received homozygous T₃ lines which were then used for the characterization of the common plant organs and flowering time. For LAUox I only characterized the T₁ generation. Therefore, some phenotypical characterizations were not possible.

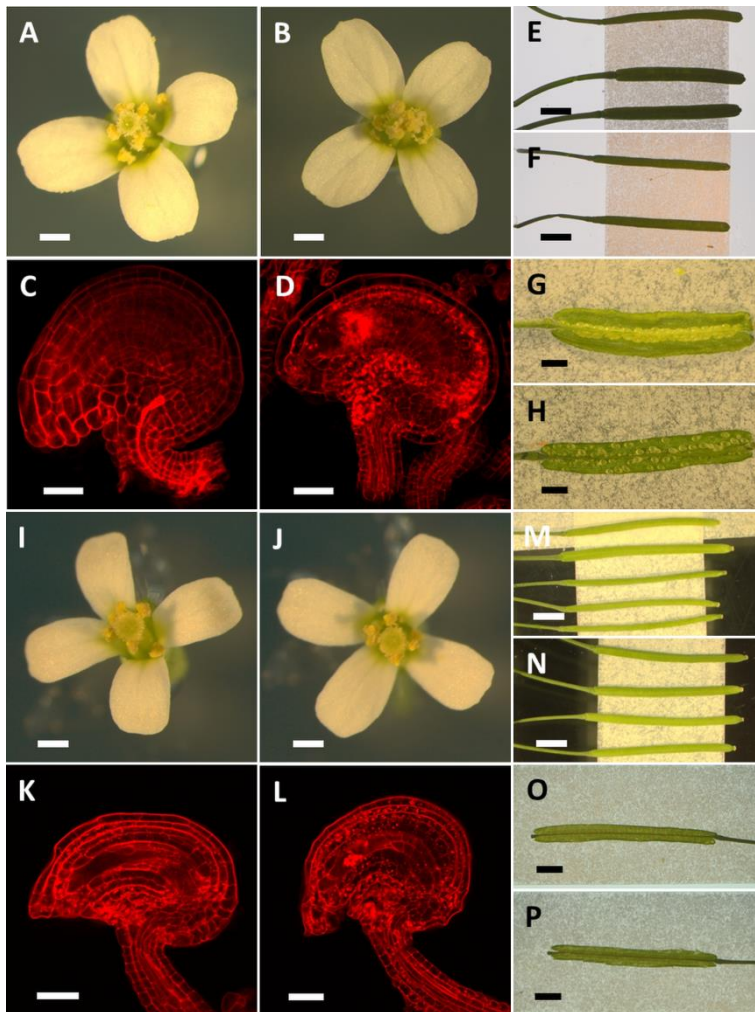


Figure 3.11.4: Analysis of the reproductive organs of LAUox (A to H) and CAUox (I to P).

(A), (B), (I), and (J) The flowers of LAUox (B) and CAUox (J) are indistinguishable from *Ler* (A) or *Col-0* (I) flowers. (C), (D), (K), and (L) The ovules of LAUox (D) and CAUox (L) also show no specialties compared to *Ler* (C) or *Col-0* (K) ovules. (E) to (H) and (M) to (P) The siliques of LAUox (F) and CAUox (N) are also shaped like wild-type siliques of *Ler* (E) or *Col-0* (M). Embryo lethality is not observed either, neither in LAUox (H) nor in CAUox (P) (compare to *Ler* (G) and *Col-0* (O), respectively). Scale bars: A, B, I, J = 500 μ m; C, D, K, L = 20 μ m; E, F, M, N = 3mm; G, H, O, P = 2mm.

The reproductive organs of LAUox and CAUox show no specialties compared to the wild-types *Ler* and *Col-0*. Neither the flowers nor the ovules show any striking characteristics (see figure 3.11.4A to D and I to L). Also the germination rate is inconspicuous (see figure 3.11.5B).

The determination of the 2D seed area of CAUox revealed that the seed surface measured for the double overexpression line is almost the same like the seed surface of the wild-type (see figure 3.11.5A). In average, the 2D seed area of CAUox ($n = 258$) is 88737 μ m² while the 2D seed area of wild-type seeds ($n = 204$) is in average 87436 μ m² ($p = 0,4044$). Since CUox shows a small decrease in seed area and CAox has a bigger 2D seed area than

the wild-type, this result indicates that the overexpression of *UCN* and *ATXR7* at the same time neutralizes the effects of each other.

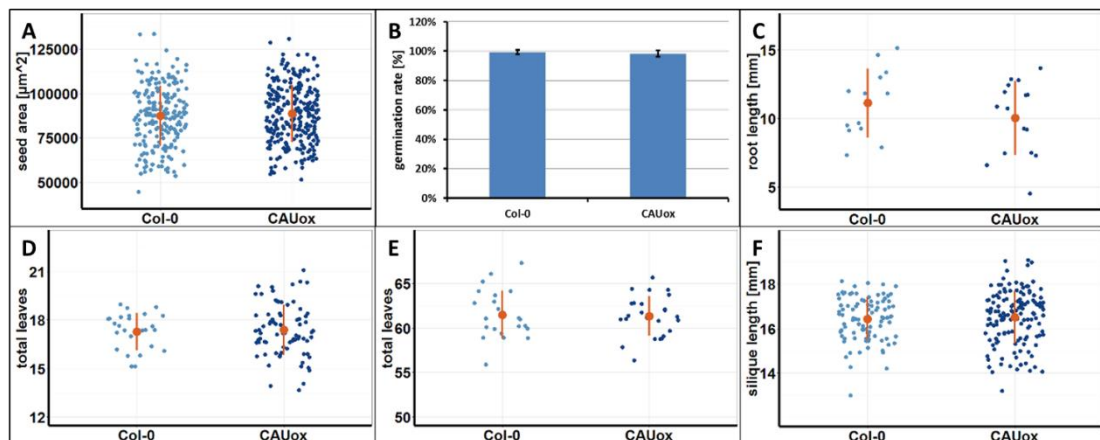


Figure 3.11.5: Analysis of the characteristics of CAUox.

(A) 2D seed area of CAUox compared to Col-0. (B) Germination rate of CAUox. (C) Root length of CAUox seedlings, 5dag. (D) Flowering time of CAUox in LD. (E) Flowering time of CAUox when grown in SD. (F) Silique length of CAUox. Each blue dot represents one sample, brown dots with lines represent average with 1x standard deviation.

The analysis of the root length of five day old seedlings revealed that in average, seedlings of CAUox ($n = 16$) have a root of 10,0mm length while wild-type seedlings of the same age ($n = 13$) have a root of 11,1mm length ($p = 0,2736$) (see figure 3.11.5C). Therefore, the smaller root of CUox seedlings is rescued by the overexpression of *ATXR7*.

The determination of the flowering time of CAUox demonstrates that in LD, CAUox ($n = 76$) starts flowering with in average 17,4 total leaves which is almost the same number of total leaves as Col-0 ($n = 26$) that starts flowering with in average 17,3 total leaves ($p = 0,6971$) (see figure 3.11.5D and 3.11.6A). In *Ler*, the T_1 generation of LAUox ($n = 38$ independent transformants) starts flowering with in average 14,2 total leaves. This is slightly later than the wild-type ($n = 10$) which starts flowering with in average 11,5 total leaves. In this experiment, LAox ($n = 29$) starts flowering with in average 12,4 total leaves and LUox ($n = 26$) starts flowering with in average 7,4 total leaves (see figure 3.11.6D and 3.11.7). Thus, the early flowering of LUox and the late flowering of CUox is rescued by the parallel overexpression of *ATXR7*.

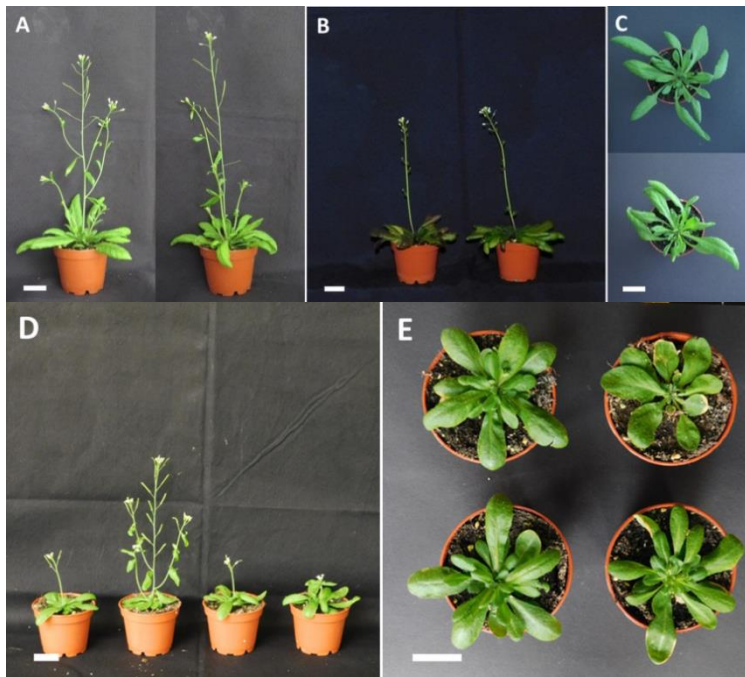


Figure 3.11.6: Phenotypal analysis of CAUox and LAUox.

The overexpression of *ATXR7* rescues the phenotype which the overexpression of *UCN* causes to wild-type plants. (A) and (B) The flowering time of CAUox in LD (A; right plant) as well as in SD (B; right plant) is the same as the flowering time of Col-0 (A and B; left plants). (C) Regarding the rosette of CAUox (C; lower plant) there are no special features compared to the wild-type rosette (C; upper plant). (D) LAUox starts flowering close to the wild-type when grown in LD (D; rightmost plant) and therefore just like wild-type (D; leftmost plant) and LAox (D; 3rd plant from the left). Hence, it rescues the early flowering of LUox (D; 2nd plant from the left). (E) In addition to the flowering time, the rosette shape of LAUox (E; lower right) is like the shape of the wild-type (E; upper left) and LAox (E; lower left), respectively, and not roundish like the rosette shape of LUox (E; upper right). Scale bars = 2cm.

I also investigated the flowering time of CAUox under SD conditions. Here, the double overexpression line ($n = 26$) starts flowering with in average 62,4 total leaves, which is not different from the 62,4 total leaves that Col-0 ($n = 22$) grows in average until the first flower opens (see figure 3.11.5E and 3.11.6B). Hence, like the single gain-of-function lines, the double gain-of-function line flowers like the wild-type when grown in SD.

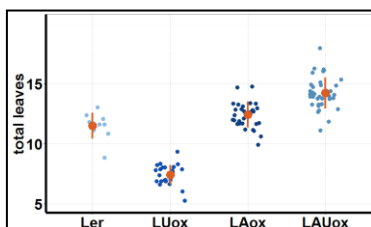


Figure 3.11.7: Flowering time of a T_1 generation of LAUox.

Figure shows the flowering time of 38 independent T_1 plants of LAUox compared to *Ler*, LUox, and LAox. Each blue dot represents one sample, brown dots with lines represent average with 1x standard deviation.

An analysis of the silique length revealed that CAUox grows siliques of a similar size than the wild-type. In average, siliques of CAUox ($n = 140$) have a length of 16,5mm compared to the average silique length of Col-0 ($n = 93$) which is 16,4mm ($p = 0,5550$) (see

figure 3.11.5F). The silique shape of CAUox is inconspicuous and no degenerated ovules are observed (see figure 3.11.4M to P). This was also the case for siliques of LAUox. I found no more siliques with more than two fused carpels. In addition, LAUox does not show ovule degeneration (see figure 3.11.4E to H). The result suggests that the negative influence of the *UCN* overexpression can be buffered by overexpression of *ATXR7* to rescue silique length in Col-0 and silique shape and ovule viability in *Ler*.

In addition to the phenotypical rescue of the LAUox siliques, the overall phenotype related to LUox is also rescued. The stature is not compressed anymore and the rosette leaves show the lanceolatic form instead of a roundish shape (see figure 3.11.6D and E). The result indicates that the parallel overexpression of *ATXR7* neutralizes the phenotypical characteristics of the *UCN* overexpression independent from the background.

In conclusion, the overexpression of *ATXR7* can neutralize all features observed for the *UCN* gain-of-function lines (see table 3.11.2). In case of LAUox, the flowering time was delayed compared to *Ler*. This might be a T_1 specific effect (see discussion).

Table 3.11.2: Comparison of the single *ATXR7* and *UCN* gain-of-function lines to the *ATXR7 UCN* double gain-of-function lines.

Only affected plant organs are listed. Seed size = 2D seed area, Root length = main root length of five day old seedlings, FT = flowering time under long day (LD) and short day (SD) conditions. All numbers are given in relation to the corresponding wild-types.

Characteristic	LAox	LUox	LAUox	CAox	CUox	CAUox
2D seed area	wild-type	105%	no data	126%	85%	wild-type
Root length	83%	53%	no data	wild-type	47%	wild-type
FT (LD)	108%	64%	123%	wild-type	124%	wild-type
FT (SD)	wild-type	66%	no data	wild-type	wild-type	wild-type
Silique length	105%	wild-type	no data	wild-type	97%	wild-type
Silique shape	wild-type	>2 fused carpels	wild-type	wild-type	wild-type	wild-type

3.11.3 Overexpressing *ATXR7* in *ucn-1* and *ucn-2*

The rescue of the effects of the *UCN* overexpression in wild-types by overexpressing *ATXR7* might be due to a posttranslational repression of *UCN* by *ATXR7*. Since *ATXR7* can possibly interact with *ucn-1* and maybe *ucn-2*, this raises the question if characteristics of *ucn-2* and especially *ucn-1* can also be rescued by the overexpression of *ATXR7* and therefore blocking the negative influence of *ucn-1*. To answer this question, the *ATXR7* overexpression construct pUBQ::*ATXR7* was transformed into *ucn-1* and *ucn-2*. Three independent T_1 lines per transformation into *ucn-1* and *ucn-2* were inbred until I gained

homozygous T_3 lines I worked with. For further reading the *ucn-1* mutants carrying pUBQ::*ATXR7* are called 1Aox (for *ucn-1* *ATXR7* overexpression line) and the *ucn-2* mutants carrying pUBQ::*ATXR7* are called 2Aox (for *ucn-2* *ATXR7* overexpression line).

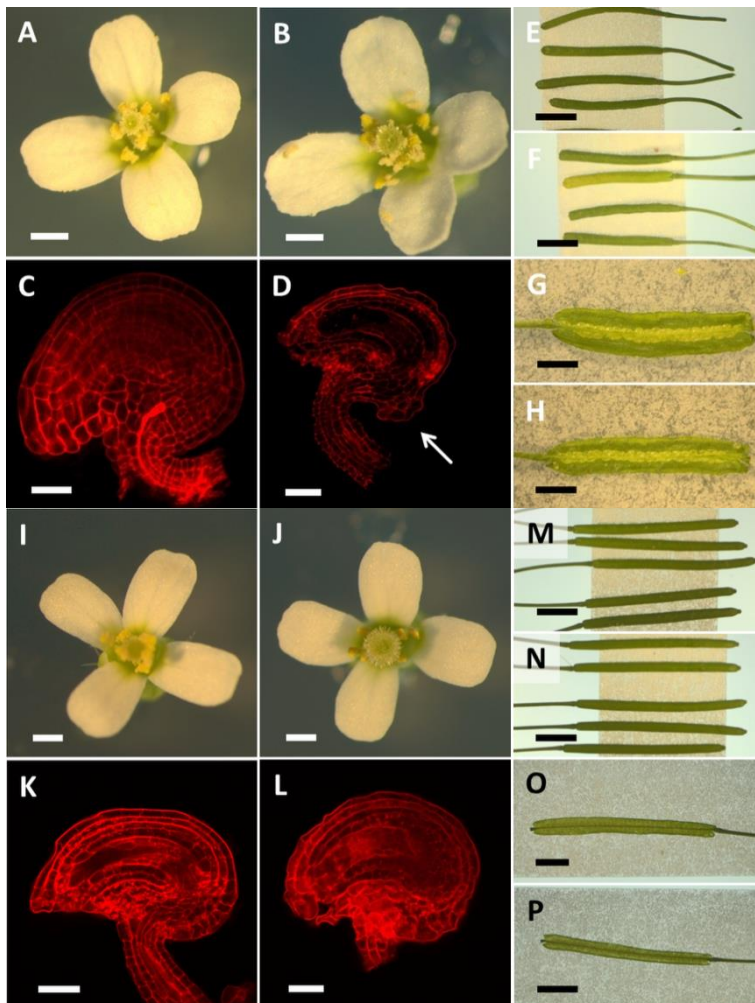


Figure 3.11.8: Phenotypal analysis of the reproductive organs of 1Aox and 2Aox.

(A) and (B) The overexpression of *ATXR7* in *ucn-1* partially rescues the flower shape. The flower shape of 1Aox (B) is much closer to *Ler* (A) than to *ucn-1* (compare also to figure 3.2.1). (C) and (D) The protrusions of the integuments are not rescued. The ovules of 1Aox (D, arrow) still show outgrowths. These are never observed on *Ler* ovules (C). (E) to (H) The siliques of 1Aox (F) are smaller than the siliques of *Ler* (E), although the siliques of 1Aox (H) contain a lot less degenerated ovules than *ucn-1* (compare also to figure 3.2.1). (I) to (P) The reproductive organs of 2Aox are inconspicuous. Flowers (J) and ovules (L) show no differences compared to wild-type flowers (I) and ovules (K). The siliques of 2Aox (N) also show no special features compared to *Col-0* (M) neither do the siliques of 2Aox (P) contain degenerated ovules (O = wild-type). Scale bars: A, B = 500 μ m; C, D = 20 μ m; E, F: 4mm; G, H: 2mm.

An analysis of the flowers and ovules of 2Aox showed no differences compared to the flowers of the wild-type, *ucn-2*, or CAox (see figure 3.11.8I to L). The flowers of 1Aox are partially rescued. Compared to *ucn-1*, which shows a very striking flower phenotype, the phenotype of 1Aox is much less severe (see figure 3.11.8A and B). On the other hand, the ovule shape is not rescued (see figure 3.11.8C and D). They still show outgrowths on their

integuments. Contrariwise, it looks as if they get bigger building knob like structures instead of the peaked ones of *ucn-1*.

The investigation of the 2D seed area revealed that seeds of 1Aox ($n = 240$) have an average 2D seed area of $83115\mu\text{m}^2$, while *Ler* ($n = 249$) seeds have an average 2D seed area of $85627\mu\text{m}^2$ ($p = 0,0299$) (see figure 3.11.9F). In average, 2Aox ($n = 215$) has a 2D seed area of $100741\mu\text{m}^2$ while *Col-0* ($n = 142$) seeds have an average 2D seed surface of $115234\mu\text{m}^2$ ($p = 9,2 * 10^{-19}$) (see figure 3.11.9A). Hence, the influence on seed size of *ucn-1* and *ucn-2* is rescued through the overexpression of *ATXR7*.

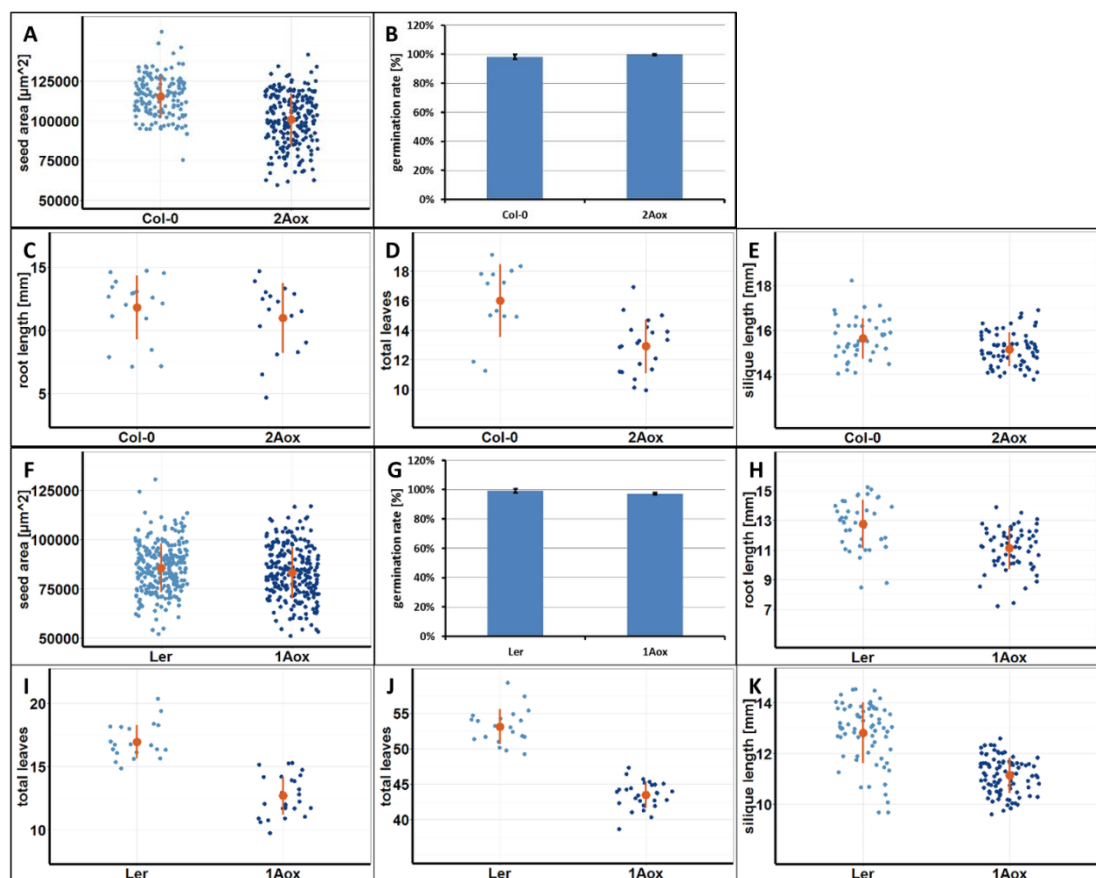


Figure 3.11.9: Analysis of the characteristics of 2Aox and 1Aox.

(A) 2D seed area of 2Aox. (B) Germination rate of 2Aox compared to *Col-0*. (C) Root length of 2Aox. (D) Flowering time of 2Aox when grown in LD conditions. (E) Silique length of 2Aox. (F) 2D seed area of 1Aox compared to *Ler*. (G) Germination rate of 1Aox. (H) Root length of 1Aox seedlings, 5dag. (I) Flowering time of 1Aox under LD conditions. (J) Flowering time of 1Aox under SD conditions. (K) Silique length of 1Aox compared to *Ler*. Each blue dot represents one sample, brown dots with lines represent average with 1x standard deviation.

The quantification of the germination rate also revealed a rescue. 153 out of 158 seeds of 1Aox germinated after seven days of incubation (97%) which is close to the wild-type germination rate (157 out of 158 seeds) (see figure 3.11.9G). Like observed before for *ucn-2* and CAox, the germination rate of 2Aox is inconspicuous (see figure 3.11.9B). For 1Aox

the result indicates that the lower germination rate of *ucn-1* is rescued through the *ATXR7* overexpression. Seeds of 2Aox show no new features regarding germination rate.

The investigation of the main root length of five days old seedlings revealed that in case of 1Aox ($n = 62$), the average root length is 11,1mm which is 15% smaller than the wild-type ($n = 39$) root length of in average 12,8mm ($p = 2,19 * 10^{-6}$) (see figure 3.11.9H). In case of 2Aox the root length of five days old seedlings ($n = 17$) is in average 11,0mm and therefore not significantly shorter ($p = 0,3682$) than the wild-type roots ($n = 18$) which measure in average 11,8mm (see figure 3.11.9C). The results indicate that in both cases the *ATXR7* overexpression rescues the shorter root of the *ucn* mutants. In case of *ucn-1* the rescue is not complete but the root length is rescued to the extent of the average root length of LAox.

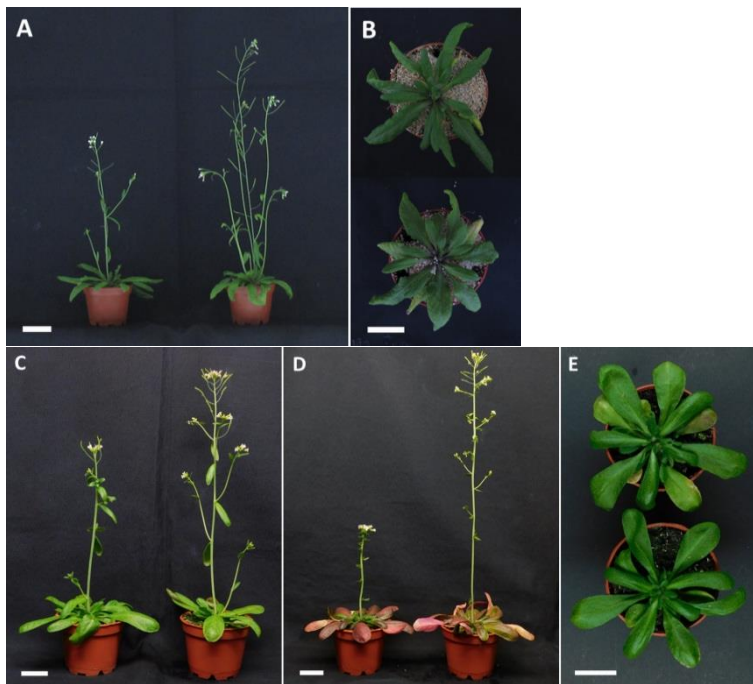


Figure 3.11.10: Phenotypical analysis of 2Aox and 1Aox.

(A), (C), and (D) Under LD conditions 2Aox (A; right plant) and 1Aox (C; right plant) flower earlier than the corresponding wild-types Col-0 (A; left plant) or Ler (C; left plant). Under SD conditions, 1Aox flowers early (D; right plant) compared to Ler (D; left plant). (B) and (E) Both *ATXR7* overexpression lines, 2Aox (B; lower plant) and 1Aox (E; lower plant), do not show any special features in rosette shape compared to Col-0 (B; upper plant) or Ler (E; upper plant). Scale bars: A: 3cm; B to E: 2cm.

The analysis of the flowering time revealed that in average, 1Aox ($n = 26$) started flowering with 12,7 total leaves while Ler ($n = 20$) starts flowering in average with 17,0 total leaves ($p = 3,82 * 10^{-13}$) (see figure 3.11.9I and 3.11.10C). In case of 2Aox ($n = 21$), the plants start flowering in average with 12,9 total leaves while the wild-type starts flowering in average with 16 total leaves ($p = 0,00082$) (see figure 3.11.9D and 3.11.10A). The results

show that the overexpression of *ATXR7* in *ucn-1* slightly enhances the early flowering while the combination of *ucn-2* and an overexpressed *ATXR7* causes early flowering.

The flowering time of 1Aox was further determined under SD conditions. In average 1Aox (n = 28) starts flowering with 43,4 total leaves. The wild-type (n = 20) starts flowering with in average 53,1 total leaves ($p = 2,13 * 10^{-16}$) (see figure 3.11.9J and 3.11.10D). Therefore, the early flowering of 1Aox is also independent of the length of day.

Siliques of 1Aox and 2Aox are inconspicuous in their shape (see figure 3.11.8E, F, M, and N). This corresponds with the observation that the siliques of the single mutants and the *ATXR7* gain-of-function lines, respectively, also show no special features in their silique shape. The analysis of the silique length revealed that the siliques of 1Aox (n = 90) have an average length of 11,1mm while siliques of *Ler* (n = 68) have an average length of 12,8mm ($p = 4,38 * 10^{-109}$) (see figure 3.11.9K). Although the silique length is not recovered the ovule viability is rescued (see figures 3.11.8G and H). No degenerated ovules can be found in siliques of 1Aox lines. The analysis of the silique length of 2Aox (n = 68) revealed that the average length is 15,1mm while the wild-type siliques (n = 41) measure in average 15,6mm ($p = 0,00512$) (see figure 3.11.9E). Siliques of 2Aox do not display any degenerated ovules (see figure 3.11.8O and P). The results suggest that the silique length of *ucn-1* and *ucn-2*, respectively, is not rescued by the overexpression of *ATXR7*. They further indicate that the ovule degeneration observed for *ucn-1* is rescued.

In conclusion, the gain-of-function of *ATXR7* rescues most features of *ucn-1* to a very great extent. 1Aox regained its germination rate, its seed size, and displays no degenerated ovules. Also the flower almost regains its wild-type shape and the root length is the same as in LAox, which is considerably longer than the root of *ucn-1*. Other features of *ucn-1* like the ovule protrusions and the early flowering are rather enhanced by the *ATXR7* overexpression than rescued or weaker. In 2Aox, the seed size and the root length is rescued whereas the silique length is not. The mutant now also shows early flowering, although neither *ucn-2* nor CAox do (see table 3.11.3).

Table 3.11.3: Comparison of the *ucn* mutants to the *ATXR7* gain-of-function lines in mutant and wild-type background.

Only affected plant organs are listed. Germ. rate = germination rate, Seed size = 2D seed area, Root length = main root length of five day old seedlings, FT = flowering time in long day (LD) and short day (SD). All numbers are given in relation to the corresponding wild-types.

Characteristic	<i>ucn-1</i>	LAox	1Aox	<i>ucn-2</i>	CAox	2Aox
Flower shape	affected	wild-type	slightly affected	wild-type	wild-type	wild-type
Ovule shape	protrusions	wild-type	protrusions	wild-type	wild-type	wild-type
Germ. rate	72%	wild-type	wild-type	wild-type	wild-type	wild-type
Seed size	78%	wild-type	97%	123%	126%	87%
Root length	64%	83%	87%	87%	wild-type	wild-type
FT (LD)	80%	wild-type	75%	wild-type	wild-type	81%
FT (SD)	81%	wild-type	82%	wild-type	wild-type	no data
Silique length	85%	105%	87%	96%	wild-type	97%
Ovule lethality	yes	wild-type	wild-type	wild-type	wild-type	wild-type

3.11.4 Overexpression of *UCN* in *atxr7-1*

The results I gained for the double overexpression of *ATXR7* and *UCN* and also for the partial rescue of *ucn-1* and *ucn-2* features through *ATXR7* overexpression suggest that *ATXR7* acts epistatic to *UCN*. To verify that relationship, I transformed the pUBQ::*UCN* construct into *atxr7-1*. Again, I inbred three independent T₁ lines until I gained homozygous T₃ lines. For further reading, these lines are called aUox (for *atxr7-1 UCN* overexpressed). I analyzed the lines for seed size, germination rate, main root length, and flowering time. If *ATXR7* acts completely epistatic to *UCN*, it should rescue the phenotypes caused by *UCN* overexpression.



Figure 3.11.11: Analysis of the *atxr7-1* line overexpressing *UCN* (aUox).

Figure shows (from left) CUox, Col-0, *atxr7-1*, and aUox. Late flowering CUox is eliminated by *atxr7-1*.

The analysis of the 2D seed surface revealed that in average, the Col-0 seeds have a surface of $97239\mu\text{m}^2$ ($n = 108$) while seeds of aUox have in average a seed surface of $84690\mu\text{m}^2$ ($n = 257$) ($p = 2,14 * 10^{-16}$) (see figure 3.11.12A). This reduction was already observed on CUox seeds. Therefore, the result indicates that the decrease in seed surface observed on CUox cannot be suppressed in *atxr7-1*. The germination rate of the seeds was inconspicuous (see figure 3.11.12B).

The measurement of the root size of five day old seedlings revealed that the main root length of Col-0 seedlings ($n = 31$) measures 10,7mm. For the average root length of aUox seedlings I measured 11,4mm ($p = 0,1400$) (see figure 3.11.12). Hence, the loss-of-function of *ATXR7* rescues the root length of the gain-of-function of *UCN* which has less than 50% of the wild-type root length.

I further checked the flowering time under LD conditions. In average, aUox ($n = 48$) grows 10,3 total leaves until flowering while Col-0 ($n = 9$) grows in average 16,4 total leaves until flowering ($p = 6,2 * 10^{-5}$) (see figure 3.11.11 and 3.11.12D). Therefore, the flowering time phenocopies the early flowering of *atxr7-1* ($n = 10$) which starts flowering with in average 10,0 total leaves ($p_{\text{aUox}} = 0,2115$). In contrast, CUox ($n = 20$) starts flowering with in average 20,5 total leaves ($p = 0,0025$). The result suggests that *UCN* represses flowering over *ATXR7*.

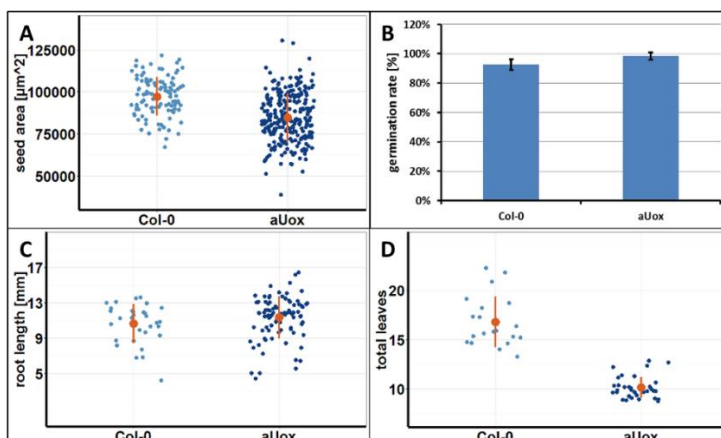


Figure 3.11.12: Analysis of the characteristics of aUox.

(A) 2D seed area of aUox compared to Col-0. (B) Germination rate of aUox. (C) Root length of aUox seedlings, 5dag. (D) Flowering time of aUox when grown under LD conditions. Each blue dot represents one sample, brown dots with lines represent average with 1x standard deviation.

In conclusion, no additive or enhancing effects are found. The seed size of *atxr7-1* is overridden by *UCN* gain-of-function. Regarding flowering time and root length the results indicate that *UCN* cannot influence them in an *atxr7-1* background (see table 3.11.4).

Table 3.11.4: Comparison of the phenotypical features observed on *atxr7-1*, CUox, and aUox.

Only affected plant organs are listed. Seed size = 2D seed area, Root length = main root length of five days old seedlings, FT (LD) = flowering timme under long day conditions. All numbers are given in relation to the wild-type.

Characteristic	<i>atxr7-1</i>	CUox	aUox
2D seed area	135%	85%	87%
Root length	wild-type	47%	wild-type
FT (LD)	61%	125%	63%

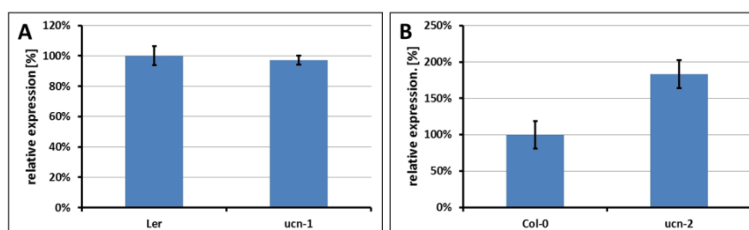
3.12 qRT-PCR results

Since I was able to demonstrate a relationship between *ATXR7* and *UCN* at least in some processes, the question raises if the two genes only affect each other on protein or also on transcriptional level. To answer that question, I performed qRT-PCRs with the mRNA of ten days old seedlings grown in long day. If *ATXR7* and *UCN* affect themselves on transcriptional level, their expression level should differ from the wild-type transcription level in the different loss- or gain-of-function lines.

3.12.1 The influence of *UCN* on *ATXR7*

To analyze if *UCN* influences *ATXR7*, I checked the expression levels of *ATXR7* in *ucn-1*, *ucn-2*, and the *UCN* gain-of-function lines.

The analysis of the *ATXR7* expression in *ucn-1* revealed that it is 97% compared to *Ler* ($p = 0,5304$) (see figure 3.12.1A). In *ucn-2* on the other hand, the *ATXR7* expression increases to 183% compared to *Col-0* ($p = 0,00566$) (see figure 3.12.1B). The result indicates that the loss-of-function in *Ler* has no influence on *ATXR7* expression while the loss-of-function in *Col-0* increases *ATXR7* expression.

**Figure 3.12.1: Analysis of the *ATXR7* expression in *ucn-1* and *ucn-2*.**

(A) In *ucn-1* *ATXR7* expression is not deregulated. (B) *ATXR7* expression increases in *ucn-2*. Data is from 10d old seedlings grown in LD. Bars represent mean value of biological triplicate with 1x standard deviation.

The analysis of the *ATXR7* expression in the *UCN* and *ucn-1* gain-of-function lines as well as their EMO offspring revealed that in *Ler* background neither the overexpression of *UCN* nor the overexpression of *ucn-1* influences *ATXR7* expression (see figure 3.12.2A and B). In *Col-0* background, only the overexpression of *ucn-1* influences *ATXR7* expression (see figure 3.12.2C and D). In *C1ox*, the expression level of *ATXR7* increases to 139% ($p = 0,000454$) compared to *Col-0*. *CUox* as well as the two EMO lines *EFC* and *EFC1* do not show any variation in their *ATXR7* expression. The results therefore suggest that *UCN* has no direct influence on the expression of *ATXR7*, although in *ucn-2* and *C1ox* the expression of *ATXR7* increases.

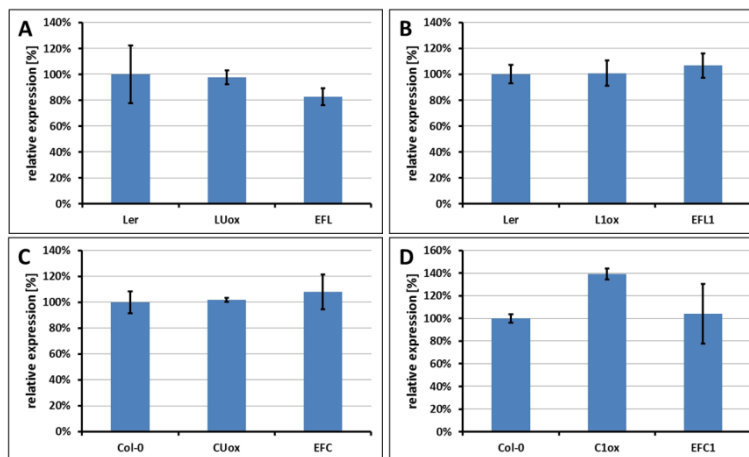


Figure 3.12.2: Analysis of the influence of *UCN/ucn-1* overexpression on *ATXR7* expression.

(A) *ATXR7* expression in *LUox* and *EFL* is not influenced. (B) The overexpression of *ucn-1* has no influence on *ATXR7* expression. (C) In *CUox* and *EFC*, *ATXR7* is expressed like in the wild-type. (D) *ATXR7* expression slightly increases in *C1ox* but not in *EFC1*. Data is from 10d old seedlings grown in LD. Bars represent mean value of biological triplicate with 1x standard deviation.

3.12.2 The influence of *ATXR7* on *UCN*

The analysis of the *UCN* expression in *atxr7-1* and the two gain-of-function lines *LAox* and *CAox* revealed that in *atxr7-1* the *UCN* expression decreases to 76% compared to *Col-0* ($p = 0,003065$) (see figure 3.12.3A). On the other hand, there is no influence on *UCN* expression in the *ATXR7* gain-of-function lines; neither in *Ler* nor in *Col-0* (see figure 3.12.3B and C). The results show that *ATXR7* has no direct influence on *UCN* expression. The loss-of-function of *ATXR7* on the other hand could indirectly decrease the expression of *UCN*.

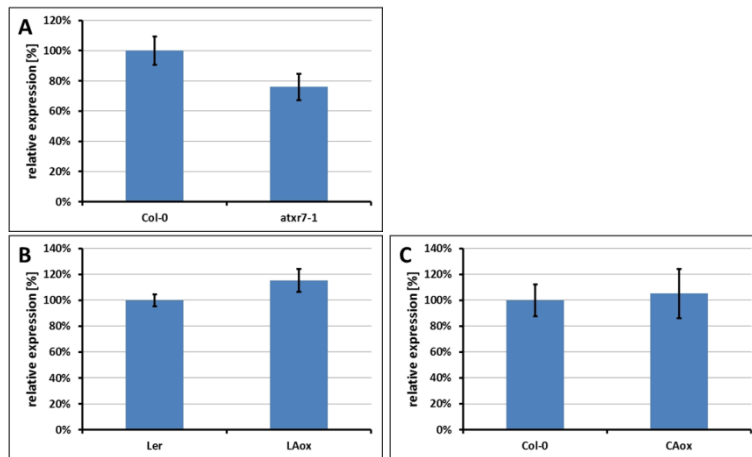


Figure 3.12.3: Analysis of the *UCN* expression in *atxr7-1* and the *ATXR7* overexpressor lines *LAox* and *CAox*. (A) In the loss-of-function mutant *atxr7-1* the expression of *UCN* shows a mild decrease. (B) In *LAox*, *UCN* expression is not affected. (C) *CAox* shows no difference in *UCN* expression compared to the wild-type. Data is from 10d old seedlings grown in LD. Bars represent mean value of biological triplicate with 1x standard deviation.

In conclusion, in *atxr7-1* the *UCN* expression mildly decreases while in *ucn-2* and also *C1ox* the *ATXR7* expression increases. A direct influence of *UCN* on *ATXR7* or vice versa is not found.

3.12.3 The influence of *UCN* on the expression of *FLC*

ATXR7 is a trithorax-like protein enhancing the expression of its targets by methylating H3K4 and H3K36 [74]. One of these targets is *FLC*, a very potent flowering repressor [104]. *FLC* represses the transcription of *FT* which is in turn a very potent flowering activator [34]. Due to the involvement of *ATXR7* in this relationship, I hypothesized that *UCN* maybe also involved in flowering time determination via influencing this relationship over *ATXR7*. The differences that I described for the two alleles *ucn-1* and *ucn-2* could also be interpreted as a support for the hypothesis: *Ler* does not contain a functional *FLC* allele [38, 104]. That could be part of an explanation why *ucn-1* flowers early while *ucn-2* only shows wild-type flowering. Also the fact that *ucn-2* does only show wild-type flowering does not necessarily exclude a role for *UCN* in flowering time determination: a prominent mutant that also shows wild-type flowering when grown under LD conditions is *flc-3*, a *FLC* loss-of-function mutant [105]. Another example would be *jmj15-1*, a *JMJ15* loss-of-function mutants that shows no flowering time deregulation while the gain-of-function line shows rapid flowering [106]. However, if *UCN* is involved in the process of flowering time determination over *ATXR7* it could have an influence on *FLC* expression. Therefore, I checked the expression of *FLC* in the *ucn-2* mutant. I further checked the *FLC* expression in the *atxr7-1 ucn-2* double mutant to verify an involvement in the same flowering pathways.

The analysis of the expression of *FLC* in *ucn-2* revealed that it is decreased to 34,8% compared to the wild-type expression ($p = 0,0316$). In *atxr7-1*, the *FLC* expression decreases to 12,3% ($p = 0,0183$). In the double mutant, the *FLC* expression decreases to 7,2% compared to the wild-type ($p = 0,0176$) (see figure 3.12.4). This indicates that *FLC* expression is impaired in *ucn-2* but not as strong as in *atxr7-1* ($p_{atxr7-1-ucn-2} = 0,0013$). On the other hand, no additive effect is found in the double mutant ($p_{atxr7-1-atxr7-1\ ucn-2} = 0,1146$).

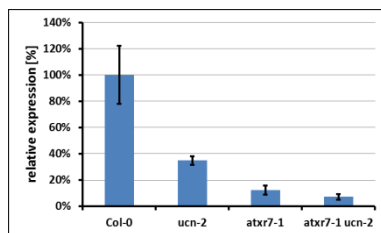


Figure 3.12.4: *FLC* expression in *ucn-2* and *atxr7-1* compared to wild-type.

RNA was extracted from ten days old seedlings grown under LD conditions. Bars represent mean value of a biological triplicate with 1x standard deviation.

The result above suggests that *UCN* is needed for *FLC* expression. To further answer the question if this role is direct or indirect, I analyzed the *FLC* expression in the gain-of-function line *CUox*. If *UCN* is directly involved in *FLC* expression, this expression should be increased in *CUox*.

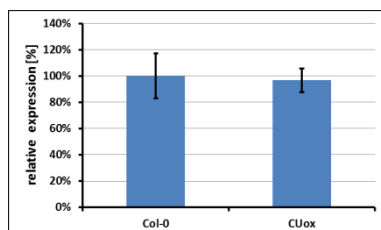


Figure 3.12.5: *FLC* expression in the *UCN* gain-of-function line *CUox*.

RNA was extracted from ten days old seedlings grown under LD conditions. Bars represent mean value of a biological triplicate with 1x standard deviation.

In *CUox*, the *FLC* expression is inconspicuous compared to the wild-type (see figure 3.12.5). Therefore, the result suggests that *UCN* is not able to actively increase the expression of *FLC*.

Summarized, the results indicate that *UCN* is needed for the proper expression of *FLC* and that *FLC* expression does not decrease further in the *atxr7-1 ucn-2* double mutant when compared to *atxr7-1*, verifying indirectly the epistasis of *ATXR7* and the involvement of *UCN* and *ATXR7* in the same flowering pathways. Furthermore, it could be shown that *UCN* is not able to actively increase *FLC* expression.

3.12.4 The influence of *UCN* on the expression of *FT*

FT, a very potent flowering activator, is known to be actively repressed by *FLC* [34]. I was able to demonstrate that *FLC* is not properly expressed in *ucn-2* (see above). Since neither *ucn-2* is flowering early nor the gain-of-function has an influence on *FLC* expression the question remains why CUox flowers early. Due to the direct coupling of *FLC* expression to *FT*, I analyzed also this expression in the loss- and gain-of-function lines of *UCN* in Col-0.

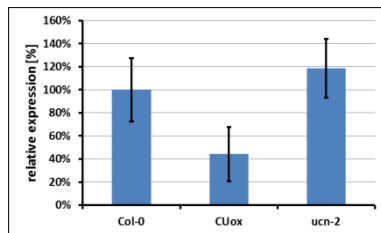


Figure 3.12.6: Expression of *FT* in *ucn-2* and CUox.

RNA was extracted from ten days old seedlings grown under LD conditions. Bars represent mean value of a biological triplicate with 1x standard deviation.

The analysis of *FT* expression in CUox and *ucn-2* revealed that the *FT* expression slightly increases to 119% ($p = 0,2543$) while the *FT* expression decreases to 44% ($p = 0,0575$) in CUox (see figure 3.12.6). Therefore, the result indicates that the loss-of-function does not influence the *FT* expression, but the gain-of-function does.

To better understand the influence of *UCN* on *FT* expression and also analyze it in an *atxr7-1* context, I also checked the *FT* expression in the double mutant *atxr7-1 ucn-2*. The *ATXR7* loss-of-function mutant shows a more than 2-fold increase in *FT* expression ($p = 0,0011$) while the double mutants *atxr7-1 ucn-2* shows an increase to 181% ($p = 0,0517$) (see figure 3.12.7). This result indicates that the loss-of-function of *ATXR7* does have an influence on *FT* expression.

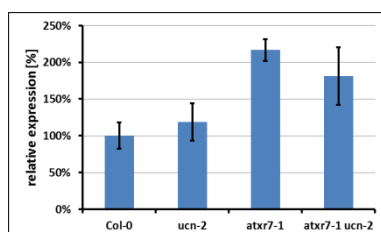


Figure 3.12.7: *FT* expression in *atxr7-1 ucn-2*

RNA was extracted from ten days old seedlings grown under LD conditions. Bars represent mean value of a biological triplicate with 1x standard deviation.

Summarized, the results indicate that the overexpression of *UCN* influences *FT* expression negatively while the *atxr7-1* loss-of-function increases the *FT* expression. Thereby, the double mutant *atxr7-1 ucn-2* shows no further increase in *FT* expression.

3.12.5 The influence of *ATXR7* gain-of-function on the expression of *FLC* and *FT*

The influence of *ATXR7* on *FLC* and also on *FT* is still not completely understood [76]. In addition it was studied in solely the loss-of-function line *atxr7-1*. Since *ATXR7* gain-of-function lines do not show late flowering and is even showing early flowering in 2Aox, I investigated *FLC* and *FT* expression in the *ATXR7* gain-of-function line.

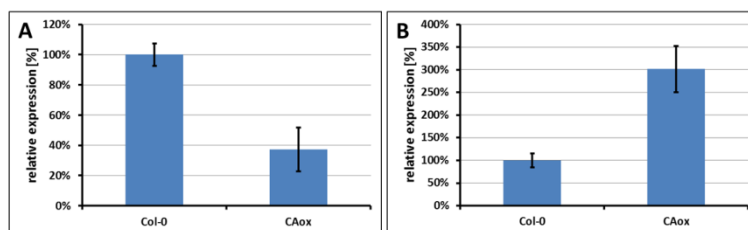


Figure 3.12.8: *FLC* and *FT* expression in CAox

(A) *FLC* expression in CAox. (B) *FT* expression in CAox. RNA was extracted from ten days old seedlings grown under LD conditions. Bars represent mean value of a biological triplicate with 1x standard deviation.

In CAox the *FLC* expression decreases to 37% ($p = 0,0067$) while the *FT* expression increases 3-fold ($p = 0,0966$) (see figure 3.12.8A and B). The result indicates that gain-of-function phenocopies the loss-of-function. Although, the influence is weaker on *FLC* expression, it is stronger on *FT* expression.

The result that the *ATXR7* gain-of-function displays reacts in the same way than the loss-of-function raises the question if the increase of *ATXR7* expression in *ucn-2* (see above) is responsible for the decrease of *FLC*. To answer the question, the *FLC* expression of 2Aox was analyzed and compared to the *FLC* expression of CAox. In addition the *FT* expression of 2Aox was also checked. An additive effect would explain why 2Aox flowers early while CAox does not. Furthermore I checked the *FLC* and *FT* expression in CAUox. This should shed more light on the question why CUox flowers late and how *UCN* and *ATXR7* influence each other or work together.

The analysis of *FLC* expression in 2Aox revealed that it decreases to 23% ($p = 0,0224$) while the *FT* expression increases to 248% ($p = 0,1317$) (see figure 3.12.9 A and B). The result indicates that 2Aox shows a similar *FLC* and *FT* expression pattern like CAox and therefore suggests no additive effect. In CAUox, the *FLC* expression is 110% compared to the wild-type ($p = 0,4870$) while the *FT* expression increases to 123% ($p = 0,2022$) (see figure

3.12.9 C and D). Therefore, the *FLC* and *FT* expression in CAUox does not differ significantly from wild-type expression.

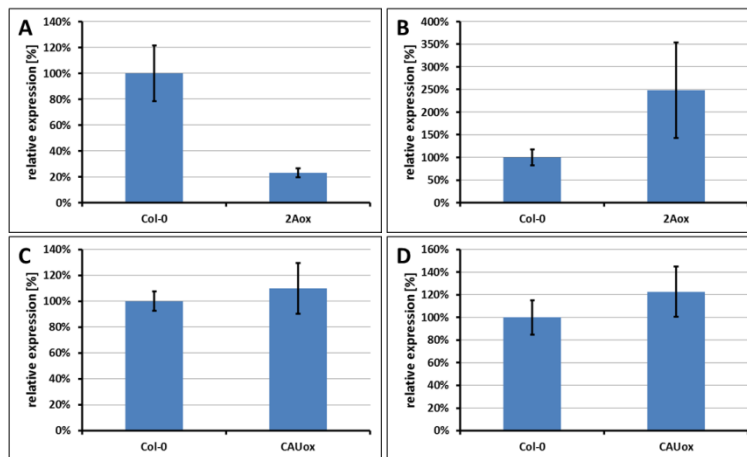


Figure 3.12.9: *FLC* and *FT* expression in 2Aox and CAUox.

(A) *FLC* expression in 2Aox. (B) *FT* expression in 2Aox. (C) *FLC* expression in CAUox. (D) *FT* expression in CAUox. RNA was extracted from ten days old seedlings grown under LD conditions. Bars represent mean value of a biological triplicate with 1x standard deviation.

3.12.6 Epigenetic influence on the expression of *FLC* and *FT* in EFC

I was able to show that the *FLC* expression as well as the *FT* expression is impaired in *ucn-2* and CUox, respectively. The epigenetic inheritance of the flowering time from CUox to EFC raises the question if one or both of these genes are also deregulated in the EMO line EFC. Therefore, I analyzed the expression pattern of the two genes in EFC seedlings.

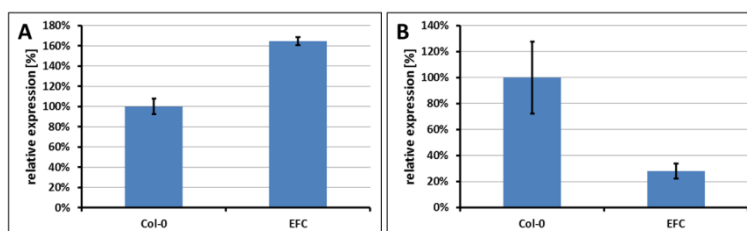


Figure 3.12.10: *FLC* and *FT* expression in EFC.

(A) *FLC* expression in EFC. (B) *FT* expression in EFC. RNA was extracted from ten days old seedlings grown under LD conditions. Bars represent mean value of a biological triplicate with 1x standard deviation.

The analysis of *FLC* expression in EFC revealed that it increases to 165% ($p = 0,0012$) (see figure 3.12.10A). The *FT* expression on the other hand decreases to 28% ($p = 0,0409$) (see figure 3.12.10B). The result indicates that the *FLC* expression increases while the *FT* expression decreases. The decrease in *FT* expression is also observed in CUox but in CUox, this decrease is not coupled to an increase in the *FLC* expression level.

Table 3.12.1: Summarized results of the analysis of the *FLC* and *FT* expression in the different loss- and gain-of-function mutants.

All numbers are given in relation to the wild-type expressions. Data is from ten days old seedlings grown under LD conditions. Numbers represent mean values of biological triplicates.

Gene	<i>ucn-2</i>	<i>atxr7-1</i>	<i>atxr7-1 ucn-2</i>	CUox	EFC	CAox	2Aox	CAUox
<i>FLC</i>	35%	12%	7%	97%	165%	37%	23%	110%
<i>FT</i>	119%	217%	181%	44%	28%	302%	248%	123%

In summary, the results suggest a role for *UCN* in *FLC* expression as well as in *FT* repression (see table 3.12.1). I was able to further demonstrate that the influence on *FLC* and *FT* can be inherited to the EMO line. Surprisingly, the EMO line is the only line showing an increase in *FLC* expression. Moreover, the effect on *FLC* expression seems to be rather indirect while the effect on *FT* might be more directly. The analysis of the *ATXR7* loss-of-function mutant verified former results: *FLC* expression decreases [74]. Consistently with that the *FT* expression increases. The expression patterns of *FLC* and *FT* in the gain-of-function lines of *ATXR7* were rather unexpected. I was able to show that the gain-of-function of *ATXR7* reacts the same way as a loss-of-function. This suggests that high *ATXR7* levels are rather activating flowering than repressing it. However, the results of the expression analysis confirm former results of the phenotyping. Furthermore, the CAUox line demonstrates the neutralization of the effects of the single overexpression of *ATXR7* or *UCN* also on transcriptional level.

4 Discussion

4.1 *UCN* is involved in processes of multiple plant organs

The AGCVIII kinase UNICORN (*UCN*), a protein that phosphorylates its targets and thereby modulates their activity, was formerly shown to be involved in ovule and flower development [89, 91]. Since one kinase is able to phosphorylate multiple different targets in the same tissue and even in the same cell, it can be involved and therefore influence multiple pathways at the same time. In addition, 4% of the Arabidopsis genome encodes for phosphorylating serine/threonine kinases [83], highlighting the importance of these proteins in development and signal transduction.

Using a *3xVenus* reporter gene coupled to the complete promoter region of *UCN*, I was able to confirm former results: the expression of *UCN* in the ovule and all floral organs. This expression pattern coincides with the observed abnormalities on these organs in *ucn-1*. In addition, the strong expression observed in the nucellus and the megaspore mother-cell (MMC), respectively, suggests a role for *UCN* in embryo sac development. This suggestion also coincides with the observation that *ucn-1* is eventually developing no embryo sac [89] and therefore at least contribute to the explanation why *ucn-1* is semi-sterile. In later stages of the ovule development, two nuclei are highlighted by their very strong signal. Due to the number and localization, this could be the synergids, but without a second reporter gene a safe statement is not possible. Anyway, the strong signal suggests that in later stages of ovule development *UCN* still plays an important role. The spatial expression pattern of *UCN* in the ovule refines the knowledge of the putative role for *UCN* in ovule development. It is likely that it is not only involved in integument development but also in the development of the embryo sac and maybe beyond. Further investigations are needed to answer the question why *ucn-1* eventually develops no embryo sac and if there is a certain stage in ovule development that fails in *ucn-1*.

With the *3xVenus* reporter line I further demonstrated that *UCN* is expressed in all plant organs. Moreover, I showed that neither *ucn-1* nor *ucn-2* carries a real null-allele, since both lines still show expression of their *ucn* alleles. I found more impaired plant organs on *ucn-1* as well as on *ucn-2*. Thus, it is likely that *UCN* plays a role in the processes of these organs, too. Both loss-of-function lines have in common that they grow smaller roots and siliques. This suggests a direct or indirect involvement in root and silique growth. Further-

more, it raises the question if the shorter siliques of *ucn-1* are due to the degenerated ovules. Since *ucn-2* also shows smaller siliques without bearing degenerated ovules, it is possible that *UCN* is involved in processes that determine silique length. However, the results I gained for the gain-of-function mutants suggest that the role of *UCN* in the processes that impairs the root and siliques is rather indirect, otherwise an opposite effect would have been expected.

Another feature both loss-of-function mutants display is the seed size, although *ucn-2* shows bigger seeds while *ucn-1* shows smaller seeds. Anyway, it is the only feature that shows an opposite result in the gain-of-function lines than in the loss-of-function lines. Hence, the result suggests a direct role for *UCN* in seed size determination. Taking in account the results I gained for the crossing experiments of the loss-of-function mutants with their corresponding wild-types, it can further be assumed that *UCN* can influence the seed size from maternal as well as from paternal side. Since seed size is determined from the integuments as well as from the endosperm [51], this further suggests that *UCN* influences seed size from both of these tissues. Moreover, the small seeds of CUox suggest that the lower germination rate of *ucn-1* is due to its background and not due to the small seeds, otherwise CUox, which also shows much smaller seeds, would also show a problem in germination rate. Due to the parent-of-origin effect on the seed size of *ucn-1* as well as of *ucn-2*, *UCN* might be involved in the imprinting of genes which would also influence seed size [55, 107]. This assumption is further supported by the epigenetic effects shown by the EMO offspring of *UCN* and *ucn-1* overexpressor lines, respectively. In contrast to some features still observable on the EMO lines, the seed size differences are not inherited to the EMO offspring. This indicates that the seed size difference is probably not due to a change in DNA methylation otherwise it would be inherited epigenetically.

All features described in this work are more severe in *Ler* background than in *Col-0*. Furthermore, *ucn-1* displays features that are not observed on *ucn-2*, like a rapid flowering or the deformed flower shape. By using a gain-of-function approach I was able to demonstrate that the overexpression not only affects different plant organs in the two accessions, but also that the overexpression influences plant organs more severe in *Ler* background than in *Col-0*. Although both lines have in common a massive reduction in root length, CUox only shows a mild phenotype while LUox shows a strong phenotype including additional features that are not observed on CUox. This suggests that the differences displayed by the loss-of-function mutants are due to the different backgrounds rather than

due to the different *ucn* alleles. If this also includes a more important or prominent role for *UCN* in *Ler* than in *Col-0* cannot be answered with the results I present.

The spatial expression pattern of *UCN* and the effect of the loss-of-function of *UCN* on multiple organs suggest a role for *UCN* in cell division. This is supported by the observation that the strongest expression is found in tissues with active cell division, like in the elongation zone of the root or young leaves and the proximal ends of older leaves, respectively. On the other hand, in mature, differentiated tissue, the signal decreased but never disappeared completely. Moreover, this assumption is supported by the former observation that cell cycle genes in *ucn-1* are deregulated [108]. It is further supported by the results of the gain-of-function lines where the root is even shorter than in the loss-of-function lines or the leaves of *LUox* which show a roundish shape rather than a lanceolate. Phenotypes like this could be explained with the interference of maturing cells which cannot properly elongate. If the loss-of-function of *UCN* is interfering with the cell cycle it can be speculated that the ectopic expression would, too. Anyway, since organ growth and therefore cell division is still possible, *UCN* is involved in the process of cell division but it is not sufficient to repress it as a loss-of-function allele. If *UCN* is sufficient to repress cell maturation when expressed ectopically, especially in *Ler* background, will need further investigations.

Another phenotype observed on *LUox* is the pistils with up to four fused carpels. When fully developed I also found degenerated ovules here, comparable to *ucn-1*, suggesting that *UCN* is not only needed for ovule development but further that it is needed in the right concentration. However, the multiple carpels could be explained by the misexpression of *UCN* in the floral meristem. Although floral meristems were not explicitly checked, unpublished data of Jan Lohmann (personal communication) indicate a *WUS* binding site in the 3' end of *UCN* used to repress its expression. This would also repress *UCN* in floral meristems where *WUS* is also active. The explanation is further supported by the missing expression of *UCN* in the SAM. However, a bigger floral meristem would explain the phenotype of multiple fused carpels and also coincides with the mapping of the *CLV1* region (unpublished data, Jin Gao), a protein involved in SAM size determination, to rescue *ucn-1* and therefore suggesting a relationship between these two proteins. Taken together, these results suggest a role for *UCN* in SAM size determination. Further experiments are needed to verify this hypothesis and also to answer the question if this role is restricted to floral meristems or if *UCN* also plays a role in the SAM or even the root meristem.

In conclusion, the results I gained broaden the view that we had from the role of *UCN* in the different plant organs. In addition to integument development, *UCN* likely contributes to in embryo sac development. I was further able to demonstrate that *UCN* is involved in processes of multiple other plant organs and therefore plays a more prominent role than thought. The phenotypes described in my comparable analysis between *ucn-1* and *ucn-2* and the phenotypes I gained from the gain-of-function of *UCN* in combination with the expression pattern points to a role in cell division. Moreover, I demonstrate that ectopically expressed *UCN* likely interferes with cell maturation. I also presented evidence that the different phenotypes of the two mutant alleles of *ucn* largely depend on background. Moreover, I propose a possible role for *UCN* in meristem size determination at least for the floral meristem.

4.2 The *ucn-1* allele displays a dominant negative behavior

In a diploid organism like *Arabidopsis thaliana* genes are usually available in two copies or alleles, one inherited from the maternal and one from the paternal side. Therefore, if one allele is defect, the other one is usually able to buffer the putative effect. Thus, the non-functional allele has no impact on the plant. In addition to these recessive mutations, dominant mutations are also observed. These are mutations where one defect allele already matters. There are multiple explanations for a dominant mutation. One explanation is haplo-insufficiency, a situation where both alleles are needed for proper function of the affected process. Another one is genetic imprinting [109, 110]. Here, the maternal or paternal allele is silenced and therefore, a mutation in the active allele cannot be buffered any more. A third explanation is a dominant-negative behavior of the affected allele which “poisons” the processes it is involved in.

The *ucn-1* mutant was formerly described as a recessive mutation [91], but the results I received in this work are questioning that statement. All features observed for homozygous *ucn-1* plants were still observed in a weaker manner for heterozygous *ucn-1* plants. These observations exclude a completely recessive behavior for *ucn-1*, although there might be exceptions like the flower that displayed no phenotype any more in the heterozygous *ucn-1* mutant. Anyway, due to the independence of the different features of the crossing direction, I was already able to exclude a genetic imprinting effect. Otherwise I would have gained different results for the two heterozygous mutants depending on the crossing direction. To exclude a haplo-insufficiency I used an *ucn-1* gain-of-function

approach. In case of a haplo-insufficiency, the resulting lines should not show any effect. However, since the overexpression of *ucn-1* does show an effect in *Ler* as well as in *Col-0*, the only conclusion possible is a “poisoning” of the system by *ucn-1* and therefore a dominant-negative role.

A dominant-negative behavior would also be observed when *ucn-1* would be a neomorphic or hypermorphic protein. A neomorphic mutation causes the mutated protein to do reactions which would not be performed by the wild-type protein. Such a mutation would therefore be dominant. Also a hypermorphic mutation, which causes a protein to over-activate its targets, would be dominant. Both of these possibilities needed to be excluded, since they would interfere with the reverse-genetics approach to investigate the function of *UCN*. I was able to exclude a neomorphic behavior because *L1ox* is a weaker phenocopy of *LUox*. This evidences that *ucn-1* causes no additional features that would be different in *L1ox* compared to *LUox*. Furthermore, the features observed in *L1ox* are always weaker than in *LUox*. Therefore, a hypermorphic behavior can also be excluded.

If *ucn-2* also represents a dominant-negative allele could not be answered. A gain-of-function approach with the truncated *ucn-2* gene was not performed. The weak phenotype of *ucn-2* probably also makes it difficult to gain clear results for answering that question. However, one approach that was not performed in this work is to grow heterozygous *ucn-2* plants under short day conditions. Here, I was able to demonstrate that also *ucn-2* grows protrusions on its integuments. Therefore, it is possible that heterozygous *ucn-2* plants also display smaller protrusions like heterozygous *ucn-1* plants do under LD conditions. However, this would still not answer the question if *ucn-2* shows a dominant-negative behavior but only if *ucn-2* is also a dominant allele.

In addition to the recessive behavior of *ucn-1* regarding flower shape, the ovules seem to suffer from a haplo-insufficiency. I observed no protrusions for *L1ox* and therefore, *ucn-1* does not behave dominant-negative. On the other hand, I observed protrusions on F_2 ovules from the crossing of *ucn-1* with *Ler*. The integuments of these ovules have a heterozygous *ucn-1* genome, since the tissue is delivered completely from the F_1 motherplant. Therefore, one *UCN* allele is not enough to determine the right cell division plane.

In conclusion, I present evidence that the *ucn-1* allele is not recessive but dominant-negative. Thereby, I was able to exclude a haplo-insufficiency and further a neo- or hypermorphic behavior. If this holds also true for the *ucn-2* allele needs further analysis.

Anyway, the dominant-negative behavior is not observed for all plant organs *ucn-1* affects. For the flower phenotype, *ucn-1* displays a recessive behavior while the ovule phenotype displays a haplo-insufficiency. All other plant organs are also affected in L1ox or C1ox. Therefore, *ucn-1* displays a dominant-negative behavior here.

4.3 UCN is involved in epigenetic modifications

“An epigenetic trait is a stably heritable phenotype resulting from changes in a chromosome without alterations in the DNA sequence” [111].

The structure of the DNA allows its modification by the methylation of cytosine which can result in changes of the expression patterns of the affected genes. While in animals, only cytosine in a CG context can be methylated, in plants also cytosine in CNG (N = any nucleotide) and CHH (H = A, C, or T) can be methylated [59]. Furthermore, the DNA is wrapped around histones, protein octamers that show certain sites for posttranslational modification (methylation, phosphorylation, acetylation, etc.) which also influence gene expression [71]. Both, DNA as well as histone modifications are inherited to the daughter cell when cells are dividing [112]. Furthermore, DNA modifications are partly inherited trans-generational, although the mechanism behind this feature is still poorly understood [68].

In this work evidence is presented that *UCN* not only influences the plant on a genetic level but also on an epigenetic level. I demonstrated that the early flowering that the *ucn-1* mutant displays can be inherited to a wild-type plant that segregates out in the F₂ generation when a heterozygous F₁ generation of *ucn-1* is self-pollinated (*Ler/+* plants). This demonstrates that the feature of early flowering can be inherited independently of the *ucn-1* allele and therefore epigenetically. Further evidence is presented that this epigenetic inheritance is not restricted to flowering time but also on plant organs like the pistils of LUox that are still observed on EFL. The inheritance is therefore not dependent on the functionality of *UCN* since the *ucn-1* gain-of-function lines also inherit features to their EMO offspring EFL1 and EFC1, although in a weaker manner. This might suggest that here, the concentration of *UCN* plays a more prominent role than the functionality. Also the physical interaction with ATXR7 which I demonstrated in this work, further supports the theory of the involvement of *UCN* into epigenetics, since ATXR7 is a known chromatin modifier [74].

Vast epigenetic reprogramming is known from mutants such as *ddm1* [113] or *met1* [61, 114] where the whole DNA suffers from hypo-methylation. These mutants both show abnormal development and demonstrate the importance of DNA methylation for development. For the *UCN* mutants I excluded a vast epigenetic reprogramming like in *ddm1* and *met1*. If this would be the case, the phenotype of the EMO lines would be instable comparable to *ddm1* and *met1* [115, 116]. However, there is one restriction that has to be made for the gain-of-function lines. In all these cases, *UCN* is ectopically over-expressed. Therefore, this trans-generational effect could be the result of a chromatin modification in a tissue *UCN* would otherwise not be expressed. However, this restriction is challenged by the putative role of *UCN* in ovule development. This could indicate that *UCN* is also active in the reprogramming of the epigenome and therefore that it should not interfere with the process since it would be expressed anyway. Anyway, the process of epigenetic reprogramming is still objective of ongoing investigations [67, 117] as is the role of *UCN* in early embryogenesis. Therefore, the exclusion of a trans-generational inheritance by misexpression of *UCN* needs further analysis.

In conclusion, I was able to demonstrate an involvement of *UCN* into epigenetic modification and maybe trans-generational inheritance. Besides the flowering time that is affected in *Ler/+* plants segregating out from an F₂ generation of heterozygous *ucn-1* mutants, I demonstrated that also the gain-of-function inherits features to its EMO offspring. This effect depends rather on high *UCN* levels than on a functional *UCN* protein, since the *ucn-1* gain-of-function lines also show this effect. The inheritance of the features suggests an involvement of *UCN* in DNA methylation but the physical interaction and the sharing of some pathways with *ATXR7* also points to a role in histone modification.

4.4 *UCN* and *ATXR7* share pathways

ATXR7 is a histone methyl transferase that methylates lysine 4 and putatively lysine 36 of histone H3 [74, 75]. One known target gene of *ATXR7* is *FLC*, more precisely the region around the ATG, although *atxr7-1* displays histone modifications throughout the entire locus [75]. The *atxr7-1* loss-of-function mutant displays rapid flowering [74], although this cannot be explained with the loss of enhancement of *FLC* expression since *flc-3*, a loss of function mutant of *FLC* displays no rapid flowering [104]. Anyway, there are multiple genes in *atxr7-1* that are affected in their expression [74] and the combination of the misexpression of

multiple genes involved in flowering time determination most likely causes the rapid flowering.

In this work, I phenotypically characterized *atxr7-1* focussing on plant organs rather than on flowering time. I was able to show that the seeds of *atxr7-1* are also bigger than wild-type seeds. Furthermore, I demonstrated that a double loss-of-function line *atxr7-1 ucn-2* does not further increase seed size. If two proteins act in two different pathways influencing the same plant organ in the same way, a double mutant then usually adds up, enhancing the feature the two proteins influence. Therefore, regarding seed size determination it is very likely that *UCN* and *ATXR7* act in the same pathway. Also the other features described for the single loss-of-function lines never add up or show an enhanced phenotype in the double loss-of-function line. This promotes the theory that *UCN* and *ATXR7* do not act independent from each other. Furthermore, it suggests that at least in some processes, *ATXR7* and *UCN* act in the same pathways.

Presently, only the loss-of-function of *ATXR7* was investigated. In this work, I also used a gain-of-function approach to further investigate the function of *ATXR7*. I found evidence that the gain-of-function of *ATXR7* is able to neutralize the gain-of-function of *UCN*. This is not only true for CAUox, but also for LAUox where the overexpression of *ATXR7* rescues the very striking phenotype of LUox. LAUox lines still show a flowering time deregulation, but this phenomenon was also observed on other T₁ lines. The reason is not a flowering time deregulation but the growing in bulks and the subsequent selection. In later generations, where plants are brought out as single seeds, this deregulation is likely not observed any more. Therefore, it can be expected that also the early flowering of LUox is rescued by the overexpression of *ATXR7*. However, this behavior further evidences that *UCN* and *ATXR7* are involved in the same pathways. In addition, it suggests that *ATXR7* acts epistatic to *UCN*.

Other lines I generated further support this idea. Phenotypically I demonstrated that *UCN* is not able to delay flowering without *ATXR7*, as shown with aUox. This also holds true regarding root length, where the loss-of-function of *ATXR7* rescues the dramatic decrease in root length CUox shows. Interestingly, regarding seed size, the smaller seeds of CUox are not rescued in *atxr7-1*. One reason might be that *UCN* is ectopically overexpressed and therefore acts in cell lines it usually not expressed or in a much smaller amount. Another explanation is that *UCN* is able to influence seed size from the endosperm and the integuments and that *ATXR7* influences seed size from only one of these tissues. This would

also explain the discrepancy between the seed size of the double loss-of-function mutants and the single mutants. However, the rescue of the features displayed in LUox and CUox by *ATXR7* overexpression further evidences the epistasis of *ATXR7* over *UCN*.

More evidence is presented with the *ATXR7* gain-of-function lines in *ucn-1* and *ucn-2* background. One reason for the phenotypes of *UCN* gain-of-function lines is that *ATXR7* is titrated out by the high protein levels of *UCN*. With the parallel overexpression of *ATXR7*, the protein concentrations are again in a homeostatic condition as in a wild-type plant resulting in the rescue of the phenotype created by the *UCN* gain-of-function. This is further supported by the partial rescue of the *ucn-1* phenotype. Although I demonstrated that the *ucn-1* product also putatively interacts with *ATXR7*, this interaction might be weaker. Therefore, the wild-type concentration of *ATXR7* is not able to counteract *ucn-1*. If *ATXR7* is overexpressed, the higher concentrations titrate out the *ucn-1* levels and therefore prevent the *ucn-1* protein from causing a severe phenotype. Therefore, it adds up to the evidence that *ATXR7* is epistatic to *UCN* and that both proteins act in the same pathways. Some other features are not rescued. Here, *ATXR7* might simply not be involved in these processes and therefore not able to rescue the feature by repressing *UCN*. Another explanation could be that a different protein prevents the interaction in these organs and therefore the feature cannot be rescued. In both hybrid loss- and gain-of-function lines 1Aox and 2Aox, the plants start flowering earlier than the wild-types. This depends most likely on a special relationship between *ATXR7* and *UCN* in determining flowering time and will be discussed later.

Using qRT-PCR, I was further able to demonstrate that there is no direct effect on transcriptional level, neither of *UCN* on *ATXR7* nor of *ATXR7* on *UCN*, since no deregulation of the genes is found in the gain-of-function lines of *UCN* or *ATXR7*. Anyway, the expression of *ATXR7* in *ucn-2* is higher than in the wild-type, while the expression of *UCN* decreases mildly in *atxr7-1*. This demonstrates an indirect effect of *ATXR7* on *UCN* and *vice versa*. The result therefore further supports a connection between these two genes.

Summarized, the results I present show clear evidence for the relationship of *UCN* and *ATXR7*. I demonstrated that it is possible that both proteins physically interact. I further present evidence that *UCN* and *ATXR7* act in the same pathways and that, at least in most cases, *ATXR7* acts epistatic to *UCN*. Furthermore, I was able to exclude a direct mutual influence on transcriptional level, although I found an indirect one.

4.5 UCN is involved in flowering time regulation

Flowering time regulation is a very complex process influenced by intrinsic as well as extrinsic signals [39]. Deregulation of genes involved in pathways that regulate flowering time is usually coupled with a delay or an acceleration of flowering in LD and/or in SD. One very potent flowering repressor is *FLOWERING LOCUS C (FLC)* [104, 118]. Amongst others, the expression of *FLC* is regulated by *ATXR7* which modulates H3K4 and H3K36 methylation to enhance the expression of *FLC* [74, 75]. It is also known that *FLC* represses *FLOWERING LOCUS T (FT)*, a very potent floral integrator that is expressed in the vascular tissue of the leaves [34, 119]. Because of the deregulation of the determination of flowering time in the *UCN* gain-of-function lines and also *ucn-1* and furthermore the possible interaction of *ATXR7* and *UCN*, it is possible that *UCN* plays a role in determining flowering time. Using the gain- and loss-of-function lines I generated in this work, combined with an analysis of the expression levels of *FLC* and *FT*, I further investigated that possibility. Thereby, I focused on Col-0 background since *FLC* is disrupted in *Ler* [104] and therefore, the pathways I want to examine might not be available in that background.

The fact that I found no flowering time deregulation for *ucn-2* does not exclude its contribution to flowering time determination. Even *flc-3*, a *FLC* loss-of-function line does not show early flowering under LD conditions, although it does show slightly early flowering in SD conditions [105]. Another example for a mutant involved in flowering time determination that only shows a flowering phenotype in a gain-of-function line is *JMJ15* [106]. Furthermore, there are multiple environmental conditions that were not investigated in this study, like ambient temperature, heat stress, etc. Therefore, the wild-type flowering of *ucn-2* does not exclude a role for *UCN* in flowering time determination.

The putative interaction of *UCN* and *ATXR7*, a protein that is clearly associated with flowering time determination, and the involvement of these proteins in the same pathways, as shown above, support a role for *UCN* in flowering time determination. Furthermore, the influence on flowering time of *CUox* is not possible in an *atxr7-1* background, suggesting that the flowering time delay of *UCN* is dependent on *ATXR7*. In addition, the gain-of-function of *ATXR7* eliminates the later flowering of *CUox*, too. To understand this result one has to take a look on the results gained for the gain-of-function of *ATXR7* in wild-type background. Usually, in an *ATXR7* gain-of-function line, a further enhancement or at least a stable expression of *FLC* would be expected, since *ATXR7* enhances *FLC* expression. Surprisingly, the *FLC* expression decreases in *CAox*. In parallel, the *FT* expression strongly increases. The reason for this

increase cannot be exclusively the decrease of *FLC*, which represses *FT* expression. Compared to *atxr7-1*, the *FT* expression is much higher although the *FLC* expression decreases weaker. Therefore, the *FT* expression in CAox is enhanced. This supports the idea that *ATXR7* is also necessary to promote *FT* expression [76]. Therefore it seems that *UCN* is repressing *ATXR7* from activating flowering. This explanation is supported by the wild-type expression of *FLC* and *FT* in CAUox. The early flowering of 2Aox further confirms this statement. The overexpression of *ATXR7* in wild-types activates flowering on genetic level but not that strong that it is phenotypically visible. Therefore, the wild-type *UCN* expression seems to be enough to repress an early flowering phenotype of CAox. Due to the loss-of-function of *UCN* in 2Aox this repression is not possible any more resulting in an early flowering.

I found more evidence for the involvement of *UCN* in flowering time regulation by checking the expression levels of *FLC* and *FT* in the different loss- and gain-of-function lines. In *ucn-2*, the *FLC* expression decreases indicating that *FLC* is not properly expressed in this loss-of-function mutant. The double mutant *atxr7-1 ucn-2* displayed the same *FLC* expression level like *atxr7-1*. Therefore, regarding flowering time determination, *UCN* is involved in the same pathways as *ATXR7* and also here, *ATXR7* is epistatic to *UCN* since *ucn-2* displays a higher *FLC* expression level than *atxr7-1*. Since the gain-of-function of *UCN* did not result in an increased *FLC* expression, it suggests that *UCN* has an indirect effect on *FLC* expression. The question why exactly *FLC* is not properly expressed in *ucn-2* remained unanswered. If *ATXR7* would need activation by *UCN* to enhance *FLC* expression, CAUox would show an enhanced late flowering phenotype. Since *UCN* seems to be somehow involved in DNA methylation which is used for tagging histones as targets, the region of the *FLC* locus where *ATXR7* is active was checked via bisulfite sequencing, but the methylation pattern showed no difference to the wild-type (data not shown). Therefore, *UCN* is not involved in the recruiting of *ATXR7* either. Maybe *UCN* deactivates another protein that blocks *ATXR7* from methylating its targets in that region. However, I was not able to completely explain the missing expression of *FLC* in *ucn-2* and the phenomenon needs further investigation.

Surprisingly, *FT* expression was not increased in *ucn-2*, although the expression of its repressor *FLC* decreased. Furthermore, in CUox the *FT* expression decreases. This suggests that *UCN* has an effect on *FT* expression although, according to the flowering time of aUox, this repression is not possible without *ATXR7*. Anyway, the repression of *FT* coincides with the late flowering phenotype of CUox. The expression pattern of *UCN* in the leaf also overlaps with the *FT* expression pattern in the vascular tissue of the leaves. Again, it is not exactly clear how the repression happens. Since *ATXR7* is also discussed as an activator of *FT*

[76] *UCN* might be able to block that activation. The results suggest that *UCN* delays flowering in Col-0 by repressing *FT* and supporting *FLC* expression.

The trans-generational inheritance of the flowering time was not investigated in detail. Nevertheless, I was able to demonstrate that *FLC* as well as *FT* are deregulated in EFC. The reason why *FLC* expression is not increased in CUox could be that *UCN* epigenetically programs *FLC* to more expression. Due to the high expression of *UCN*, an antagonist of a higher *FLC* expression gets over-activated by the gain-of-function of *UCN* blocking an increased *FLC* expression. If the overexpression decreases as in EFC, the antagonist also decreases and *FLC* expression, which is still epigenetically programmed for higher expression, can therefore increase. However, that explanation needs experimental support verifying a different methylation pattern somewhere in or around the *FLC* locus. The decrease in *FT* expression could indicate that *UCN* does not only repress the gene but further also modifies its DNA methylation pattern. As a consequence *FT* is repressed also in EFC. However, the low *FT* expression explains the later flowering of CUox as well as of EFC.

I demonstrated that when grown under SD conditions, CUox as well as EFC flower like the wild-type. This suggests that the SD conditions override the late flowering caused by *UCN*. It is known that SD conditions activate different pathways for flowering than LD conditions do, independent of *FT* [31, 32]. These pathways are likely activating flowering under SD conditions overriding the repression of *FT* by *UCN*.

The observations I made for the possible role of *UCN* in flowering time determination also match the observations I made for the spatial expression pattern. *UCN* expression was found stronger in young organs where cell division still takes place. With the maturation of the cells, *UCN* expression decreased and according to the results I gained for the gain-of-function lines, it might even be counterproductive. However, the more the cells, and with them the organs, mature, the less *UCN* expression is found. This would result in less *FLC* activation and less *FT* repression and therefore, flowering can occur. If this assumption is correct it would further connect *ATXR7*, and therefore *FLC* expression, to plant age. The observation that *UCN* expression is rather constant in the vascular tissue while getting weaker in the surrounding cells suggests an additional player in the repression of *FT*. *FT* is expressed in the vascular tissue of the leaves and therefore, the repression by *UCN* needs to be neutralized. This could happen by repressing the unknown third player or by an environmental influence that represses the interaction between *UCN* and its partner that is needed for the repression of *FT*.

In conclusion, it is very likely that *UCN* is involved in flowering time determination. I was able to show that *UCN* represses flowering over *ATXR7* in Col-0. On the one hand it is needed for the proper expression of *FLC* and it represses *FT* expression. These observations also coincide with the spatial expression pattern that I found, where *UCN* expression decreases with the age of the cells and the organs, respectively. The results further suggest that *UCN* represses *ATXR7* from flowering activation since high *ATXR7* levels are counterproductive for flowering repression, decreasing *FLC* expression and increasing *FT* expression. Furthermore, *UCN* is involved in processes that epigenetically inherit the flowering time to the offspring.

Thus, the results point to the following model (see figure 4.5.1): *ATXR7* enhances the expression of *FLC* as well as of *FT*. *UCN* shifts these activations to the benefit of *FLC*. Therefore, *FLC* is not properly expressed in *ucn-2*. In CUox, the activation of *FLC* via *ATXR7* is not further possible; therefore, the *FLC* expression is not further increased. The repression of the *FT* activation on the other hand is enhanced and therefore, *FT* expression decreases. This results in the late flowering phenotype of CUox. In *atxr7-1* *UCN* is redundant, since the whole regulation runs over *ATXR7*. Hence, neither gain- nor loss-of-function of *UCN* further influences the flowering time of *atxr7-1*. In CAox, *UCN* is titrated out. Why this happens to the benefit of *FT* activation instead of *FLC* activation is unknown. It is possible that other factors that activate *FLC* and further repress *FT* activation are missing in Col-0 background. However, the gain-of-function of *ATXR7* activates *FT* and decreases *FLC* expression. In CAUox, this is reset by the high levels of *UCN* that now can again control the high levels of *ATXR7*: the wild-type situation is re-established.

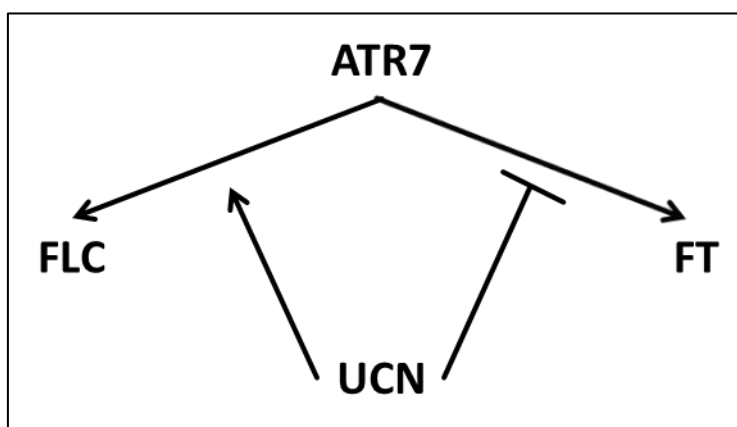


Figure 4.5.1: Model for the contribution of *UCN* to flowering time determination.

The model is based on the assumption that *FLC* and *FT* is activated by *ATXR7*. *UCN* promotes the activation of *FLC* while it represses the activation of *FT*.

5 Conclusion

In this work, the role of *UCN* in the involvement of different processes of the plant organs and, in more detail, its role in flowering time regulation of *Arabidopsis thaliana* was investigated. I was able to demonstrate that *UCN* is expressed ubiquitously in all plant organs. Further, the expression is found predominantly in the parts where cell division takes place, for example in the elongation zone of the root or young, developing leaves. Elsewhere the expression decreases but never disappears completely. Also, parts of the meristems, SAM as well as root meristem are left out. This expression pattern coincides with the observation that in the loss-of-function mutants, multiple plant organs are affected. It is therefore likely, that *UCN* is needed not only for proper ovule and flower development, which was further verified in this work, but also in processes of other plant organs. I further show that seed size is not only maternally influenced by *UCN* but also paternally. Thereby, the results suggest that the maternal behavior dominates over the paternal.

With a gain-of-function approach I demonstrated that the ectopic expression also affects almost all plant organs. Therefore, the regulation and repression is most likely necessary for proper cell maturation. The gain-of-function of *UCN* also affects *Ler* much more than *Col-0*. This coincides with the observation that *ucn-1* displays more and more severe features than *ucn-2* and that the reason for that is most likely the different ecotypes and not the different *ucn* alleles. However, the results and observations I gained suggest a role for *UCN* in cell division. This also covers former results that cell cycle genes are deregulated in *ucn-1*.

Using an *ucn-1* gain-of-function approach, I was also able to demonstrate that *ucn-1* is a dominant-negative allele. Not only do heterozygous *ucn-1* plants still show a phenotype, the *ucn-1* gain-of-function also affects many plant organs. Thereby, I excluded neomorphic or hypermorphic behavior. In addition, the dominant-negative behavior does not affect flowers, where *UCN* behaves recessive or ovules, where the observations suggest a haplo-insufficiency.

It was further demonstrated that *UCN* plays a role in epigenetics. Due to the inheritance of several features to siblings that do not carry mutated alleles anymore, it could be shown that *UCN* contributes to an epigenetic memory, especially for flowering time. These results were additionally supported by the transcriptional level of some genes

associated with flowering time regulation which were deregulated in gain-of-function lines and whose transcription was resembled by the corresponding EMO lines.

In yeast and in protoplasts, evidence was found for a physical interaction of UCN with ATXR7, a known enhancer of *FLC* expression. The ATXR7-UCN dependency was additionally demonstrated by crossing *ucn-2* with *atxr7-1* and parallel overexpression of *ATXR7* and *UCN*. These lines verify that *UCN* and *ATXR7* act in the same pathway, but furthermore, that *UCN* depends on *ATXR7* for flowering time repression in Col-0 and that *ATXR7* is epistatic to *UCN*. The deregulated flowering time displayed by the gain-of-function of *UCN* in Col-0 was investigated in more detail, since *ATXR7* is a known enhancer of *FLC*. I presented evidence that *UCN* has a role in the expression of *FLC* and the repression of *FT*. With gain-of-function lines I was further able to demonstrate that a too high *ATXR7* level is counterproductive for flowering repression. Therefore, I concluded that *UCN* represses *ATXR7* from flowering activation.

6 Supplements

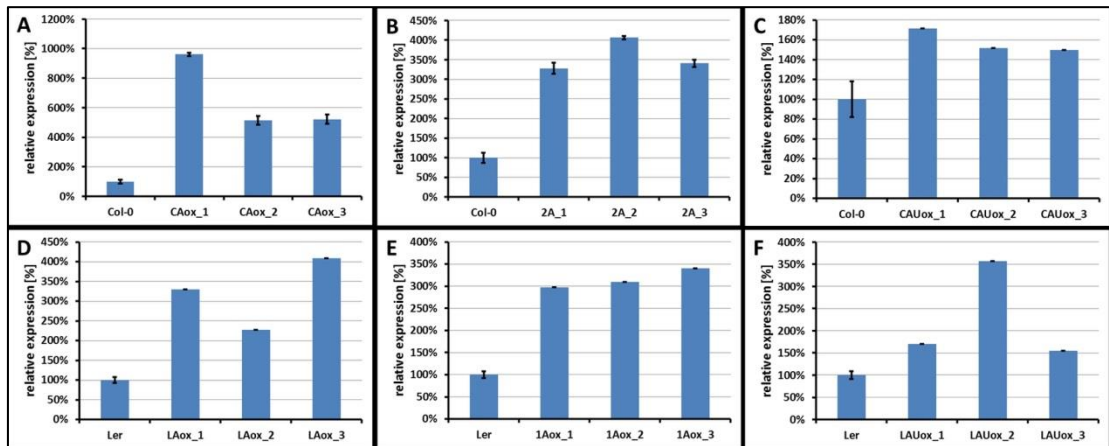


Figure S1: Expression of *ATXR7* in *ATXR7* overexpression lines

Expression of *ATXR7* in (A) CAox, (B) 2Aox, (C) CAUox, (D) LAox, (E) 1Aox, and (F) LAUox. Expression levels were checked with qRT-PCR. Figure shows expression level of three working lines compared to a biological triplicate of the corresponding wild-type expression.

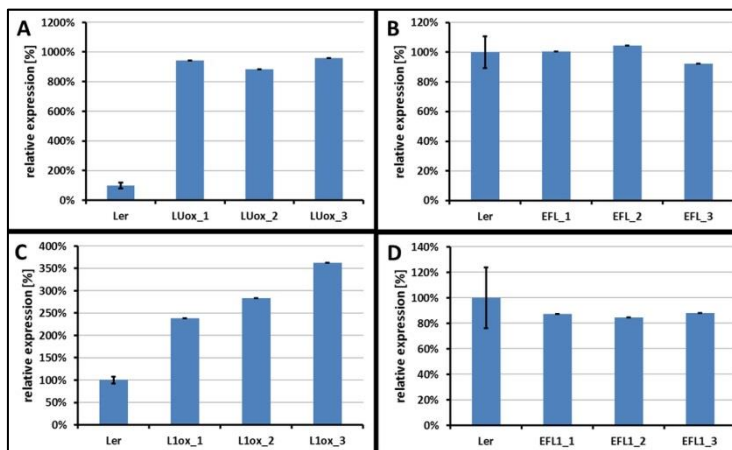


Figure S2: Expression of *UCN* and *ucn-1* in *UCN* and *ucn-1* overexpression lines (*Ler* background) incl. EMO offspring

Expression of *UCN/ucn-1* in (A) LUox, (B) EFL, (C) L1ox, and (D) EFL1. Expression levels were checked with sqRT-PCR. Figure shows expression level of three working lines compared to a biological triplicate of the corresponding wild-type expression.

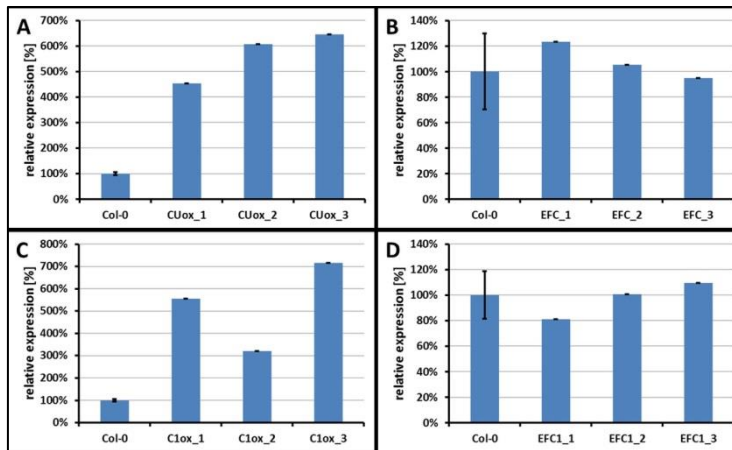


Figure S3: Expression of *UCN* and *ucn-1* in *UCN* and *ucn-1* overexpression lines (Col-0 background) incl. EMO offspring

Expression of *UCN/ucn-1* in (A) CUox, (B) EFC, (C) C1ox, and (D) EFC1. Expression levels were checked with sqRT-PCR. Figure shows expression level of three working lines compared to a biological triplicate of the corresponding wild-type expression.

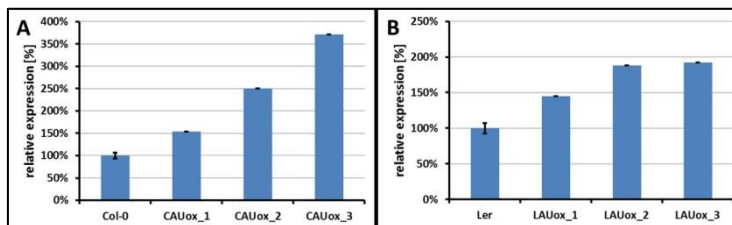


Figure S4: Expression of *UCN* in double overexpression lines.

Expression of *UCN* in (A) CAUox and (B) LAUox. Expression levels were checked with sqRT-PCR. Figure shows expression level of three working lines compared to a biological triplicate of the corresponding wild-type expression.

Table S1: Abbreviations used in the Y2H assay.

AD-plasmids were numbered with A, BD-plasmids were numbered with B. For combinations tested see table S2. ATXR7 fragments are given in numbers of basepairs.

AD	Insert	BD	Insert
A1	empty	B1	empty
A2	UCN	B2	UCN
A3	<i>ucn-1</i>	B3	<i>ucn-1</i>
A4	ATXR7 (1 – 999)	B4	ATXR7 (1 – 999)
A5	ATXR7 (501 – 1500)	B5	ATXR7 (501 – 1500)
A6	ATXR7 (999 – 1998)	B6	ATXR7 (999 – 1998)
A7	ATXR7 (1500 – 2499)	B7	ATXR7 (1500 – 2499)
A8	ATXR7 (1998 – 2997)	B8	ATXR7 (1998 – 2997)
A9	ATXR7 (2499 – 3498)	B9	ATXR7 (2499 – 3498)
A10	ATXR7 (2997 – 3996)	B10	ATXR7 (2997 – 3996)
A11	ATXR7 (3498 – 4167)	B11	ATXR7 (3498 – 4167)
A12	PDK1.2	B12	PDK1.2
A13	ATXR7	B13	AXTR7

Table S2: Combinations tested in the Y2H assay.

For abbreviations see table S1. Red boxes were not tested.

BD/AD	A1	A2	A3	A4	A5	A6	A7	A8	A9	A10	A11	A12	A13
B1	1	2	3	4	5	6	7	8	9	10	11	12	13
B2	14	15	16	17	18	19	20	21	22	23	24	25	26
B3	27	28	29	30	31	32	33	34	35	36	37	38	39
B4	40	41	42									43	44
B5	45	46	47									48	49
B6	50	51	52									53	54
B7	55	56	57									58	59
B8	60	61	62									63	64
B9	65	66	67									68	69
B10	70	71	72									73	74
B11	75	76	77									78	79
B12	80	81	82	83	84	85	86	87	88	89	90	91	92
B13	93	94	95	96	97	98	99	100	101	102	103	104	105

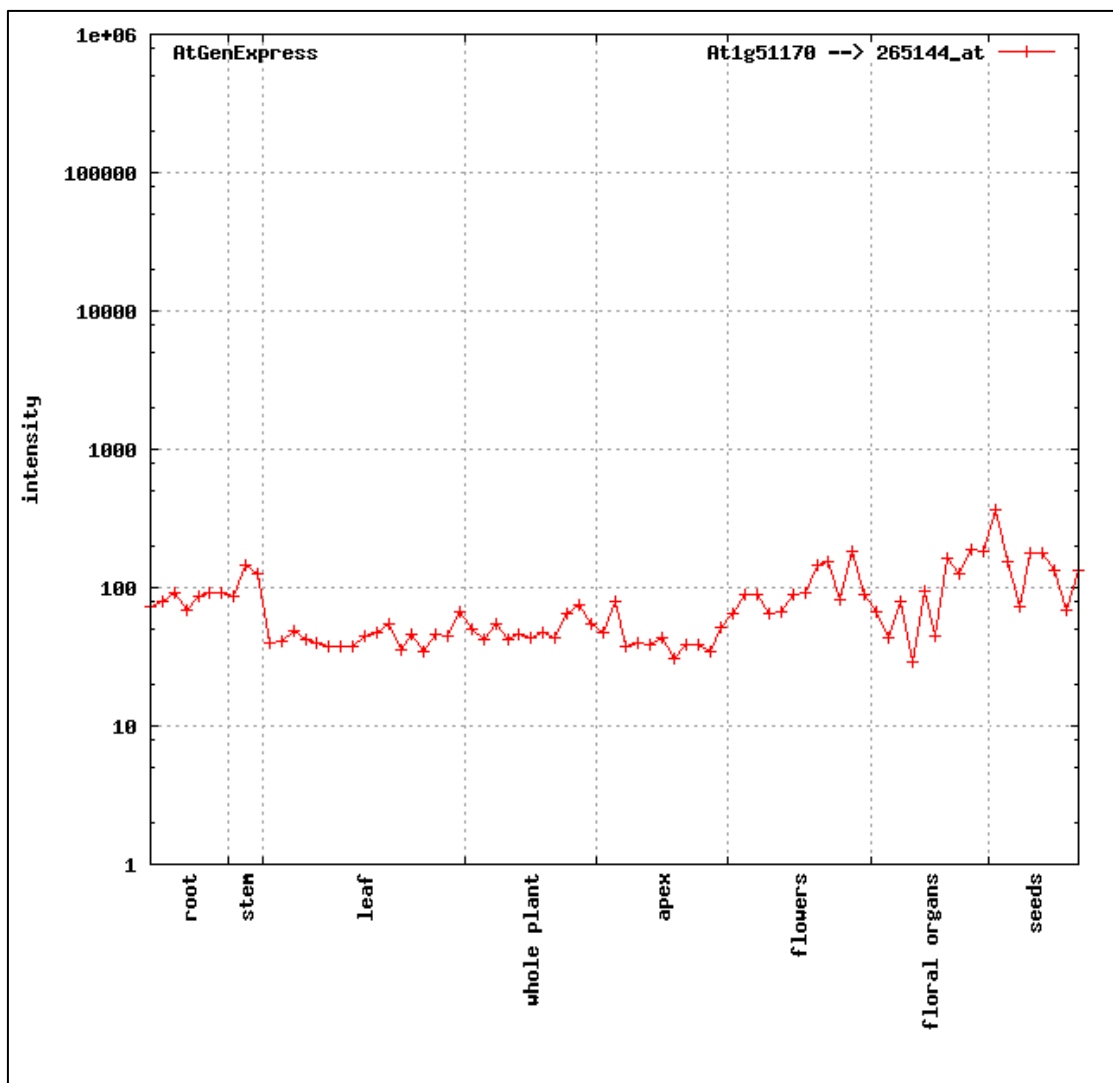
**Figure S5: Expression pattern of UCN from [120].**

Table S3: Summary of the characteristics of all lines phenotyped in this work.

Characteristic	ucn-1	ucn-2	atxr7-1	atxr7-1 ucn-2	LUox	EFL	L1ox	EFL1	CUox	EFC	C1ox	EFC1	LAox	1Aox	CAox	2Aox	aUox	CAUox	LAUox	
Seed size	82%	123%	135%	119%	105%	wild-type	89%	wild-type	85%	wild-type	116%	wild-type	wild-type	97%	126%	87%	87%	wild-type	no data	
Germination rate	72%	wild-type	wild-type	wild-type	wild-type	type	wild-type	wild-type	wild-type	wild-type	wild-type	wild-type	wild-type	wild-type	wild-type	wild-type	wild-type	wild-type	wild-type	no data
Root length	56%	87%	wild-type	92%	53%	43%	61%	83%	47%	91%	92%	82%	83%	87%	wild-type	wild-type	wild-type	wild-type	no data	
FT (LD)	75%	wild-type	71%	70%	55%	61%	88%	90%	124%	115%	113%	109%	wild-type	75%	wild-type	81%	63%	wild-type	123%	
FT (SD)	77%	wild-type	84%	82%	66%	67%	87%	90%	wild-type	wild-type	wild-type	wild-type	wild-type	82%	wild-type	no data	no data	wild-type	no data	
Overall plant stature	wild-type	wild-type	wild-type	wild-type	compressed	compressed	wild-type	wild-type	wild-type	wild-type	wild-type	wild-type	wild-type	wild-type	wild-type	wild-type	wild-type	wild-type	wild-type	
Rosette leaves	wild-type	wild-type	wild-type	wild-type	roundish	roundish-lanceolate	wild-type	wild-type	wild-type	wild-type	wild-type	wild-type	wild-type	wild-type	wild-type	wild-type	wild-type	wild-type	wild-type	
Flower shape	affected	wild-type	wild-type	wild-type	wild-type	wild-type	wild-type	wild-type	wild-type	wild-type	wild-type	wild-type	wild-type	slightly affected	wild-type	wild-type	wild-type	wild-type	wild-type	
Silique length	85%	96%	wild-type	93%	wild-type	wild-type	wild-type	105%	97%	wild-type	wild-type	wild-type	105%	87%	wild-type	97%	wild-type	wild-type	no data	
Silique shape	wild-type	wild-type	wild-type	wild-type	>2 fused carpels	>2 fused carpels	wild-type	wild-type	wild-type	wild-type	wild-type	wild-type	wild-type	wild-type	wild-type	wild-type	wild-type	wild-type	wild-type	
Ovule degeneration	yes	no	no	no	yes	yes	no	no	no	no	no	no	no	wild-type	wild-type	wild-type	wild-type	wild-type	wild-type	
Ovule shape	protrusions	wild-type	wild-type	wild-type	wild-type	wild-type	wild-type	wild-type	wild-type	wild-type	wild-type	wild-type	wild-type	protrusions (bigger?)	wild-type	wild-type	wild-type	wild-type	wild-type	

7 References

1. Simpson GG, Dean C (2002) Arabidopsis, the Rosetta Stone of Flowering Time? *Science* **296**: 285–289.
2. Hensel LL, Grbić V, Baumgarten DA, Bleecker AB (1993) Developmental and Age-Related Processes That Influence the Longevity and Senescence of Photosynthetic Tissues in Arabidopsis. *Plant Cell* **5**: 553–564.
3. Holdsworth MJ, Bentsink L, Soppe WJ (2008) Molecular networks regulating Arabidopsis seed maturation, after-ripening, dormancy and germination. *New Phytol* **179**: 33–54.
4. Bewley JD (1997) Seed Germination and Dormancy. *Plant Cell* **9**: 1055–1066.
5. West M, Harada JJ (1993) Embryogenesis in Higher Plants: An Overview. *Plant Cell* **5**: 1361–1369.
6. Dolan L, Janmaat K, Willemsen V, Linstead P, Poethig S, Roberts K, Scheres B (1993) Cellular organisation of the *Arabidopsis thaliana* root. *Development* **119**: 71–84.
7. Barlow PW (2002) The Root Cap: Cell Dynamics, Cell Differentiation and Cap Function. *J Plant Growth Regul* **21**: 261–286.
8. Petricka JJ, Winter CM, Benfey PN (2012) Control of *Arabidopsis* Root Development. *Annu Rev Plant Biol* **63**: 563–590.
9. Ding Z, Friml J (2010) Auxin regulates distal stem cell differentiation in *Arabidopsis* roots. *Proc Natl Acad Sci* **107**: 12046–12051.
10. Grieneisen VA, Xu J, Marée AFM, Hogeweg P, Scheres B (2007) Auxin transport is sufficient to generate a maximum and gradient guiding root growth. *Nature* **449**: 1008–1013.
11. De Smet I, Tetsumura T, De Rybel B, Frey NF d., Laplaze L, Casimiro I, Swarup R, Naudts M, Vanneste S, Audenaert D, et al. (2007) Auxin-dependent regulation of lateral root positioning in the basal meristem of *Arabidopsis*. *Development* **134**: 681–690.
12. Péret B, De Rybel B, Casimiro I, Benková E, Swarup R, Laplaze L, Beeckman T, Bennett MJ (2009) *Arabidopsis* lateral root development: an emerging story. *Trends Plant Sci* **14**: 399–408.
13. Bowman JL, Eshed Y (2000) Formation and maintenance of the shoot apical meristem. *Trends Plant Sci* **5**: 110–115.
14. Laux T, Mayer KF, Berger J, Jürgens G (1996) The *WUSCHEL* gene is required for shoot and floral meristem integrity in *Arabidopsis*. *Development* **122**: 87–96.
15. Yadav RK, Perales M, Gruel J, Girke T, Jönsson H, Reddy GV (2011) WUSCHEL protein movement mediates stem cell homeostasis in the *Arabidopsis* shoot apex. *Genes Dev* **25**: 2025–2030.
16. Steeves TA, Sussex IM (1989) Patterns in Plant Development. *Cambridge University Press*.
17. Donnelly PM, Bonetta D, Tsukaya H, Dengler RE, Dengler NG (1999) Cell Cycling and Cell Enlargement in Developing Leaves of *Arabidopsis*. *Dev Biol* **215**: 407–419.
18. Byrne ME (2006) Shoot Meristem Function and Leaf Polarity: The Role of Class III HD-ZIP Genes. *PLoS Genet* **2**: 785–790.
19. Boscá S, Knauer S, Laux T (2011) Embryonic development in *Arabidopsis thaliana*: from the zygote division to the shoot meristem. *Front Plant Sci* **2**: 1–6.
20. Long J, Barton MK (2000) Initiation of Axillary and Floral Meristems in *Arabidopsis*. *Dev Biol* **218**: 341–353.
21. Martinez-Zapater JM, Coupland G, Dean C, Koornneef M (1994) The Transition to Flowering in *Arabidopsis*. *Cold Spring Harb Monogr Arch* **27**: 403–433.
22. Parcy F, Bomblies K, Weigel D (2002) Interaction of *LEAFY*, *AGAMOUS* and *TERMINAL FLOWER1* in maintaining floral meristem identity in *Arabidopsis*. *Development* **129**: 2519–2527.

23. Higashiyama T (2002) The synergid cell: attractor and acceptor of the pollen tube for double fertilization. *J Plant Res* **115**: 149–160.
24. Faure J-E, Rotman N, Fortuné P, Dumas C (2002) Fertilization in *Arabidopsis thaliana* wild type: Developmental stages and time course. *Plant J* **30**: 481–488.
25. De Smet I, Lau S, Mayer U, Jürgens G (2010) Embryogenesis – the humble beginnings of plant life. *Plant J* **61**: 959–970.
26. Jürgens G, Mayer U, Torres Ruiz RA, Berleth T, Miséra S (1991) Genetic analysis of pattern formation in the *Arabidopsis* embryo. *Development* **113**: 27–38.
27. Napp-Zinn K (1957) Die Abhängigkeit des Vernalisationseffektes bei *Arabidopsis thaliana* vom Quellungsgrad der Samen und vom Lichtgenuß der Pflanzen nach der Kältebehandlung. *Flora Oder Allg Bot Ztg* **144**: 403–419.
28. Putterill J, Laurie R, Macknight R (2004) It's time to flower: the genetic control of flowering time. *BioEssays* **26**: 363–373.
29. Simpson GG (2004) The autonomous pathway: epigenetic and post-transcriptional gene regulation in the control of *Arabidopsis* flowering time. *Curr Opin Plant Biol* **7**: 570–574.
30. Blázquez MA, Green R, Nilsson O, Sussman MR, Weigel D (1998) Gibberellins Promote Flowering of *Arabidopsis* by Activating the *LEAFY* Promoter. *Plant Cell* **10**: 791–800.
31. Hisamatsu T, King RW (2008) The nature of floral signals in *Arabidopsis*. II. Roles for *FLOWERING LOCUS T (FT)* and gibberellin. *J Exp Bot* **59**: 3821–3829.
32. Wilson RN, Heckman JW, Somerville CR (1992) Gibberellin is Required for Flowering in *Arabidopsis thaliana* under Short Days. *Plant Physiol* **100**: 403–408.
33. Amasino RM (2005) Vernalization and flowering time. *Curr Opin Biotechnol* **16**: 154–158.
34. Helliwell CA, Wood CC, Robertson M, James Peacock W, Dennis ES (2006) The *Arabidopsis* FLC protein interacts directly *in vivo* with *SOC1* and *FT* chromatin and is part of a high-molecular-weight protein complex. *Plant J* **46**: 183–192.
35. Choi K, Kim J, Hwang H-J, Kim S, Park C, Kim SY, Lee I (2011) The FRIGIDA Complex Activates Transcription of *FLC*, a Strong Flowering Repressor in *Arabidopsis*, by Recruiting Chromatin Modification Factors. *Plant Cell* **23**: 289–303.
36. Gazzani S, Gendall AR, Lister C, Dean C (2003) Analysis of the Molecular Basis of Flowering Time Variation in *Arabidopsis* Accessions. *Plant Physiol* **132**: 1107–1114.
37. Schmalenbach I, Zhang L, Rynhajillo M, Jiménez-Gómez JM (2014) Functional analysis of the Landsberg *erecta* allele of *FRIGIDA*. *BMC Plant Biol* **14**: 218 (1–11).
38. Sheldon CC, Conn AB, Dennis ES, James Peacock W (2002) Different Regulatory Regions Are Required for the Vernalization-Induced Repression of *FLOWERING LOCUS C* and for the Epigenetic Maintenance of Repression. *Plant Cell* **14**: 2527–2537.
39. Boss PK, Bastow RM, Mylne JS, Dean C (2004) Multiple Pathways in the Decision to Flower: Enabling, Promoting, and Resetting. *Plant Cell* **16**: S18–S31.
40. Corbesier L, Vincent C, Jang S, Fornara F, Fan Q, Searle I, Giakountis A, Farrona S, Gissot L, Turnbull C, Coupland G (2007) FT Protein Movement Contributes to Long-Distance Signaling in Floral Induction of *Arabidopsis*. *Science* **316**: 1030–1033.
41. An H, Roussot C, Suárez-López P, Corbesier L, Vincent C, Piñeiro M, Hepworth S, Mouradov A, Justin S, Turnbull C, Coupland G (2004) CONSTANS acts in the phloem to regulate a systemic signal that induces photoperiodic flowering of *Arabidopsis*. *Development* **131**: 3615–3626.
42. Huang T, Böhlenius H, Eriksson S, Parcy F, Nilsson O (2005) The mRNA of the *Arabidopsis* Gene *FT* Moves from Leaf to Shoot Apex and Induces Flowering. *Science* **309**: 1694–1696.
43. Wigge PA, Kim MC, Jaeger KE, Busch W, Schmid M, Lohmann JU, Weigel D (2005) Integration of Spatial and Temporal Information During Floral Induction in *Arabidopsis*. *Science* **309**: 1056–1059.
44. Mandel MA, Gustafson-Brown C, Savidge B, Yanofsky MF (1992) Molecular characterization of the *Arabidopsis* floral homeotic gene *APETALA1*. *Nature* **360**: 273–277.

45. Weigel D, Alvarez J, Smyth DR, Yanofsky MF, Meyerowitz EM (1992) *LEAFY* Controls Floral Meristem Identity in Arabidopsis. *Cell* **69**: 843–859.
46. Coen ES, Meyerowitz EM (1991) The war of the whorls: genetic interactions controlling flower development. *Nature* **353**: 31–37.
47. Yanofsky MF, Ma H, Bowman JL, Drews GN, Feldmann KA, Meyerowitz EM (1990) The protein encoded by the *Arabidopsis* homeotic gene *agamous* resembles transcription factors. *Nature* **346**: 35–39.
48. Krizek BA, Meyerowitz EM (1996) The *Arabidopsis* homeotic genes *APETALA3* and *PISTILLATA* are sufficient to provide the B class organ identity function. *Development* **122**: 11–22.
49. Irish VF, Sussex IM (1990) Function of the *apetala-1* Gene during *Arabidopsis* Floral Development. *Plant Cell* **2**: 741–753.
50. Kunst L, Klenz JE, Martinez-Zapater J, Haughn GW (1989) *AP2* Gene Determines the Identity of Perianth Organs in Flowers of *Arabidopsis thaliana*. *Plant Cell* **1**: 1195–1208.
51. Garcia D, Fitz Gerald JN, Berger F (2005) Maternal Control of Integument Cell Elongation and Zygotic Control of Endosperm Growth Are Coordinated to Determine Seed Size in Arabidopsis. *Plant Cell* **17**: 52–60.
52. Angenent GC, Colombo L (1996) Molecular control of ovule development. *Trends Plant Sci* **1**: 228–232.
53. Schneitz K, Hülskamp M, Pruitt RE (1995) Wild-type ovule development in *Arabidopsis thaliana*: a light microscope study of cleared whole-mount tissue. *Plant J* **7**: 731–749.
54. Baud S, Boutin J-P, Miquel M, Lepiniec L, Rochat C (2002) An integrated overview of seed development in *Arabidopsis thaliana* ecotype WS. *Plant Physiol Biochem* **40**: 151–160.
55. Scott RJ, Spielman M, Bailey J, Dickinson HG (1998) Parent-of-origin effects on seed development in *Arabidopsis thaliana*. *Development* **125**: 3329–3341.
56. Xiao W, Brown RC, Lemmon BE, Harada JJ, Goldberg RB, Fischer RL (2006) Regulation of Seed Size by Hypomethylation of Maternal and Paternal Genomes. *Plant Physiol* **142**: 1160–1168.
57. Zhang X, Yazaki J, Sundaresan A, Cokus S, Chan SWL, Chen H, Henderson IR, Shinn P, Pellegrini M, Jacobsen SE, Ecker JR (2006) Genome-wide High-Resolution Mapping and Functional Analysis of DNA Methylation in *Arabidopsis*. *Cell* **126**: 1189–1201.
58. Zhang X (2008) The Epigenetic Landscape of Plants. *Science* **320**: 489–492.
59. Chan SWL, Henderson IR, Jacobsen SE (2005) Gardening the genome: DNA methylation in *Arabidopsis thaliana*. *Nat Rev Genet* **6**: 351–360.
60. Li S, Liu L, Li S, Gao L, Zhao Y, Kim YJ, Chen X (2015) SUVH1, a Su(var)3–9 family member, promotes the expression of genes targeted by DNA methylation. *Nucleic Acids Res* **44**: 608–620.
61. Finnegan EJ, Peacock WJ, Dennis ES (1996) Reduced DNA methylation in *Arabidopsis thaliana* results in abnormal plant development. *Proc Natl Acad Sci* **93**: 8449–8454.
62. Barteel L, Malagnac F, Bender J (2001) *Arabidopsis cmt3* chromomethylase mutations block non-CG methylation and silencing of an endogenous gene. *Genes Dev* **15**: 1753–1758.
63. Lindroth AM, Cao X, Jackson JP, Zilberman D, McCallum CM, Henikoff S, Jacobsen SE (2001) Requirement of *CHROMOMETHYLASE3* for Maintenance of CpXpG Methylation. *Science* **292**: 2077–2080.
64. Cao X, Jacobsen SE (2002) Role of the Arabidopsis DRM methyltransferases in de novo DNA methylation and gene silencing. *Curr Biol* **12**: 1138–1144.
65. Chan SW-L, Zilberman D, Xie Z, Johansen LK, Carrington JC, Jacobsen SE (2004) RNA silencing genes control de novo DNA methylation. *Science* **303**: 1336.
66. Zhang X, Jacobsen SE (2006) Genetic Analyses of DNA Methyltransferases in *Arabidopsis thaliana*. *Cold Spring Harbor Symposia on Quantitative Biology* **71**: 439–447.

67. Feng S, Jacobsen SE, Reik W (2010) Epigenetic Reprogramming in Plant and Animal Development. *Science* **330**: 622–627.
68. Hauser M-T, Aufsatz W, Jonak C, Luschnig C (2011) Transgenerational epigenetic inheritance in plants. *Biochim Biophys Acta BBA – Gene Regul Mech* **1809**: 459–468.
69. Talbert PB, Henikoff S (2010) Histone variants – ancient wrap artists of the epigenome. *Nat Rev Mol Cell Biol* **11**: 264–275.
70. Houben A, Demidov D, Caperta AD, Karimi R, Agueci F, Vlasenko L (2007) Phosphorylation of histone H3 in plants — A dynamic affair. *Biochim Biophys Acta BBA – Gene Struct Expr* **1769**: 308–315.
71. Bannister AJ, Kouzarides T (2011) Regulation of chromatin by histone modifications. *Cell Res* **21**: 381–395.
72. Dillon SC, Zhang X, Trievel RC, Cheng X (2005) The SET-domain protein superfamily: protein lysine methyltransferases. *Genome Biol* **6**: 227 (1–10).
73. Pien S, Fleury D, Mylne JS, Crevillen P, Inzé D, Avramova Z, Dean C, Grossniklaus U (2008) ARABIDOPSIS TRITHORAX1 Dynamically Regulates FLOWERING LOCUS C Activation via Histone 3 Lysine 4 Trimethylation. *Plant Cell* **20**: 580–588.
74. Berr A, Xu L, Gao J, Cognat V, Steinmetz A, Dong A, Shen W-H (2009) SET DOMAIN GROUP25 Encodes a Histone Methyltransferase and Is Involved in FLOWERING LOCUS C Activation and Repression of Flowering. *Plant Physiol* **151**: 1476–1485.
75. Tamada Y, Yun J-Y, Woo S c., Amasino RM (2009) ARABIDOPSIS TRITHORAX-RELATED7 Is Required for Methylation of Lysine 4 of Histone H3 and for Transcriptional Activation of FLOWERING LOCUS C. *Plant Cell* **21**: 3257–3269.
76. Shafiq S, Berr A, Shen W-H (2014) Combinatorial functions of diverse histone methylations in *Arabidopsis thaliana* flowering time regulation. *New Phytol* **201**: 312–322.
77. Xu L, Zhao Z, Dong A, Soubigou-Taconnat L, Renou J-P, Steinmetz A, Shen W-H (2008) Di- and Tri- but Not Monomethylation on Histone H3 Lysine 36 Marks Active Transcription of Genes Involved in Flowering Time Regulation and Other Processes in *Arabidopsis thaliana*. *Mol Cell Biol* **28**: 1348–1360.
78. Berger SL (2007) The complex language of chromatin regulation during transcription. *Nature* **447**: 407–412.
79. Soppe WJJ, Jasencakova Z, Houben A, Kakutani T, Meister A, Huang MS, Jacobsen SE, Schubert I, Fransz PF (2002) DNA methylation controls histone H3 lysine 9 methylation and heterochromatin assembly in *Arabidopsis*. *EMBO J* **21**: 6549–6559.
80. Jackson JP, Johnson L, Jasencakova Z, Zhang X, PerezBurgos L, Singh PB, Cheng X, Schubert I, Jenuwein T, Jacobsen SE (2004) Dimethylation of histone H3 lysine 9 is a critical mark for DNA methylation and gene silencing in *Arabidopsis thaliana*. *Chromosoma* **112**: 308–315.
81. Zegzouti H, Li W, Lorenz TC, Xie M, Payne CT, Smith K, Glennly S, Payne GS, Christensen SK (2006) Structural and Functional Insights into the Regulation of *Arabidopsis* AGC VIIIa Kinases. *J Biol Chem* **281**: 35520–35530.
82. Stone JM, Walker JC (1995) Plant Protein Kinase Families and Signal Transduction. *Plant Physiol* **108**: 451–457.
83. Champion A, Kreis M, Mockaitis K, Picaud A, Henry Y (2004) *Arabidopsis* kinome: after the casting. *Funct Integr Genomics* **4**: 163–187.
84. Hanks SK, Hunter T (1995) Protein kinases 6. The eukaryotic protein kinase superfamily: kinase (catalytic) domain structure and classification. *FASEB J* **9**: 576–596.
85. Sobko A (2006) Systems Biology of AGC Kinases in Fungi. *Sci Signal* **352**: 9 (1–8).
86. Mora A, Komander D, van Aalten DMF, Alessi DR (2004) PDK1, the master regulator of AGC kinase signal transduction. *Semin Cell Dev Biol* **15**: 161–170.
87. Bögre L, Ökrész L, Henriques R, Anthony RG (2003) Growth signalling pathways in *Arabidopsis* and the AGC protein kinases. *Trends Plant Sci* **8**: 424–431.

88. Zhang Y, McCormick S (2009) AGCVIII kinases: at the crossroads of cellular signaling. *Trends Plant Sci* **14**: 689–695.
89. Schneitz K, Hülskamp M, Kopczak SD, Pruitt RE (1997) Dissection of sexual organ ontogenesis: a genetic analysis of ovule development in *Arabidopsis thaliana*. *Development* **124**: 1367–1376.
90. Kelley DR, Arreola A, Gallagher TL, Gasser CS (2012) ETTIN (ARF3) physically interacts with KANADI proteins to form a functional complex essential for integument development and polarity determination in *Arabidopsis*. *Development* **139**: 1105–1109.
91. Enugutti B, Kirchhelle C, Oelschner M, Torres Ruiz RA, Schliebner I, Leister D, Schneitz K (2012) Regulation of planar growth by the *Arabidopsis* AGC protein kinase UNICORN. *Proc Natl Acad Sci* **109**: 15060–15065.
92. Enugutti B, Schneitz K (2013) Genetic analysis of ectopic growth suppression during planar growth of integuments mediated by the *Arabidopsis* AGC protein kinase UNICORN. *BMC Plant Biol* **13**: 2 (1–9).
93. Sambrook J, Russell DW (1989) *Molecular Cloning – A Laboratory Manual*. Cold Spring Harbor Laboratory Press.
94. Lampropoulos A, Sutikovic Z, Wenzl C, Lohmann JU, Forner J (2013) GreenGate – a novel, versatile, and efficient cloning system for plant transgenesis. *PLoS One* **8**: e83043.
95. Truernit E, Bauby H, Dubreucq B, Grandjean O, Runions J, Barthélémy J, Palauqui J-C (2008) High-Resolution Whole-Mount Imaging of Three-Dimensional Tissue Organization and Gene Expression Enables the Study of Phloem Development and Structure in *Arabidopsis*. *Plant Cell* **20**: 1494–1503.
96. Koncz C, Schell J (1986) The promoter of T₁-DNA gene 5 controls the tissue-specific expression of chimaeric genes carried by a novel type of *Agrobacterium* binary vector. *Mol Gen Genet MGG* **204**: 383–396.
97. Dreze M, Monachello D, Lurin C, Cusick ME, Hill DE, Vidal M, Braun P (2010) High-Quality Binary Interactome Mapping. *Methods in Enzymology* **470**: 281–315.
98. Walter M, Chaban C, Schütze K, Batistic O, Weckermann K, Näke C, Blazevic D, Grefen C, Schumacher K, Oecking C, et al. (2004) Visualization of protein interactions in living plant cells using bimolecular fluorescence complementation. *Plant J* **40**: 428–438.
99. Yoo S-D, Cho Y-H, Sheen J (2007) *Arabidopsis* mesophyll protoplasts: a versatile cell system for transient gene expression analysis. *Nat Protoc* **2**: 1565–1572.
100. Czechowski T, Stitt M, Altmann T, Udvardi MK, Scheible W-R (2005) Genome-Wide Identification and Testing of Superior Reference Genes for Transcript Normalization in *Arabidopsis*. *Plant Physiol* **139**: 5–17.
101. Airoidi CA, McKay M, Davies B (2015) *MAF2* Is Regulated by Temperature-Dependent Splicing and Represses Flowering at Low Temperatures in Parallel with *FLM*. *PLoS One* **10**: e0126516.
102. Ausín I, Alonso-Blanco C, Martínez-Zapater J-M (2005) Environmental regulation of flowering. *Int J Dev Biol* **49**: 689–705.
103. Dennis ES, Peacock WJ (2007) Epigenetic regulation of flowering. *Curr Opin Plant Biol* **10**: 520–527.
104. Koornneef M, Blankestijn-de Vries H, Hanhart C, Soppe W, Peeters T (1994) The phenotype of some late-flowering mutants is enhanced by a locus on chromosome 5 that is not effective in the Landsberg *erecta* wild-type. *Plant J* **6**: 911–919.
105. Michaels SD, Amasino RM (2001) Loss of *FLOWERING LOCUS C* Activity Eliminates the Late-Flowering Phenotype of *FRIGIDA* and Autonomous Pathway Mutations but Not Responsiveness to Vernalization. *Plant Cell* **13**: 935–941.
106. Yang H, Mo H, Fan D, Cao Y, Cui S, Ma L (2012) Overexpression of a histone H3K4 demethylase, JMJ15, accelerates flowering time in *Arabidopsis*. *Plant Cell Rep* **31**: 1297–1308.

107. Köhler C, Makarevich G (2006) Epigenetic mechanisms governing seed development in plants. *EMBO Rep* **7**: 1223–1227.
108. Kirchhelle C (2012) Functional analysis of the *Arabidopsis* AGC kinase UCN.
109. Neumann B, Barlow DP (1996) Multiple roles for DNA methylation in gametic imprinting. *Curr Opin Genet Dev* **6**: 159–163.
110. John RM, Surani MA (1996) Imprinted genes and regulation of gene expression by epigenetic inheritance. *Curr Opin Cell Biol* **8**: 348–353.
111. Berger SL, Kouzarides T, Shiekhattar R, Shilatifard A (2009) An operational definition of epigenetics. *Genes Dev* **23**: 781–783.
112. Liu Q, Gong Z (2011) The coupling of epigenome replication with DNA replication. *Curr Opin Plant Biol* **14**: 187–194.
113. Vongs A, Kakutani T, Martienssen RA, Richards EJ (1993) *Arabidopsis thaliana* DNA Methylation Mutants. *Science* **260**: 1926–1928.
114. Finnegan EJ, Dennis ES (1993) Isolation and identification by sequence homology of a putative cytosine methyltransferase from *Arabidopsis thaliana*. *Nucleic Acids Res* **21**: 2383–2388.
115. Kakutani T, Jeddelloh JA, Flowers SK, Munakata K, Richards EJ (1996) Developmental abnormalities and epimutations associated with DNA hypomethylation mutations. *Proc Natl Acad Sci* **93**: 12406–12411.
116. Mathieu O, Reinders J, Čaikovski M, Smathajitt C, Paszkowski J (2007) Transgenerational Stability of the *Arabidopsis* Epigenome Is Coordinated by CG Methylation. *Cell* **130**: 851–862.
117. Kawashima T, Berger F (2014) Epigenetic reprogramming in plant sexual reproduction. *Nat Rev Genet* **15**: 613–624.
118. Lee I, Michaels SD, Masshardt AS, Amasino RM (1994) The late-flowering phenotype of *FRIGIDA* and mutations in *LUMINIDEPENDENS* is suppressed in the Landsberg *erecta* strain of *Arabidopsis*. *Plant J* **6**: 903–909.
119. Takada S, Goto K (2003) TERMINAL FLOWER2, an *Arabidopsis* Homolog of HETEROCHROMATIN PROTEIN1, Counteracts the Activation of *FLOWERING LOCUS T* by CONSTANS in the Vascular Tissues of Leaves to Regulate Flowering Time. *Plant Cell* **15**: 2856–2865.
120. Schmid M, Davison TS, Henz SR, Pape UJ, Demar M, Vingron M, Schölkopf B, Weigel D, Lohmann JU (2005) A gene expression map of *Arabidopsis thaliana* development. *Nat Genet* **37**: 501–506.

8 Acknowledgements

I would like to thank Prof. Dr. Kay Schneitz for giving me the opportunity to work on this project. I am particularly grateful for his trust in my knowledge and motivation for the project and giving me the freedom to follow my ideas. Nevertheless, he always had an open door when I needed further scientific input.

I would like to thank Balaji for introducing me to the lab and the project and his guidance through my early days in the lab.

I would like to thank present and past members of the lab: Charlotte, Anja, Claudia, Prasad, Sebastian, Ajeet, Jin, Katrin, and Regina. It was a great pleasure working with you. Thank you for the friendly atmosphere and also the helpfulness.

I would like to thank my research assistants Enikö and Yue. Your effort has been outstanding.

I would like to thank the members of Lehrstuhl für Botanik and Lehrstuhl für Systembiologie der Pflanzen for their help.

The greatest thank goes to my wife for her outstanding patience. This work would not have been possible without you.

9 Curriculum Vitae

Persönliche Angaben

Name	Janys Peter Pleßmann
Geburtsdatum	25.03.1981
Geburtsort	Würzburg
Staatsangehörigkeit	Deutsch

Studium und Beruf

07/2012 – 02/2017	Wissenschaftlicher Mitarbeiter, Entwicklungsbiologie der Pflanzen, TU München
30.09.2011	Diplom in Biologie
10/2006 – 09/2011	Studium Biologie, RWTH Aachen
04/2003 – 09/2006	Studium Biologie, TU Darmstadt
10/2001 – 03/2003	Studium Informatik, TU Darmstadt
30.06.2000	Abitur / Allgemeine Hochschulreife, Karl-Ernst-Gymnasium, Amorbach